2019

TESTING THE USE OF VEGETATION INDICES AS INDICATORS OF PRE-ERUPTIVE VOLCANIC UNREST AT KILAUEA VOLCANO, HAWAII

Quelyn Bekkering

TESTING THE USE OF VEGETATION INDICES AS INDICATORS OF PRE-ERUPTIVE VOLCANIC UNREST AT KILAUEA VOLCANO, HAWAII

By

Quelyn R. Bekkering

A THESIS

Submitted in partial fulfillment of the requirements for the degree of

MASTER OF SCIENCE

In Geology

MICHIGAN TECHNOLOGICAL UNIVERSITY

2019

This thesis has been approved in partial fulfillment of the requirements for the Degree of MASTER OF SCIENCE in Geology.

Department of Geological & Mining Engineering & Sciences

Thesis Co-Advisor:	*Dr. Chad D. Deering*
Thesis Co-Advisor:	*Dr. Simon A. Carn*
Committee Member:	*Dr. Ann L. Maclean*
Committee Member:	*Dr. Catherine S. Hayer*
Department Chair:	*Dr. John S. Gierke*

Table of Contents

List of figures

List of tables

Acknowledgements

I would first like to thank my advisors, Chad and Simon, for agreeing to advise me as I made my way into the area of remote sensing. Thank you for being patient and guiding me along as I learned the necessary skills in order to put this project together. I would also like to thank Dr. Ann Maclean. Without your (almost weekly) help with learning coding and ArcGIS, this project most certainly would never have been finished. And a special thank you to Dr. Cat Hayer, who not only helped extensively with my writing, but also advised me in the capacity of my committee member and also my friend.

Special thanks to Planet Labs for providing free satellite data for my project. It has been an awesome experience learning how to work with different satellite products, all of which is only possible with companies who choose to invest in academia and students in particular.

I would also like to acknowledge the many great faculty and staff at Michigan Tech who have showed me what truly makes Tech great: a willingness to invest in the students they interact with, and a desire for each and every one of us to succeed. I would like to specifically thank Dr. John Gierke and Jeanne Watts. You have each invested in me from my very first days at Michigan Tech, and without you I would not have seen the potential in myself to know just how far I can come. Thank you for always believing in me.

And above all, I would like to thank my family and Sean. You are the best people in my life. Thank you for always supporting me and being there for me, no matter how far apart we are.

List of Abbreviations

CO_2	Carbon Dioxide
DN	Digital Number
ERDAS	ERDAS Imagine 2015
ERZ	East Rift Zone
H_2S	Hydrogen Sulfide
Hg	Mercury
LERZ	Lower East Rift Zone
NDVI	Normalized Difference Vegetation Index
NIR	Near Infra-red
ROD	Rapid Ohia Death
TOA	Top of Atmosphere
UTM	Universal Transverse Mercator

Abstract

Satellite remote sensing has become an integral part of pre-eruptive and long-term volcano monitoring due to its low cost, spatial and temporal coverage, and time-series analysis capabilities. Pre-eruptive unrest at volcanoes can include increased fluxes of heat and volcanic gases, which can be manifested either directly (e.g., the appearance of thermal anomalies or fumaroles) or indirectly (e.g., through impacts on vegetation health and extent). We are evaluating the use of novel, high spatial and temporal resolution data from the Planet Labs cubesat constellation to monitor changes in vegetation related to volcanic unrest. We present results from a study of key locations, including known geothermal areas, within the East Rift Zone (ERZ) of Kilauea volcano, Hawaii, prior to and during the May-August 2018 eruption on the Lower ERZ (LERZ). This proof of concept study investigates possible correlations between the Normalized Difference Vegetation Index (NDVI) stress signature and the formation or growth of geothermal features as well as eruptive events throughout the ERZ. There are a number of factors that can influence the NDVI signature, including changes in soil gas (CO_2, H_2S) emission rates and ground temperature. Both of these factors can be correlated to subsurface magma movement and migration in the ERZ.

Using the PlanetScope OrthoTile dataset (at 3.125 m resolution, with daily revisit time at nadir) from Planet Labs, the NDVI is calculated across the study areas within the ERZ. Using ArcGIS and ERDAS Imagine, pixels are classified according to spectral values in order to delineate different zones of vegetation coverage within the region of interest.

The Puhimau geothermal feature shows a clear decrease in NDVI in the lead up to the 2018 eruption. Significant changes in the distribution and general health of vegetation in the region directly surrounding the geothermal vents in the year preceding the eruption show a clear correlation between NDVI and increased volcanic unrest.

1 Introduction

Volcanic eruptions impact humans and landscapes on a large scale [Demarée et. al., 2001]. Understanding pre-eruptive behavior, eruption timing, repose periods, and associated hazards is increasingly important, especially for persistently active volcanic regions. Numerous techniques are utilized to monitor pre-eruptive volcanic behavior, including seismic, ground deformation, gravity, and remote or in-situ gas measurements [Tilling, 2008; Scarpa, 1996]. These tools, however, can be costly in terms of equipment price, operating costs and time in the field, and human risk while in close proximity to an active volcano. Another limitation of these techniques is that they fail to comprehensively observe the entire volcanic system through space and time. Remote sensing imagery provides extensive datasets with multiple applications by utilizing just one data collection method.

Since the advent of satellite technology, remote sensing has become a cornerstone technique to observe volcanic systems, reducing costs while increasing spatiotemporal coverage. Monitoring of volcanic phenomena such as landscape change, thermal sensing, gas output, and lava flow paths are all enhanced by remote sensing techniques. While remote sensing imagery is important for these types of observations, the data require extensive processing to elucidate key features that best represent active volcanic processes and eruptive precursors. This study aims to use multispectral remote sensing data to investigate the correlation between stressed vegetation signatures and increases in volcanic unrest prior to eruption.

Vegetation shows potential as a key eruptive indicator because it intakes a number of gases through both the air and soil, including carbon dioxide (CO_2) and hydrogen sulfide (H_2S), both of which are emitted from volcanoes [Cawse-Nicholson et. al., 2018]. During magma ascent, CO_2 and H_2S exsolve, and are released by the volcanic system [Shinohara, 2008]. These species are usually released at greater depths and higher pressures than other magma-associated gases. We hypothesize that an observable response in the vegetation overlying an active volcanic plumbing system should be seen. We also hypothesize that this may manifest itself as improved plant foliage health due to increased CO_2 availability. As of yet, however, the threshold at which increased CO_2 enrichment becomes detrimental is unknown. On the other hand, it is known that increased soil temperatures and acidic gas effusion certainly damage overlying vegetation and inhibit regrowth [Burns, 1997].

To assess vegetation health, vegetation indices (e.g., the Normalized Difference Vegetation Index – NDVI) are applied to collected remote sensing data [Lillesand, 1987]. The NDVI algorithm assigns a number to plant health and assesses health on a scale ranging from -1.0 to 1.0. Clouds, water, and snow typically occupy values close to -1; bare rock and soil occupy values close to zero, and healthy vegetation occupy values closer to 1.0 (typically 0.6 to 0.9) [Jensen, 2000].

The NDVI not only shows plant health, but other features such as buildings, rocks, sand, pavement, and more using spectral response values. These spectral response values allow the user to differentiate between different land cover types in a processed image, and thus assess vegetation health [Lillesand, 1987]. The NDVI is a normalized ratio comparing reflectance values from the red and near-infrared (NIR) channels of the satellite source

[Jensen, 1986]. These channels are used because plants with abundant chlorophyll will reflect highly in the NIR channel and absorb strongly in the red channel. The NDVI equation is as follows:

$$NDVI = \frac{NIR - red}{NIR + red}$$

The resulting ratio will be higher (closer to 1.0) for healthy vegetation, and lower for unhealthy vegetation. The use of the NDVI was twofold. It is considered a standard vegetation index because its ratioing concept reduces many types of sensor noise, allowing for meaningful comparisons in vegetation growth throughout the growing cycle [Tortini, 2017]. While the NDVI does have its weaknesses (it can be influenced by atmospheric attenuation and display scaling problems for high biomass conditions), it was deemed sufficient for this study based on vegetation present in each study area [Huete, 1988]. Additionally, this study continues on the work that C. Torres completed in May 2019, and the NDVI is used to keep methods consistent between studies for later analysis [Torres, 2019].

The utilization of the NDVI algorithm has been predominantly used for agricultural purposes to assess different crop health and growing seasons [Lillesand, 1987]. As of yet, NDVI has not been widely applied to studying volcanic activity correlated with vegetation, with the exception of a few studies. Previous work includes the application of NDVI to vegetative "kill zones" in Costa Rica, where increased SO_2 emissions directly correlate to a decline in vegetative health downwind of vents at Turrialba volcano [Tortini, 2017]. NDVI has also been used to attempt to identify naturally produced CO_2 storage sites and

degassing patterns at Latera, Italy. Of the various remote sensing methods used in this study, NDVI proved to have the highest success rate of 47%, though it failed to identify some known vents [Bateson et al., 2008].

Similar NDVI satellite studies have been performed at Mount Etna, Italy and Nyiragonog during November 2002. Increased vegetation health was observed across the North East rift zone and a strong correlation was seen between these improved vegetative health areas due to dyke injection and later lava fissure formation during 2003-2004 [Houlie et al., 2006].

Analysis of temperature and precipitation over the same time period showed no correlation with high-altitude tree ring growth, suggesting that these external climate factors do not account for the increased NDVI signal [Seiler, 2017].

The aim of this study is to ascertain if an increased NDVI signature was present in the year leading up to the May-August 2018 Kilauea eruption in Hawaii. This research integrates remote sensing data and geospatial analysis techniques of post-classification thematic change detection to analyze seven study areas in Kilauea's East Rift Zone (ERZ). Through the use of these techniques, this study addresses the following objectives: 1) determine if previously identified geothermal features within the ERZ experienced changes in vegetative health leading up to the 2018 Kilauea eruption; 2) ascertain if environmental factors played a role in increasing vegetative health; and 3) determine if an increased NDVI signature (if seen) was prevalent throughout multiple study areas in order to more thoroughly understand magma migration and movement within Kilauea's ERZ.

2 Geologic Background

Hawaii is part of the Hawaii-Emperor seamount volcanic chain which formed as a result of the Pacific Plate's northwest movement over the Hawaii hotspot. The hotspot is the main driver for the Hawaiian volcanic plumbing system through the mantle plume, resulting in nearly constant basaltic magma production and thus near constant volcanic activity [Morgan, 1972]. Kilauea volcano is contained within the Hawaii's ERZ and together this system is the most well monitored and studied volcanic region on the planet.

The ERZ has a rich eruptive history and complex surficial geology due to the frequency of its eruptions. Documented eruptions begain in 1924 with the Halema'uma'u crater eruption [USGS, 2018] and activity has continued in various locations throughout the ERZ, including the 1983 Pu'u'O'o eruption which is still ongoing today [USGS, 2019]. The most recent eruption and the focus of this study is the 2018 rift eruption and summit collapse of Kilauea in May to August of 2018.

2.1 Kilauea Volcano Activity Prior to the 2018 Eruption

Prior to the May-August 2018 eruption, Kilauea had been erupting predominantly from the Halema'uma'u crater at the summit, and the Pu'u'O'o cone and nearby vents [Neal et al., 2018]. By mid-March of 2018, tilt-meter observations showed inflation at the Pu'u'O'o cone, with continued pressurization increase through April. This pressurization caused the Pu'u'O'o lava pond to rise, eventually overflowing the summit lava lake onto the Halema'uma'u crater floor [Neal et al., 2018]. It was not until April 30 that rapidly changing geophysical data in the middle of the ERZ indicated that magmatic activity was

heading in an eastward direction toward the lower ERZ Leilani Estates area, where the first eruptive fissures would form [Neal et al., 2018].

Given that previous eruptions within the ERZ have shown increased seismic activity and fissure propagation within the active zone in the months leading up to an eruption (i.e.; the Puna district eruption in 1955) [USGS, 2018], the utilization of NDVI analyses provides an opportunistic tool for earlier detection of changes in the activity level of the volcano and to investigate any cyclicity in the activity.

2.2 Description of Field Locality

For this study, NDVI was analyzed for the 2018 Kilauea eruption at seven key areas within the ERZ (Figure 1). Areas 1 through 5 are all previously known active geothermal areas [pers. comm., C Deering]. Additionally, Areas 1 through 4 have been identified as having higher thermal activity than the majority of the ERZ [USGS, 2011]. Area 1 and 2 lie in close proximity to the Kamoamoa eruptive fissure. Area 3 lies near the Pauahi-Hi'iaka Crater. Area 4 is the well-known Puhimau geothermal feature, and Area 5 is within Leilani Estates where the first eruptive fissures formed in 2018. Areas 6 and 7 were chosen as control areas in the heavily vegetated Ohia forest, away from known geothermal activity. Both areas were chosen in order to assess overall vegetation health (Area 6), and whether a directional aspect to vegetation resurgence on the edges of the lava field was present (Area 7).

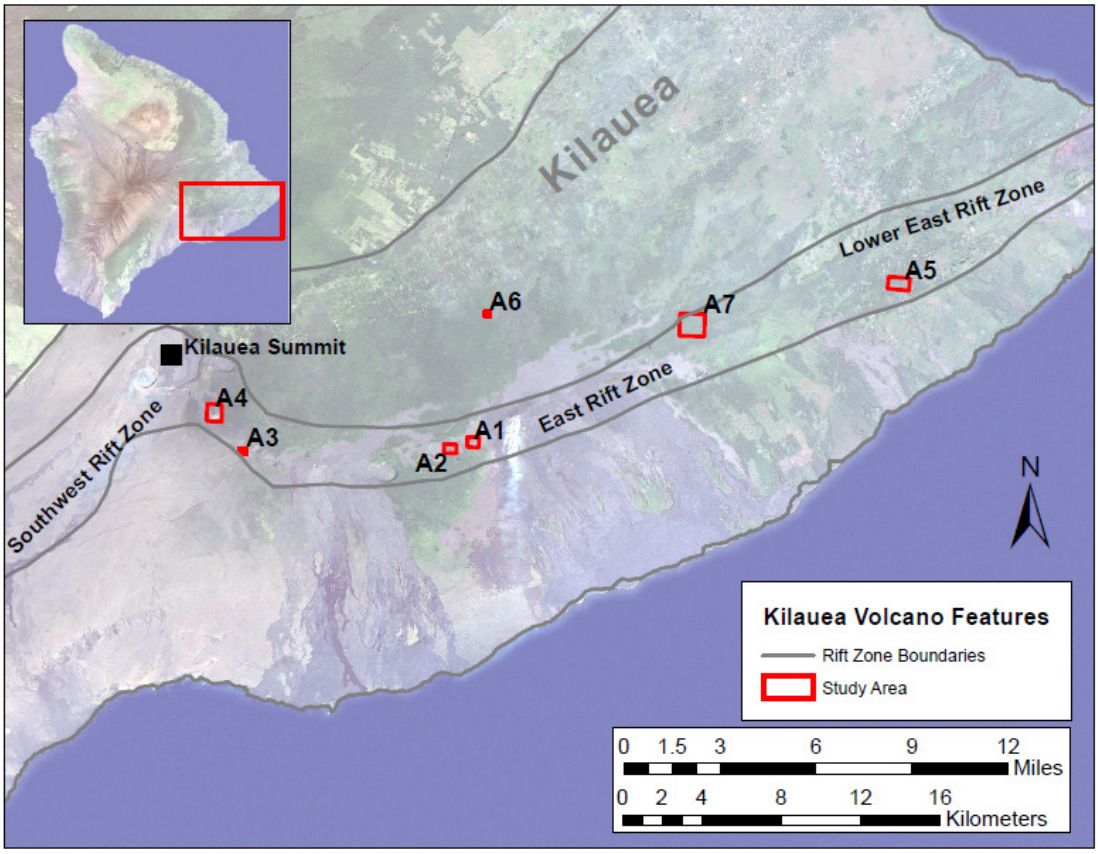

Figure 1: Location of Kilauea Volcano, Hawaii and its associated rift zones.

2.3 Description of Puhimau Geothermal Area

The Puhimau geothermal feature is thought to have formed in 1936 due to degassing from an intrusion directly below the feature [McGee et. al., 2006]. On the surface, soil temperatures have been highly elevated [McGee et. al., 2006; Torres, 2019], and the area releases anomalous amounts of CO_2, H_2S, and Mercury (Hg) compared to the surrounding region [Hinkle, 1978]. The CO_2 that is released from the feature is known to have magmatic origins [Gerlach and Taylor, 1900], and intrusive events at the Kilauea summit have been

linked with transient CO_2 measured at the Puhimau feature [Decker, 1987]. Additionally, the vegetation surrounding the Puhimau feature ranges from lichen to large Ohia trees further away from the feature, which provides an ideal setting to assess NDVI and vegetation health and extent in a single study area.

3 Methodology

A suite of high-resolution multispectral imagery was collected through a student partnership with Planet Labs, Inc. (http://www.planet.com). This imagery was used to determine if a spatiotemporal correlation existed between vegetation health in volcanic geothermal areas and volcanic unrest prior to eruption (volcanic predictors). The two main goals of this portion of the study were to: 1) ascertain if key geothermal areas within the ERZ experienced changes in vegetation health prior to the May 2018 Kilauea eruption, and 2) determine if this change (if detected) was prevalent throughout multiple study areas within the ERZ in order to determine possible related causation.

To achieve this, two analyses were performed, following a similar methodology to that outlined in Torres [2019]. The first was the application of the NDVI, and the second was land cover change detection using thematic matrix operations.

3.1 Planet Labs Imagery

The Planet Labs Cubesat constellation provides the highest rate of near-constant coverage of predetermined study areas, as it has over 130 satellites covering the entire Earth with a daily revisit time of one day at nadir [Planet Labs, 2017]. All imagery utilized were the Planet Labs Level 3A PlanetScope Analytic OrthoTile product, a 4-band multispectral image. The four bands are blue (455 – 515 nm), green (500 – 590 nm), red (590 – 670 nm), and near-infrared (NIR) (780 – 860 nm). This product is radiometrically and geometrically corrected at the time of image download. Additionally, it is orthorectified and projected to a Universal Transverse Mercator (UTM) projected coordinate system, with a spatial

resolution of 3.125 m [Planet Labs, 2017]. This product was chosen to minimize the amount of image preprocessing needed, and ensures positional and geometric accuracy for time-series imagery comparison.

A total of 50 images were downloaded for seven predetermined study areas within the ERZ of Kilauea. The first five study areas were chosen due to proximity of a geothermal feature within the ERZ (Figure 1). Area 6 and Area 7 are control areas, and not related to known geothermal activity. Area 6 is a completely vegetated area within Hawaii Volcanoes National Park. Area 7 includes vegetation and lava fields. These two control areas were included to ascertain if precipitation, temperature, or directional vegetation growth had an impact on the NDVI signature. It was thought that environmental factors may have an impact on vegetation growth, as well as the possibility for vegetation to grow in accordance to regional restrictors (e.g., older lava flow boundaries), and so these variables needed to be analyzed.

The OrthoTile images are downloaded with a data mask. Unusable pixels either contain clouds or the satellite could not gather information from a certain band [Planet Labs, 2017]. Applying a cloud mask when processing imagery is then impossible, so cloud-free imagery is necessary. Preference was given to images that shared the same acquisition dates for consistent analysis across all seven study areas. If an image of the same date could not be chosen due to cloud cover or imagery that was not as clear, the closest date to the rest of the study areas was selected. Imagery was downloaded following the tutorial provided by Planet Labs (see tutorial link in Appendix B).

3.2 Converting Analytic OrthoTile Products from TOA Radiance to Reflectance Values

All PlanetScope Analytic OrthoTile products are downloaded in units of radiance (W sr^{-1} m^{-2}). Therefore, it is necessary to convert each image to top of atmosphere (TOA) reflectance (unitless) to remove any atmospheric effects so that images can be directly compared. Planet Labs provides a Python script to aid in calculating TOA reflectance from radiance values. The script works by extracting the conversion coefficients from each spectral band, found in the associated image metadata file. It converts radiance values to reflectance via a simple scalar multiplication, where the digital number (DN) values in each band are multiplied by TOA reflectance coefficients, and writes these to new files [Planet Labs, 2017].

The current version of the script has an error writing the unscaled percentages to the output file, resulting in a completely unusable black image. As such, the Python script was modified to write correctly scaled values. This provides a valid set of values and a usable image. The output reflectance images are 32-bit float images. Links to the original Python script provided by Planet Labs, as well as the modified script, are provided in Appendix B.

3.3 Image Processing Utilizing ArcGIS

The corrected images were loaded into ArcMap 10.6. Pyramids were built for each image using nearest neighbor interpolation and default pyramid compression type. Each image was then masked (cropped using *Extract by Mask*) to the corresponding study area using the shapefile made in Mapshaper during the Planet Labs tutorial for downloading imagery

(see tutorial link in Appendix C). The *Extract by Mask* step limits the range and number of DNs in each image's histogram. See Figure 2 for this tool's input options.

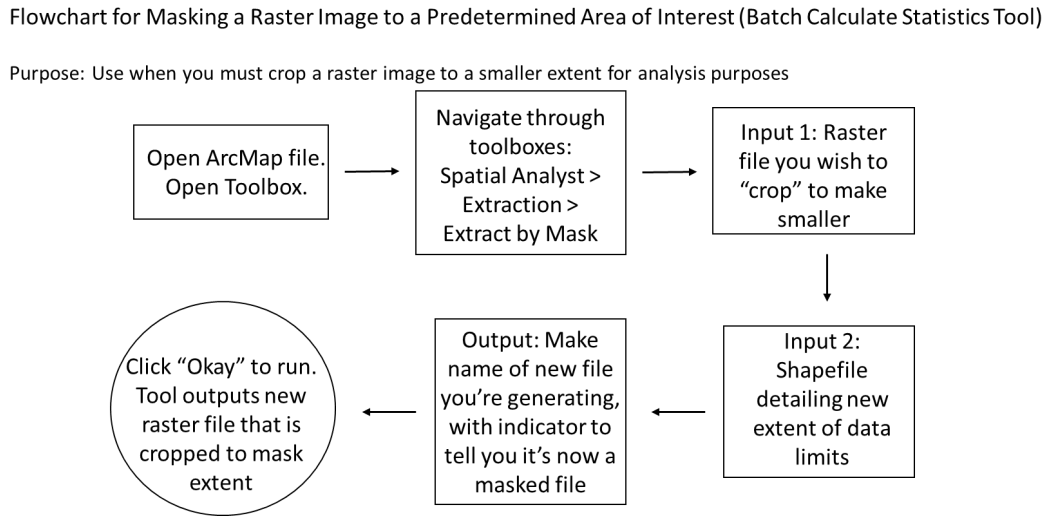

Figure 2: Flowchart for *Extract by Mask* tool in ArcGIS.

Due to a bug in ArcMap, spatial data was lost for each image after using the *Extract by Mask* tool. To rectify this, the *Define Projection* tool was used to define the projection for each image. This step should not be necessary under normal circumstances. As each study area was within the ERZ of Hawaii, the appropriate projection was WGS 1984 UTM Zone 5N. See Figure 3 for this tool's input options.

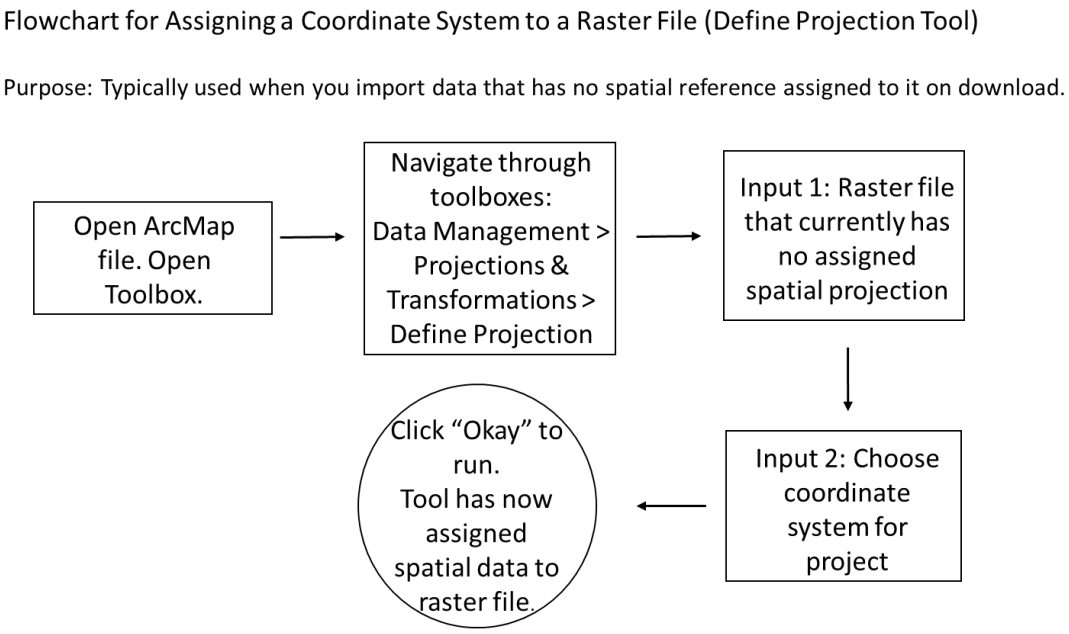

Figure 3: Flowchart for Define Projection tool in ArcGIS.

The resulting images did not have statistics, so these were calculated on the masked images using the *Batch Calculate Statistics* tool in ArcMap, keeping the tool's defaults. The lack of statistics is presumed to be resultant of the same bug in ArcMap that eliminated the image projection information. See Figure 4 for this tool's input options.

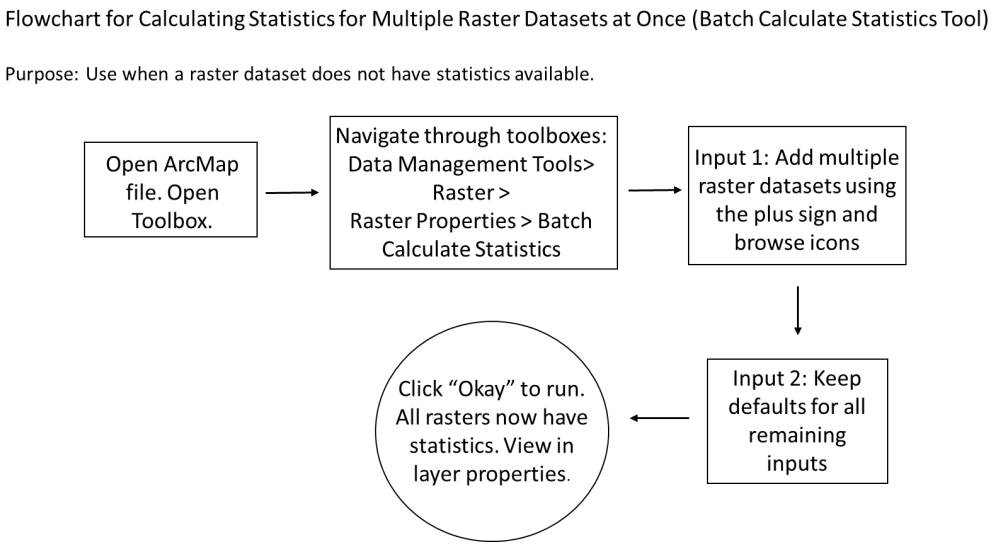

Figure 4: Flowchart for *Batch Calculate Statistics* tool in ArcGIS.

When downloading imagery from Planet Labs, there were multiple dates that required two images to be mosaicked in order to cover the entire study area. This was done in a two-step process: first, by using the *Create Mosaic Dataset* tool, and then using the *Add Rasters to Mosaic Dataset* tool. The *Create Mosaic Dataset* function simply creates an empty raster on the hard disk for the user to upload images for mosaicking. The *Add Rasters to Mosaic Dataset* tool allows the empty space to be populated with two or more rasters to make a composite image. The resulting mosaicked image was then processed through the *Extract by Mask* and *Define Projection* tools. See Figures 5 for tool input options.

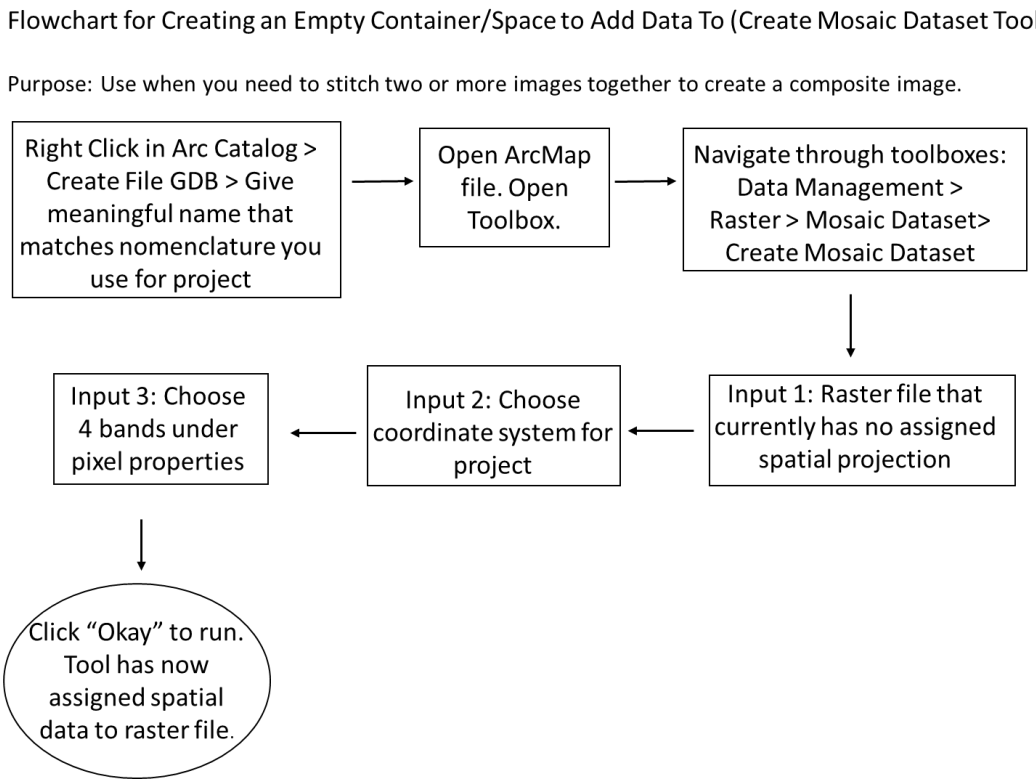

Figure 5: Flowchart for *Create Mosaic Dataset* in ArcGIS.

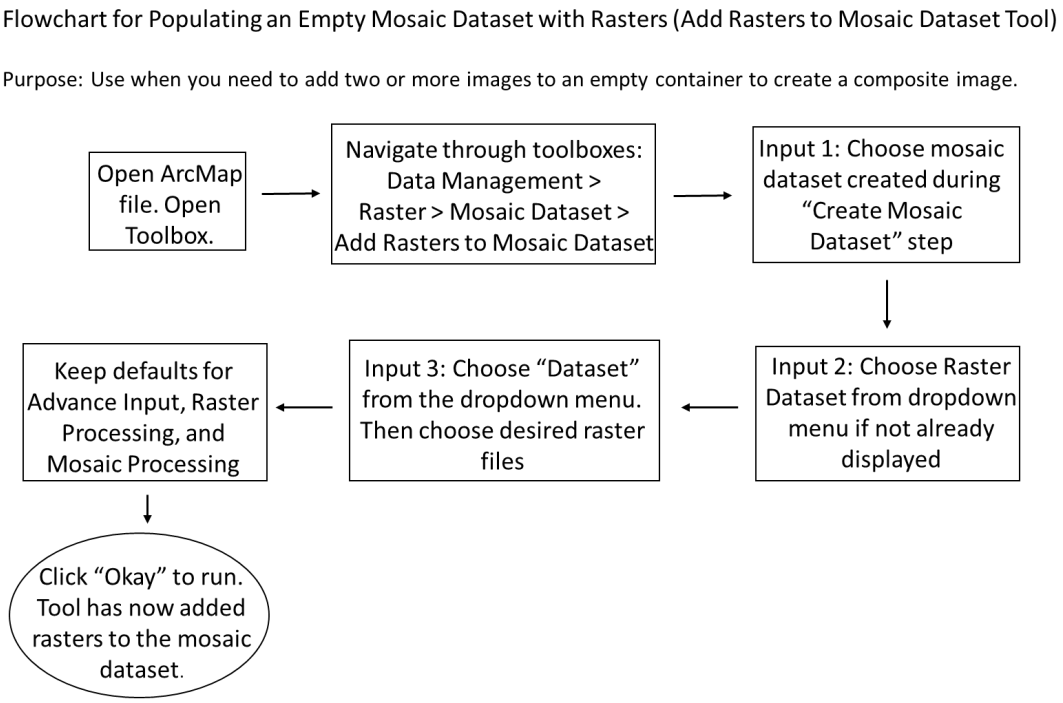

Figure 6: Flowchart for *Add Rasters to Mosaic Dataset* tool in ArcGIS.

The last image processing step in ArcMap was to resample all imagery to standardize the spatial resolution. The OrthoTile product is essentially a strip of individual scenes stitched together, and often have different pixel sizes. A majority of the downloaded imagery for this study had a spatial resolution of 3.125 m, but a few images had a pixel size of 3.0 m. Images were resampled using the *Resample* tool in ArcMap, using the tool defaults and a spatial resolution of 3.125 m. See Figure 7 for this tool's input options. The resampled files were exported as TIFF files so ERDAS Imagine 2015 could read a native file type to calculate NDVI.

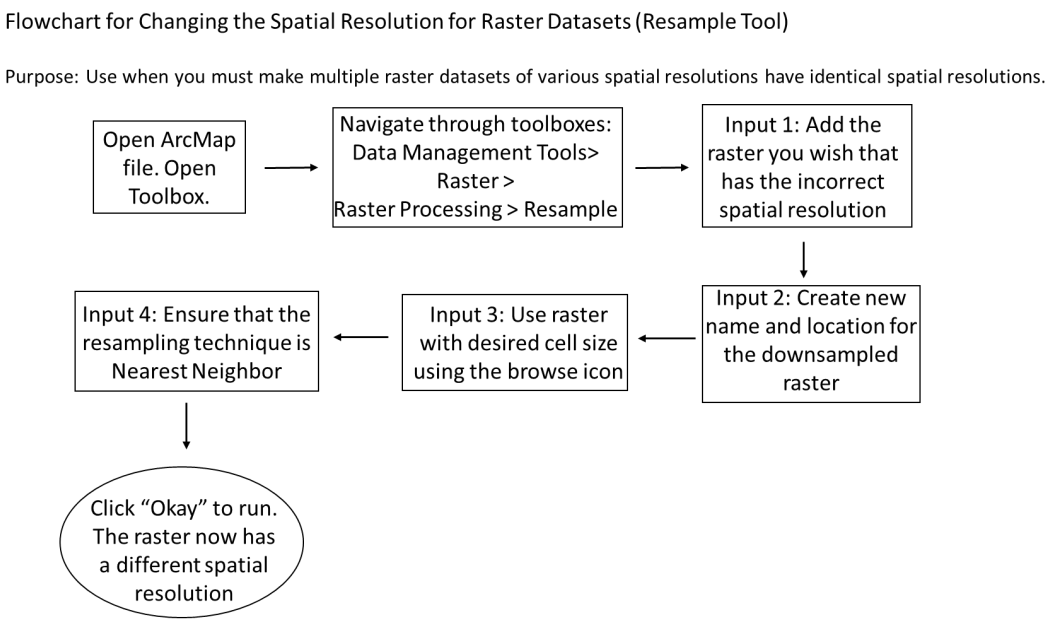

Figure 7: Flowchart for *Resample* tool in ArcGIS.

3.4 NDVI Calculation and Supervised Classification Utilizing ERDAS

After exporting each image as a TIFF file, the NDVI was calculated using ERDAS Imagine 2015 (ERDAS). The *NDVI* tool creates a composite NDVI image from the calculated ratio of the red and NIR bands of a multispectral input image. The tool provides the option to select from a common list of sensors or satellite platforms, but as the Planet Labs Cubesats were not on this list, this option was left blank. The defaults were chosen for the index options, ensuring that NDVI was selected. The tool automatically calculates DNs based on the chosen index. See Figure 8 for this tool's input options flowchart.

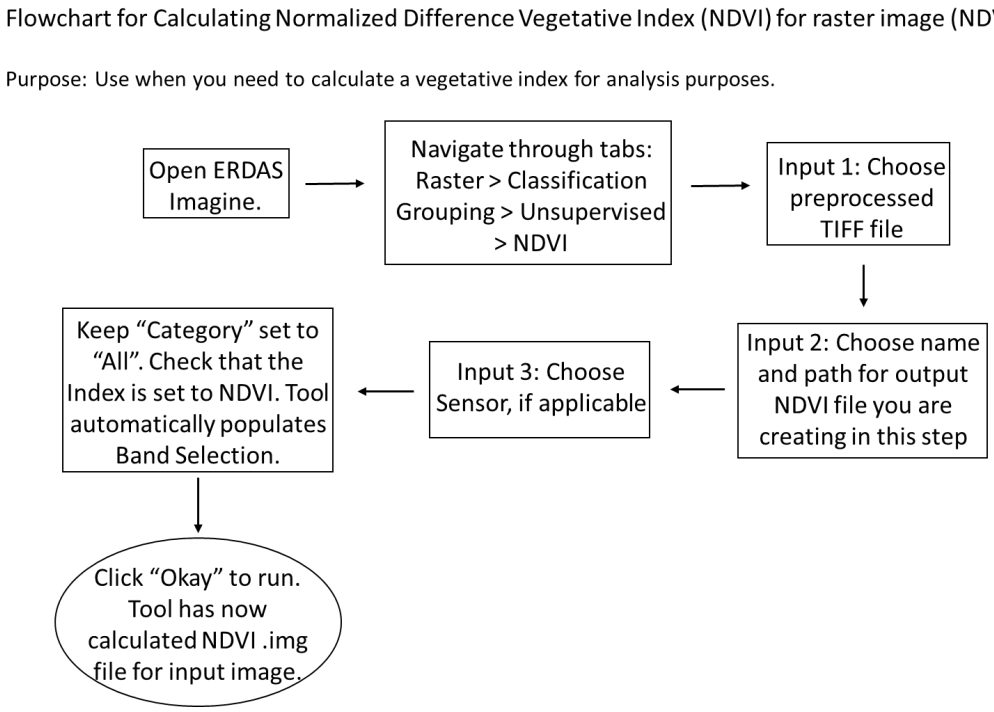

Figure 8: Flowchart for *NDVI* tool in ERDAS.

The output NDVI image file is a greyscale image. For easier interpretation of different vegetation zones and to compare change in these zones over time, a supervised classification was performed, ultimately assigning a color map to the original greyscale image. Using previous knowledge of spectral response curve values and corroboration with the study area imagery in Arc and Google Earth 3D, the generated NDVI image values were subdivided by thresholding into five vegetation information classes: non-vegetation, sparse vegetation, moderate vegetation, high vegetation, and dense vegetation. Each study site is dynamic due to weather or time of year and therefore will have slightly varying

spectral values for each of the five vegetation information classes. Mean spectral values for each study area are detailed in Table 1.

	Non Veg Mean	Sparse Veg Mean	Moderate Veg Mean	High Veg Mean	Dense Veg Mean
Area 1	0.00	0.18	0.27	0.38	0.46
Area 2	-0.02	0.14	0.21	0.33	0.44
Area 3	0.28	0.32	0.36	0.39	0.42
Area 4	0.04	0.20	0.34	0.44	0.48
Area 5	0.08	0.32	0.45	0.55	0.65
Area 6	0.40	0.44	0.46	0.48	0.50
Area 7	0.06	0.28	0.40	0.52	0.59

Table 1: Mean spectral reflectance value for each vegetation information class.

To begin the classification, the NDVI greyscale image is loaded into ERDAS. The same image, along with the resampled imagery file was loaded into ArcMap and used as a reference. Next, the signature editor was used to create thirty statistically valid training sets with a minimum of thirty pixels for each vegetation information class using the *Grow Tool*.

The *Grow Tool* allows the user to selectively click on one pixel, and the tool creates a polygon that adheres to user specified settings of spectral and spatial distances and univariate statistics. Determining settings to create an accurate classification is often an iterative process, depending on the statistical structure of the imagery and the spectral distinction between the classes. In this study, settings were refined to a neighborhood using eight surrounding pixels, but limiting to a search area of 94 meters (30 pixels), with a spectral Euclidean distance of 0.50. This essentially means that for every seed pixel, the tool looks at the eight surrounding pixels, up to 94 meters (30 pixels) away. By setting the spectral Euclidean distance to a value of 0.50, the tool does not include a pixel that has a spectral value more than half a standard deviation away from that of the seed pixel, though

it can continue to grow the polygon region until all other parameters are met. See Figure 9 for this tool's input options.

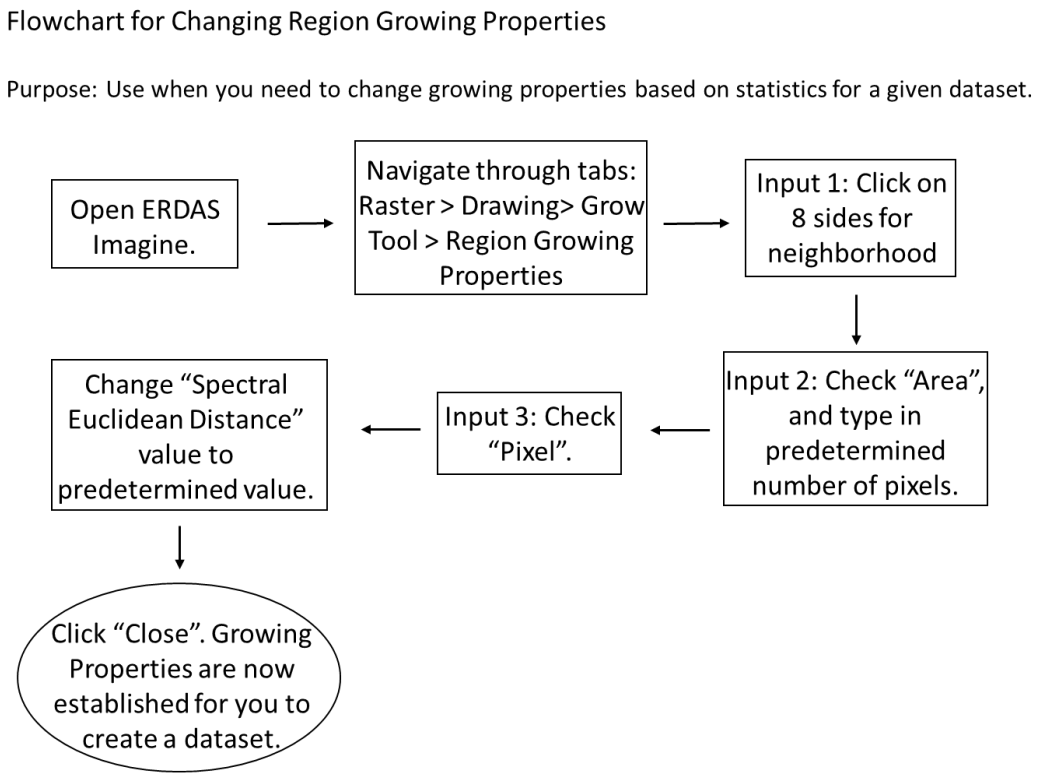

Figure 9: Flowchart for *Region Growing Properties* in ERDAS.

Thirty samples per class is deemed an appropriate number for a normal distribution [Congalton, 1957]. A total of thirty training sets for each of the five vegetation information classes is loaded into the signature editor and saved. These training sets are then condensed to five final information classes and then assigned the color map via thresholding. See Appendix D for attached tutorial on this procedure. The complete set of final classifications for each study area are smoothed and then used as the inputs for the change detection matrix.

3.5 NDVI Smoothing Algorithm Utilizing ERDAS

After generating the NDVI image and assigning the color map, each image was run through a majority smoothing algorithm in ERDAS. The smoothing algorithm reduces any data artifacts (the "salt and pepper" effect) created by the supervised classification. It also helps to create smoother boundaries between vegetation information classes, aiding in easier interpretation of spatiotemporal change.

The majority smoothing algorithm uses a neighborhood function and a 3x3 moving kernel window to move over each pixel within the image. The result is an image with smoother boundaries between vegetation classes than the original NDVI generated image. See Figure 10 for this tool's input options.

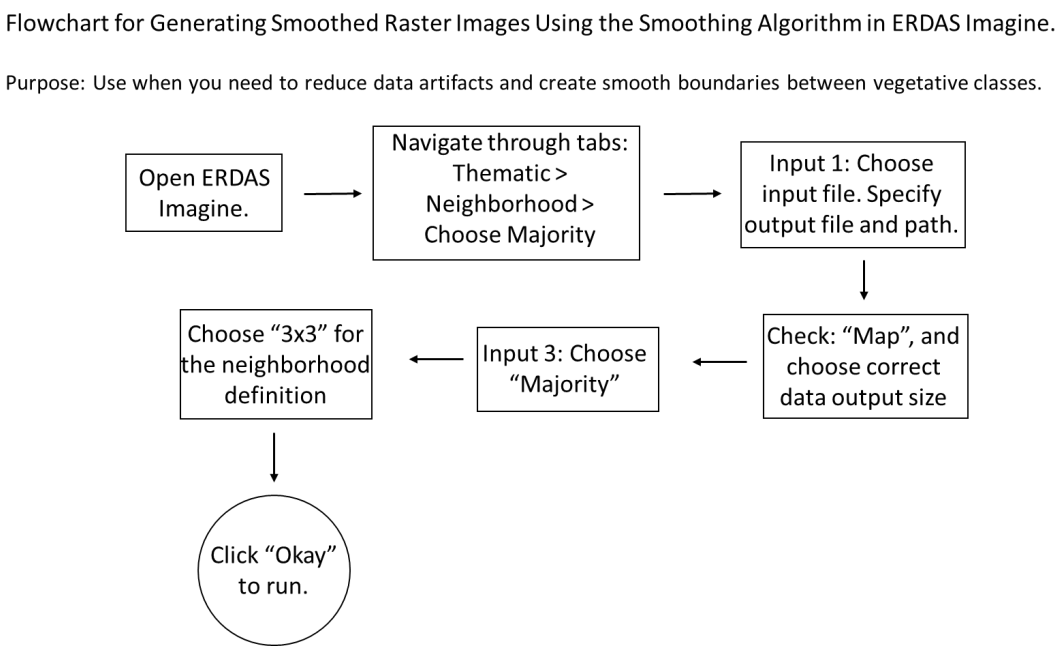

Figure 10: Flowchart for *Majority Smoothing Algorithm* in ERDAS.

3.6 Change Detection Utilizing ERDAS

The last step for image processing is to determine the amount and location of land cover change between two image dates. However, it is also imperative to know not only the proportion of change between each image, but also the classification change, or "what has changed to what". Utilizing the *Matrix Union* tool within ERDAS provides both pieces of information.

Two temporally sequential images are input into the tool, with the older image as the first input. In this study, the *Setup Recode* function was not used for the images due to the thresholding process in earlier image processing steps. By thresholding, each information class already had a set code of one through five (correlating to non-vegetation through dense vegetation, respectively), rendering the *Recode* unnecessary. The user specifies the output file name and location and ensures that the intersection box is checked. The data type for the output file must be large enough to hold the data for the new combined file (in this case, unsigned 16-bit), and the tool is run. The user can also generate a file using the *Summary Report of Matrix* tool. This file provides all of the numbers for each vegetation information class within the change detection file. See Figure 11 for this tool's input options.

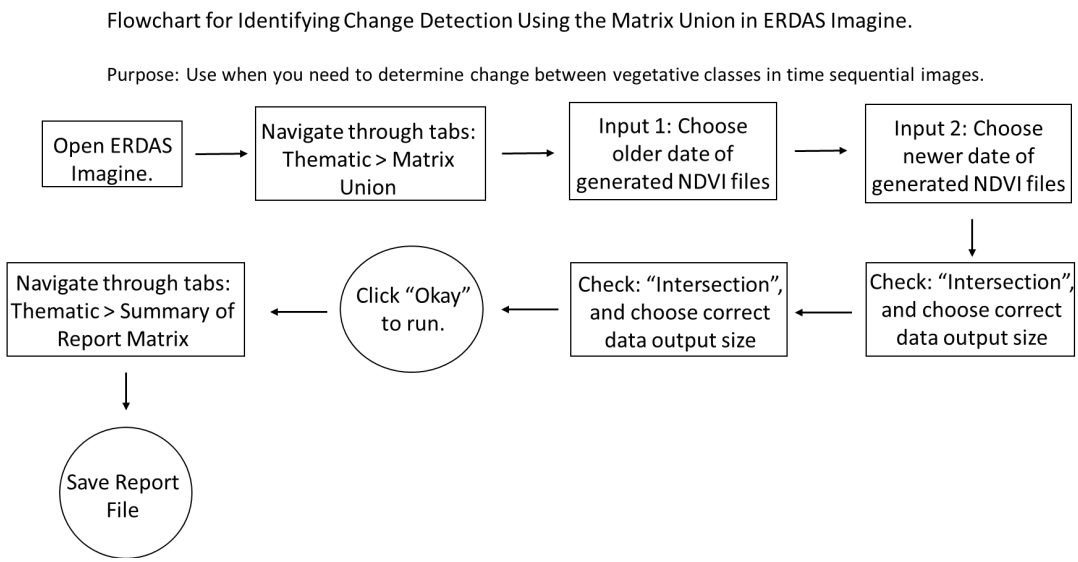

Figure 11: Flowchart for *Matrix Union* and *Summary Report* tools in ERDAS.

4 Results

4.1 NDVI Vegetation Class Derived Area

The following vegetation cover graphs show the area in hectares classified for each vegetation information class utilizing the *NDVI* tool in ERDAS. Each study area is displayed in terms of the percentage of the total study area each vegetation information class occupies.

Data were acquired for 10 of the 14 total months analyzed for Area 1. Cloud free data could not be found for May, July, October and November 2017, as well as April 2018. Area 1 covers a total of 29.88 hectares, with a small vegetated region surrounded by lava field (called a *kipuka*). While there are minor changes in vegetation cover, this study area experienced no significant vegetation change in the year prior to the eruption (Figure 12).

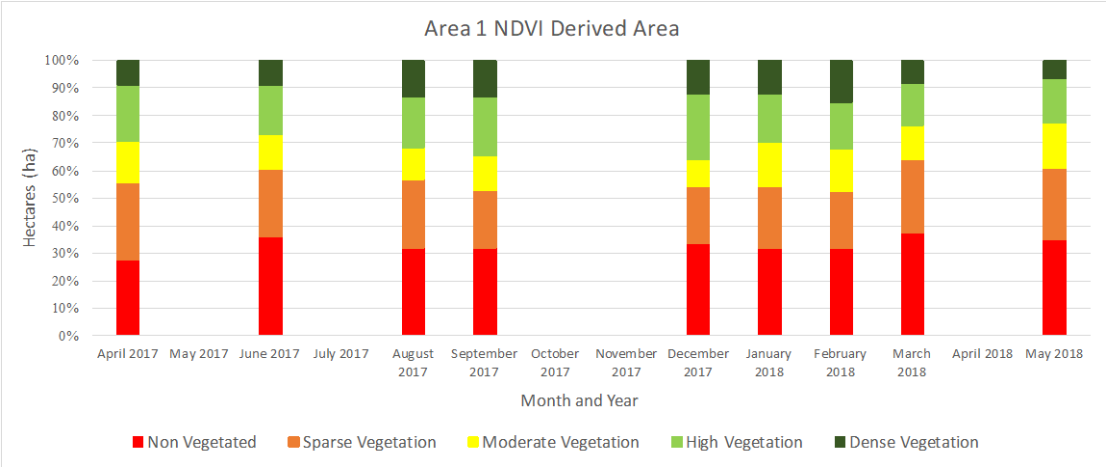

Figure 12: NDVI derived area of classes from April 2017 to May 2018 for Study Area 1.

Data were acquired for 8 of the 14 total months analyzed for Area 2. Cloud free data could not be found for May, July, October and November 2017, as well as March and April 2018.

Area 2 covers a total of 27.78 hectares, with a small vegetated region surrounded by lava field. This study area is located quite close to Area 1, and likewise experienced very little vegetation change in the year prior to the eruption. Upon cross-examination of NDVI classification images, Area 2 appears to experience fluctuation of land cover between non-vegetated and sparse vegetation classes (Figure 13). It is believed that these areas remain relatively fixed in their values and that any fluctuation is a result of the NDVI algorithm misclassifying what is actually lava flow as sparse vegetation.

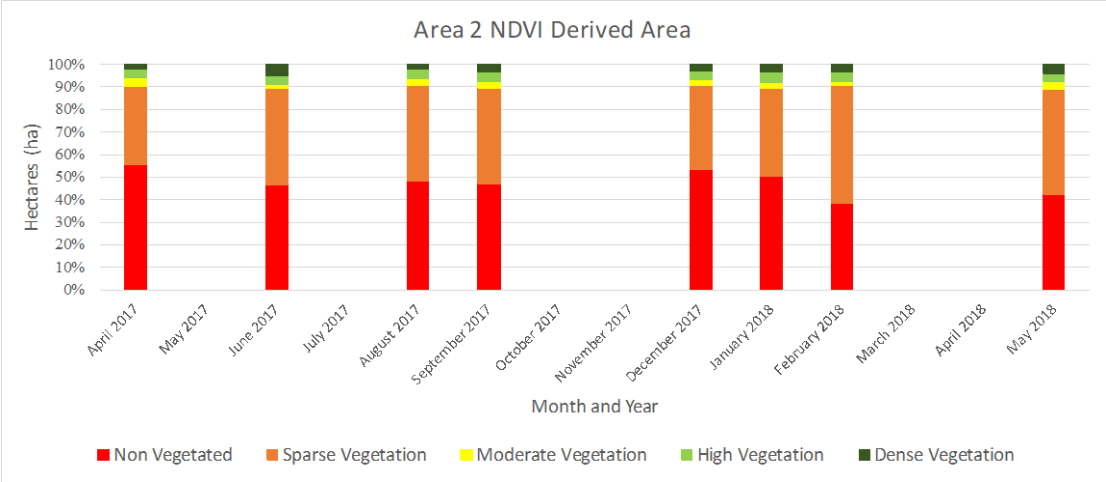

Figure 13: NDVI derived area of classes from April 2017 to May 2018 for Study Area 2.

Data were acquired for 7 of the 14 total months analyzed for Area 3. Cloud free data could not be found for May, July, October and November 2017, as well as February, March and April 2018. Area 3 covers a total of 7.88 hectares, with a small vegetated region surrounded by lava field. This study area experienced some variability in land cover change in the year prior to the eruption (Figure 14). Dense vegetation remains relatively stable, fluctuating

between 11-13% of total land cover within this study area. However, there is moderate to high variability within the sparse, moderate, and high vegetation classes.

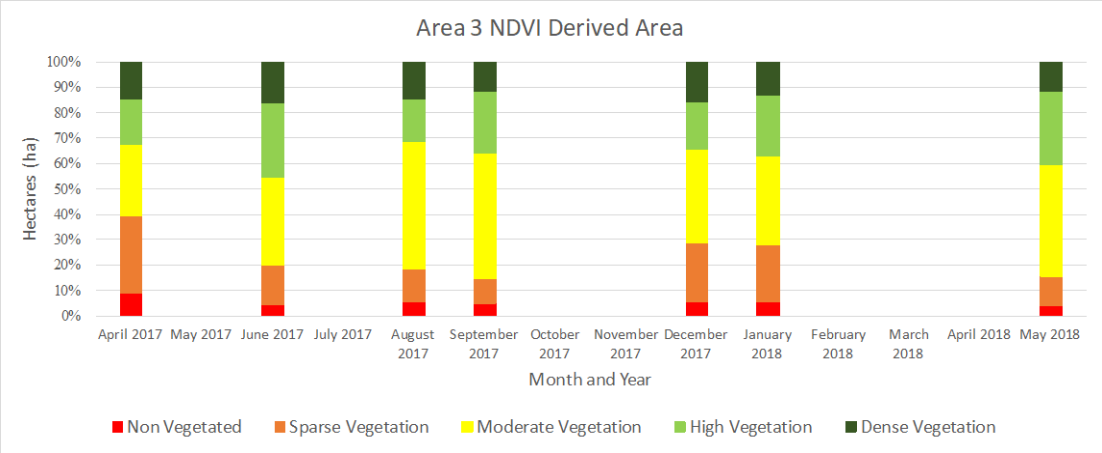

Figure 14: NDVI derived area of classes from April 2017 to May 2018 for Study Area 3.

Data were acquired for 9 of the 14 total months analyzed for Area 4. Cloud free data could not be found for May, July, October and November 2017, as well as April 2018. Area 4 covers a total of 64.33 hectares, and includes the Puhimau geothermal feature as well as a large crater in the northeast corner. This study area experienced notable variability in land cover change in the year prior to the eruption. While non-vegetation and sparse vegetation remain relatively stable, the moderate, high, and dense vegetation classes see noteworthy changes (Figure 15). The most prevalent change is the large increase in dense vegetation in May 2018, directly prior to the eruption. In May 2018, moderate and dense vegetation had increased to cover 50% of the study area.

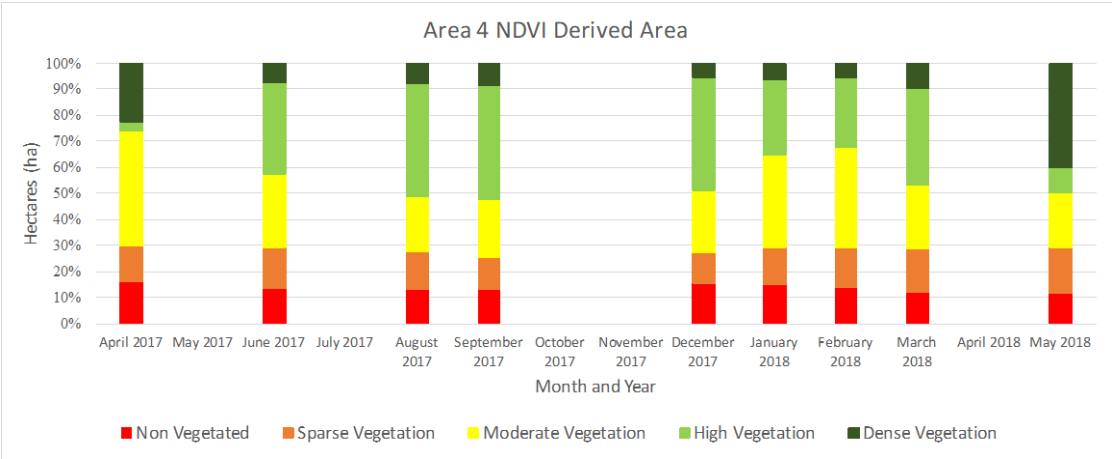

Figure 15: NDVI derived area of classes from April 2017 to May 2018 for Study Area 4.

Data were acquired for only 5 of the 14 total months analyzed for Area 5. Cloud free data could not be found for May-August and October-December 2017, as well as March and May 2018. Area 5 covers a total of 66.26 hectares, and includes Leilani Estates, dense forest, and a small area of lava field. Area 5 also experienced notable variability in land cover change in the year prior to the eruption. A year prior to the eruption (April 2017), there was a significant amount of moderate vegetation (totaling roughly 37% of the total study area). By September 2017, however, moderate vegetation comprised only 18% - effectively reduced by nearly half (Figure 16). For the remaining months prior to the 2018 eruption, high vegetation dominates in this study area. Dense vegetation also increased significantly during this time frame. In April 2017, dense vegetation only accounted for 5% of the total study area. Between September 2017 and April 2018, this percentage had risen to 13.5% and higher, nearly tripling.

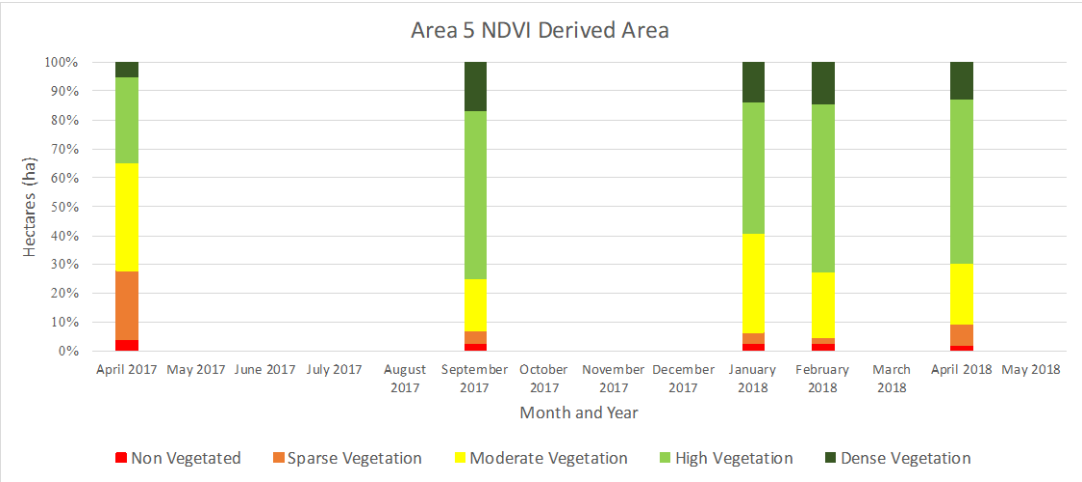

Figure 16: NDVI derived area of classes from April 2017 to May 2018 for Study Area 5.

Data were acquired for 6 of the 14 total months analyzed for Area 6. Cloud free data could not be found for May-August and October-November 2017, as well as March and April 2018. Area 6 covers a total of 5.77 hectares, and is comprised of the densely vegetated Ohia forest. This study area experienced some variability across all vegetation classes. With the exception of April 2017, non-vegetation land cover comprises less than 15% of the total study area, and sparse vegetation fluctuates between 23.5% and 34%. Moderate, high, and dense vegetation experience the least amount of variability (Figure 17).

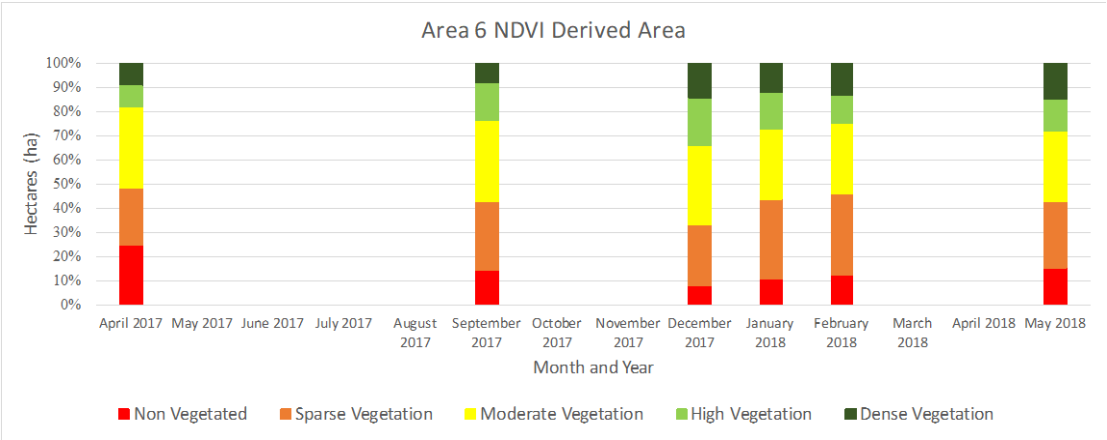

Figure 17: NDVI derived area of classes from April 2017 to May 2018 for Study Area 6.

Data were only acquired for 5 of the 14 total months analyzed for Area 7. Cloud free data could not be found for May-November 2017, as well as March 2018. Area 7 covers a total of 140.79 hectares, and is comprised of the densely vegetated Ohia forest as well as lava field. This study area experienced some variability among the moderate and high vegetation classes, while the non-, sparse, and dense vegetation classes remained very stable (Figure 18). Upon cross-examination of NDVI vegetation information class figures, this fluctuation appears to happen mainly on the edges of the lava field regions.

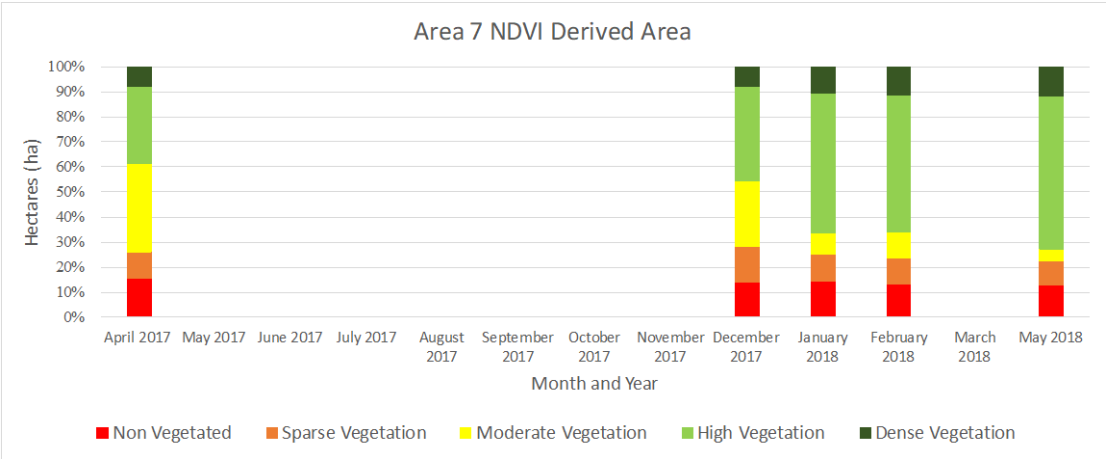

Figure 18: NDVI derived area of classes from April 2017 to May 2018 for Study Area 6.

4.2 NDVI Change Detection

Figures 19-25 show the amount of change each study area underwent between imagery dates (see original NDVI figures for each study area in Appendix A). Change is shown as significant decrease (shown as red) up through significant increase (dark green). A significant increase (dark green) means that vegetation health increased two or more classes, or that it changed to dense vegetation. Likewise, a significant decrease (red) means that vegetation health decreased two or more classes, or that it changed to non vegetation. A moderate increase (green) means that vegetation increased only one vegetation class; similarly, a moderate decrease (orange) means that vegetation decreased only one vegetative class. Yellow areas denote no change.

Area 1 (Figure 19) and Area 2 (Figure 20) display vegetation class change concentric to the vegetated region of the study area as well as change that follows lava field delineations.

The lava field change alternates between sequential images, and is attributed to misclassification of vegetation within a pixel area by the NDVI algorithm.

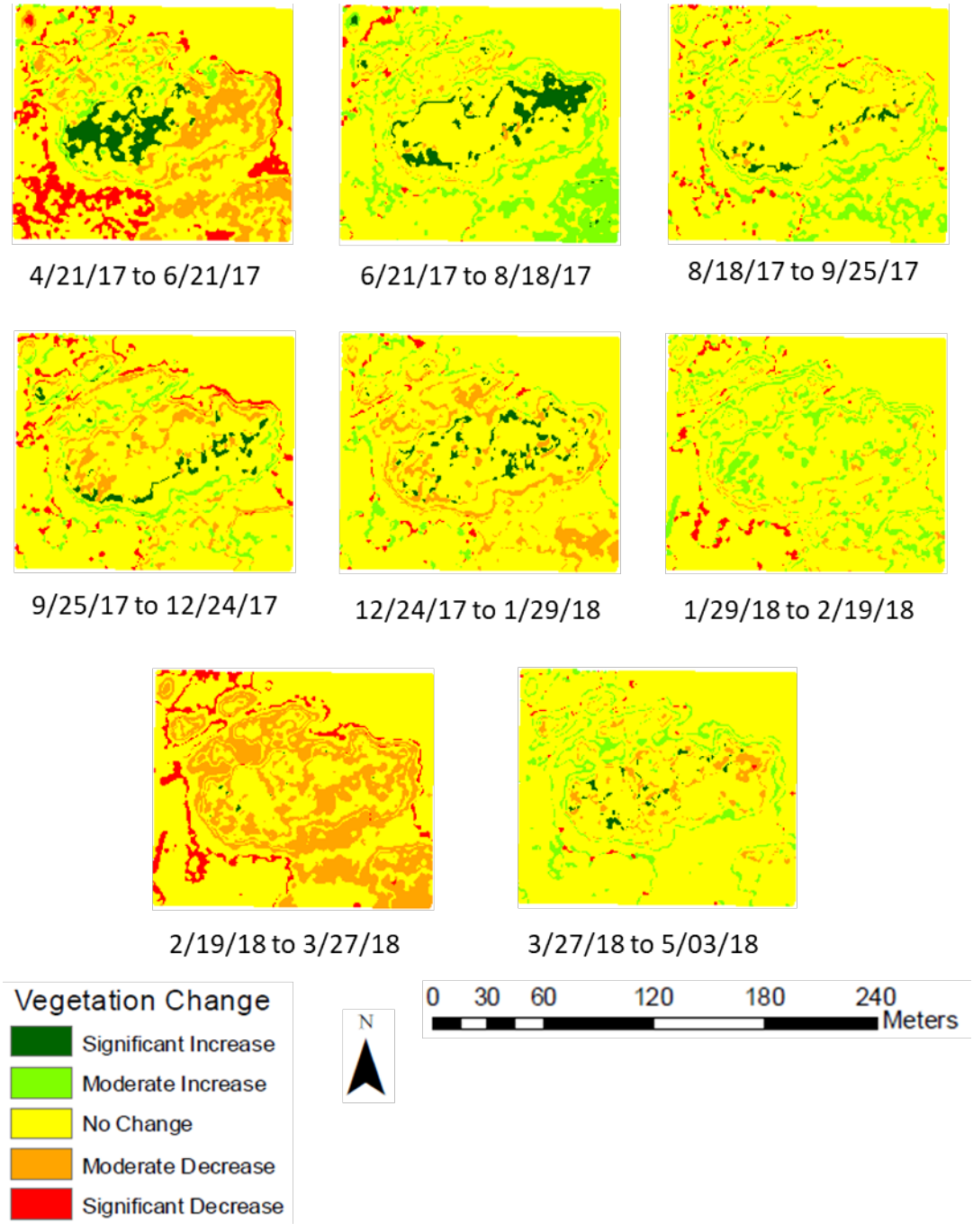

Figure 19: Map of vegetation change from April 2017 to May 2018 for Area 1.

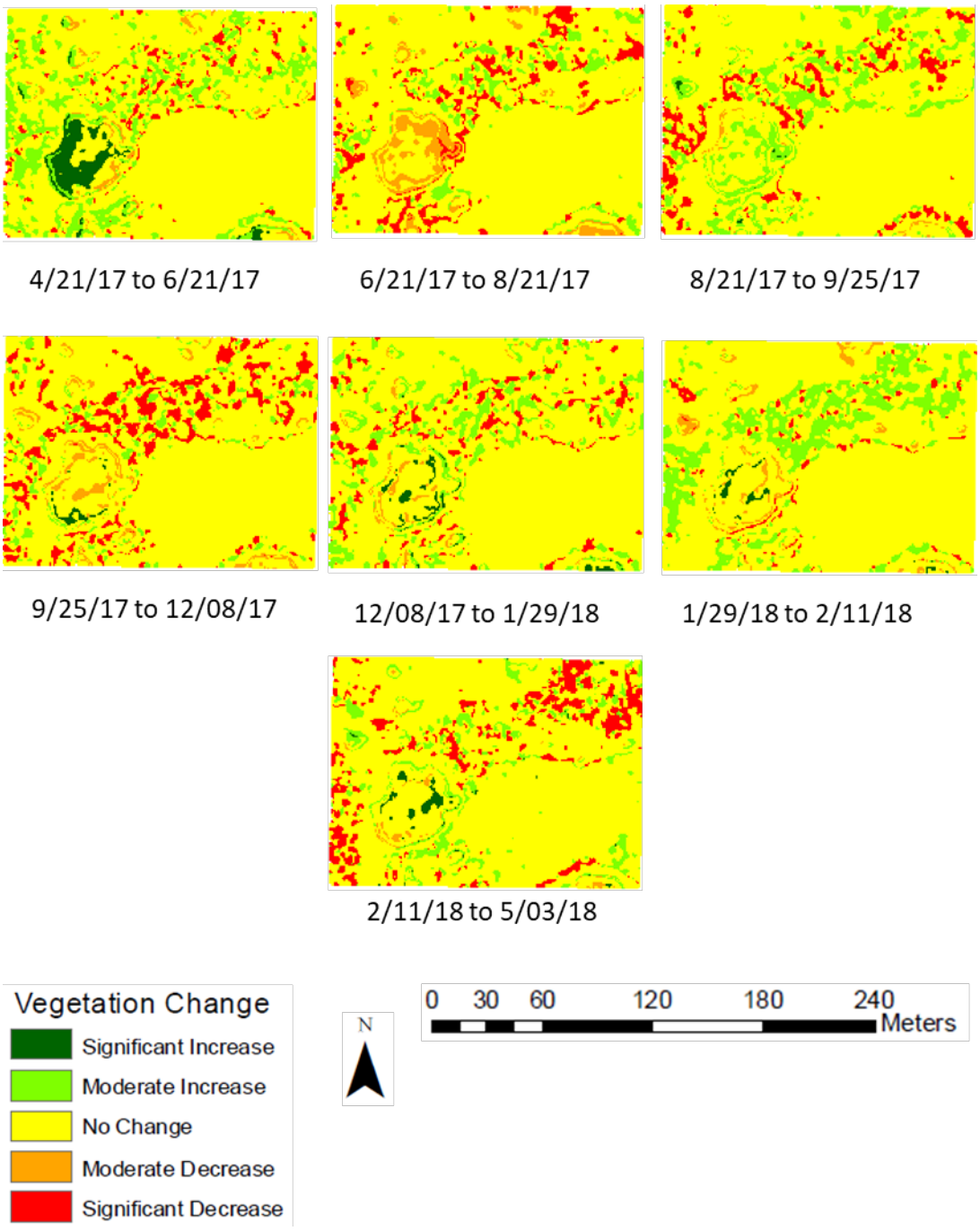

Figure 20: Map of vegetation change from April 2017 to May 2018 for Area 2.

When analyzing the change detection images for Area 3, it experiences notable change between images (Figure 21). Comparing vegetation cover in Figure 14 shows that the vegetation classes do not fluctuate significantly in their percentage of total study area. Overall, vegetation increases or decreases moderately (light green or orange, respectively) over the study time period, but very few areas experience significant change (red or dark green), nor are they spatially consistent with time.

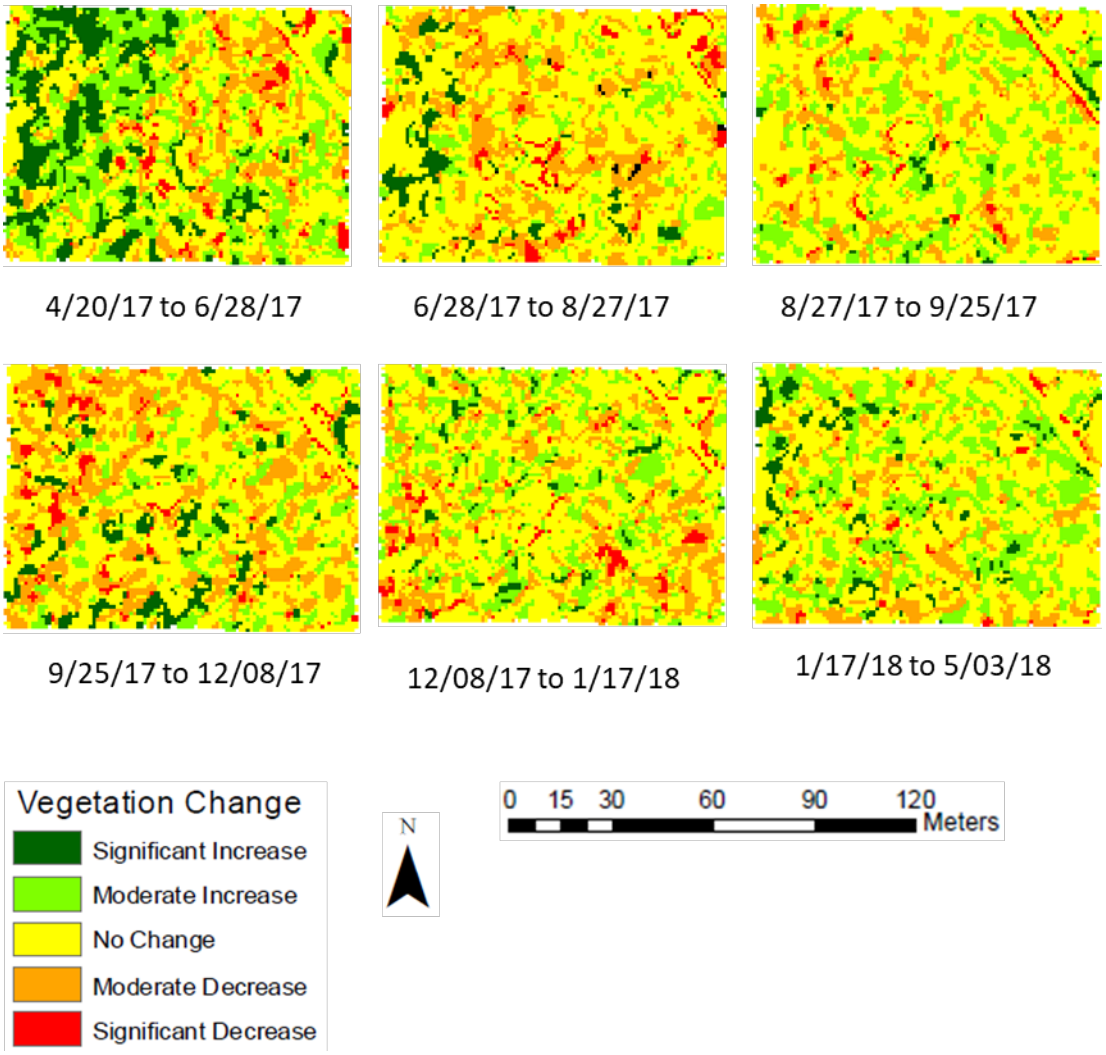

Figure 21: Map of vegetation change from April 2017 to May 2018 for Area 3.

Area 4 is also a highly vegetated area, similar to Area 3. It experiences many of the same alternating vegetation health patterns as Area 3, but there are a few key features to assess within Area 4; the first being the outline of the Puhimau geothermal feature (Figure 22). In general, the increasing and decreasing vegetation patterns of entire innermost region of the feature are quite noticeable, while the outside edges are not quite as distinct. These changes are most notable for the timespans of 4/17-6/17, 9/17-12/17, and 3/18-5/18.

The innermost region also experiences a few months (1/18-2/18 and 2/18-3/18) where the feature has increasing and decreasing NDVI in a directional aspect. The timespan of 1/18-2/18 shows that the feature has declining NDVI on the western-most portion of the inner feature, but has increasing NDVI on the middle and eastern-most portions. The next timespan (2/18-3/18) shows the reverse of this.

Additionally, the vegetated area surrounding the feature begins to experience a moderate increase in vegetation across a broad expanse of the study area beginning in the timespan of 2/18-3/18. This vegetation increase is most notably seen during the timespan of 3/18-5/18, where nearly the entire study area (that is not lava field or geothermal feature) experiences a significant vegetation increase.

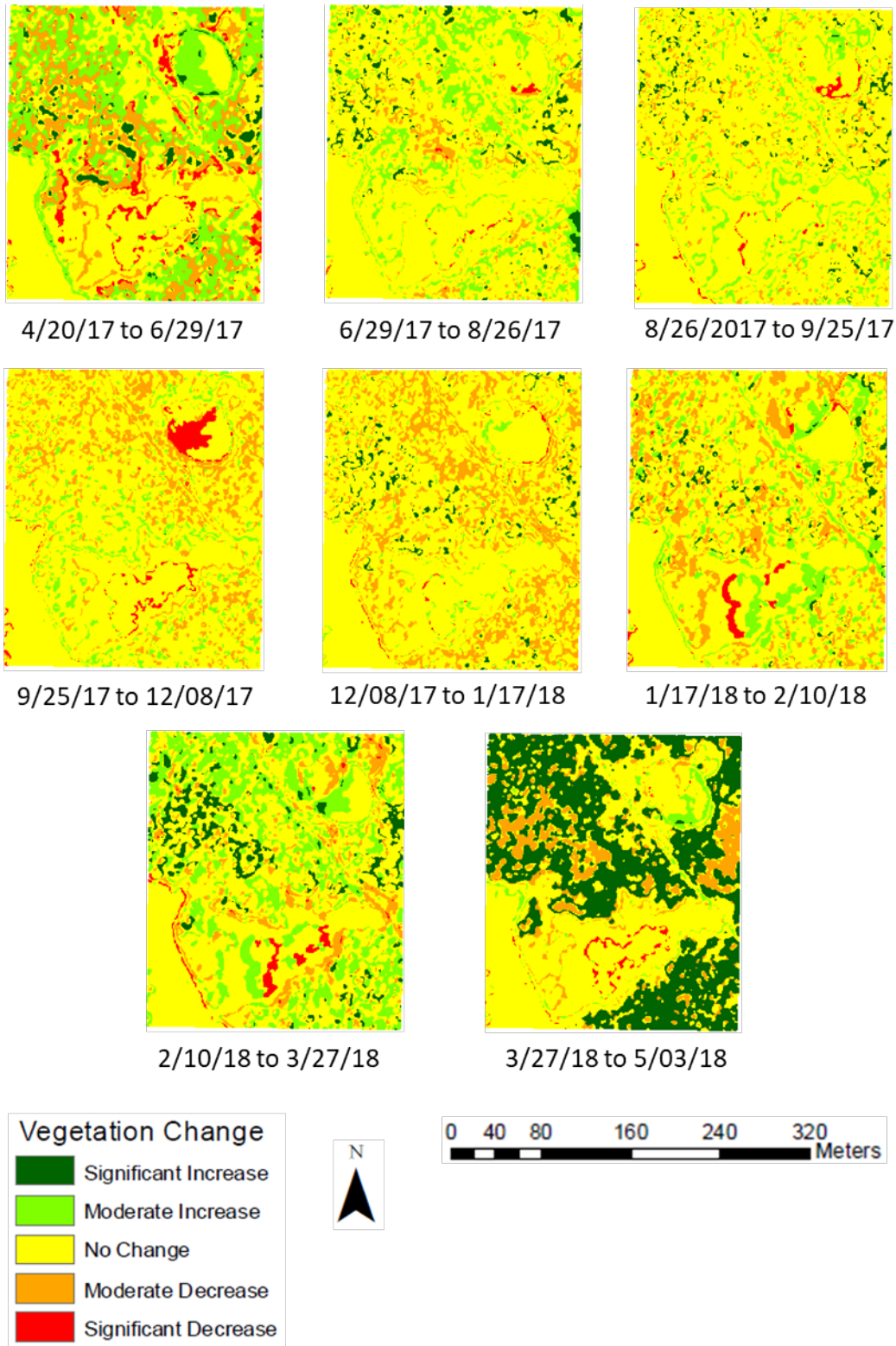

Figure 22: Map of vegetation change from April 2017 to May 2018 for Area 4.

In Figure 23, the black line in each figure panel indicates the fissures that formed during the 2018 eruption. The large time frame between the dates in the first panel of the figure below indicate that there is drastic change between the two image dates. While there is a significant vegetation change between 4/17 and 9/17, there is no cloud-free data available for this study to determine if this was gradual or not. However, for the 4/17-9/17 image, much of the lower central portion of the study area was moderate vegetation in 4/17, which had increased to high vegetation by 9/17.

This study area experienced a general decline in vegetation health during the 9/17-1/18 time period. Most notable is the general north-eastern expansion and decline in vegetation health of the lower vegetated region (see original NDVI figures for each study area in Appendix A).

After 1/18, the vegetation in Area 5 began to increase in health overall; this increase is most notable within the 2/18-4/18 panel in the figure below. Overall, the majority of the study area remains yellow (no change in vegetation health) from 2/18-4/18. There are significant increases in vegetation health in the top left area, and moderate vegetation health increases throughout the lower left to central portion of the study area.

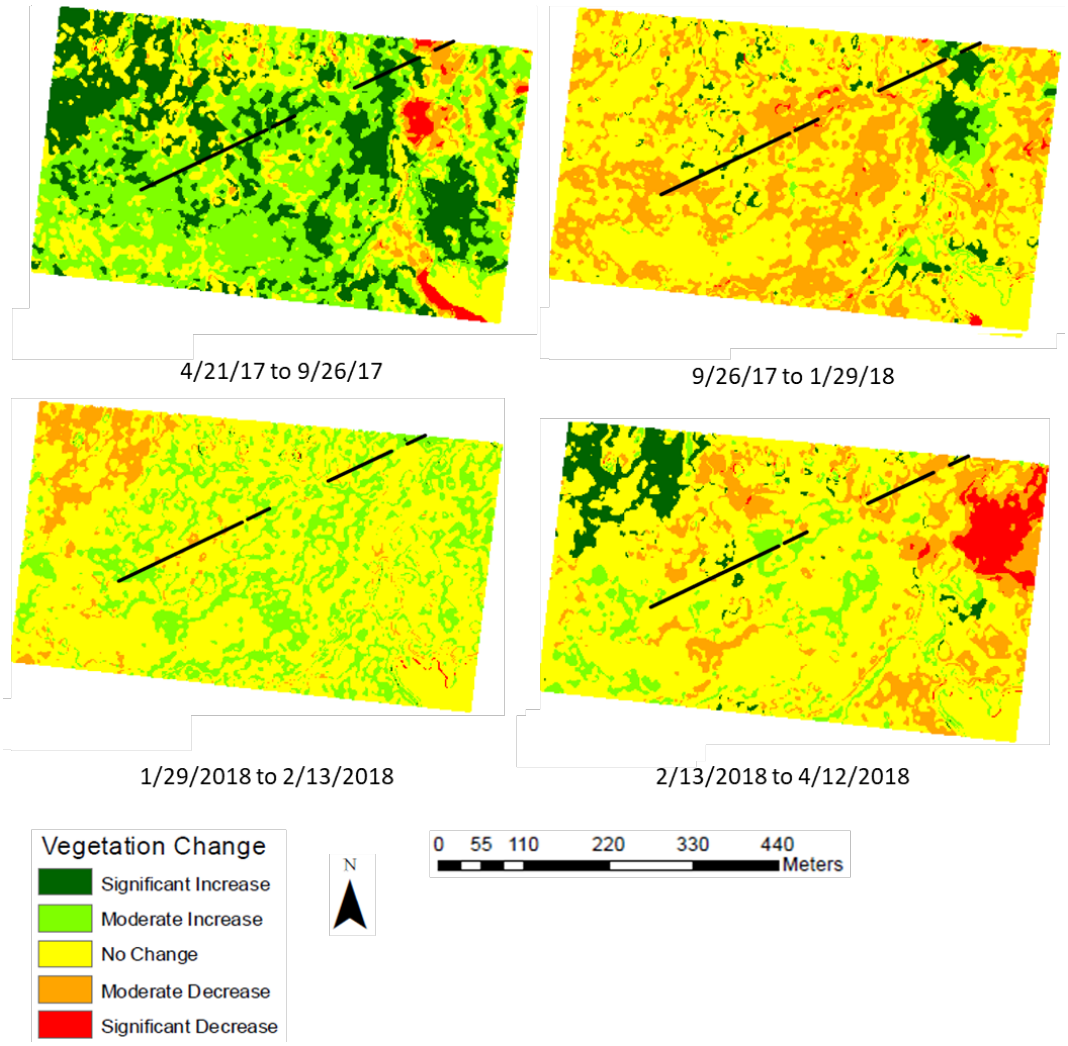

Figure 23: Map of vegetation change from April 2017 to April 2018 for Area 5.

Study Area 6 and Area 7 are densely vegetated Ohia forest, and Ohia forest with lava field, respectively. Area 6 experiences vegetation health flux much like Area 3, and is not deemed significant in respect to the overall percentage that each vegetation class covers over the duration of the study time period (Figure 24). Vegetation health for Area 7 is relatively stable, with a moderate increase in health for the 12/17-1/18 time period (Figure 25).

Alternating health and decline of vegetation along lava field boundaries is seen throughout each panel.

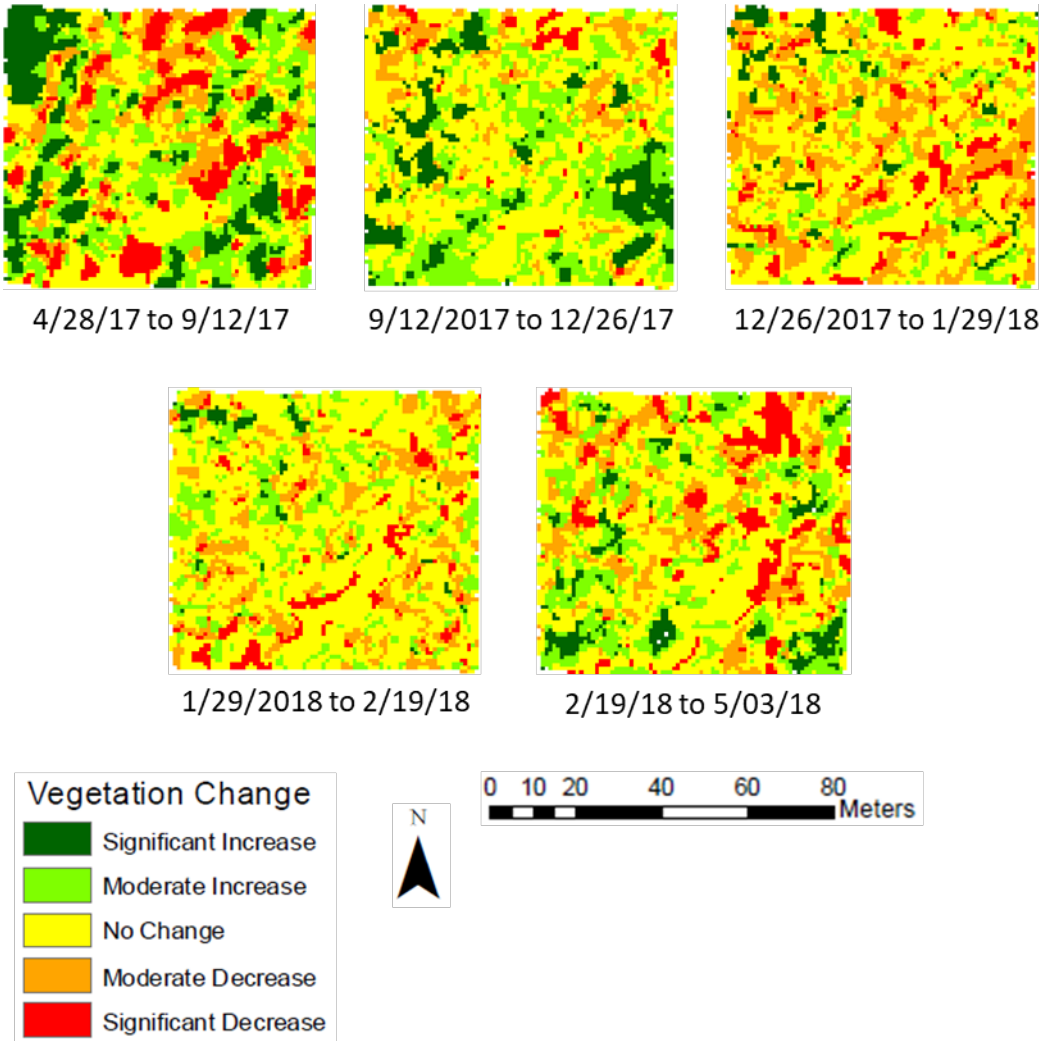

Figure 24: Map of vegetation change from April 2017 to May 2018 for Area 6.

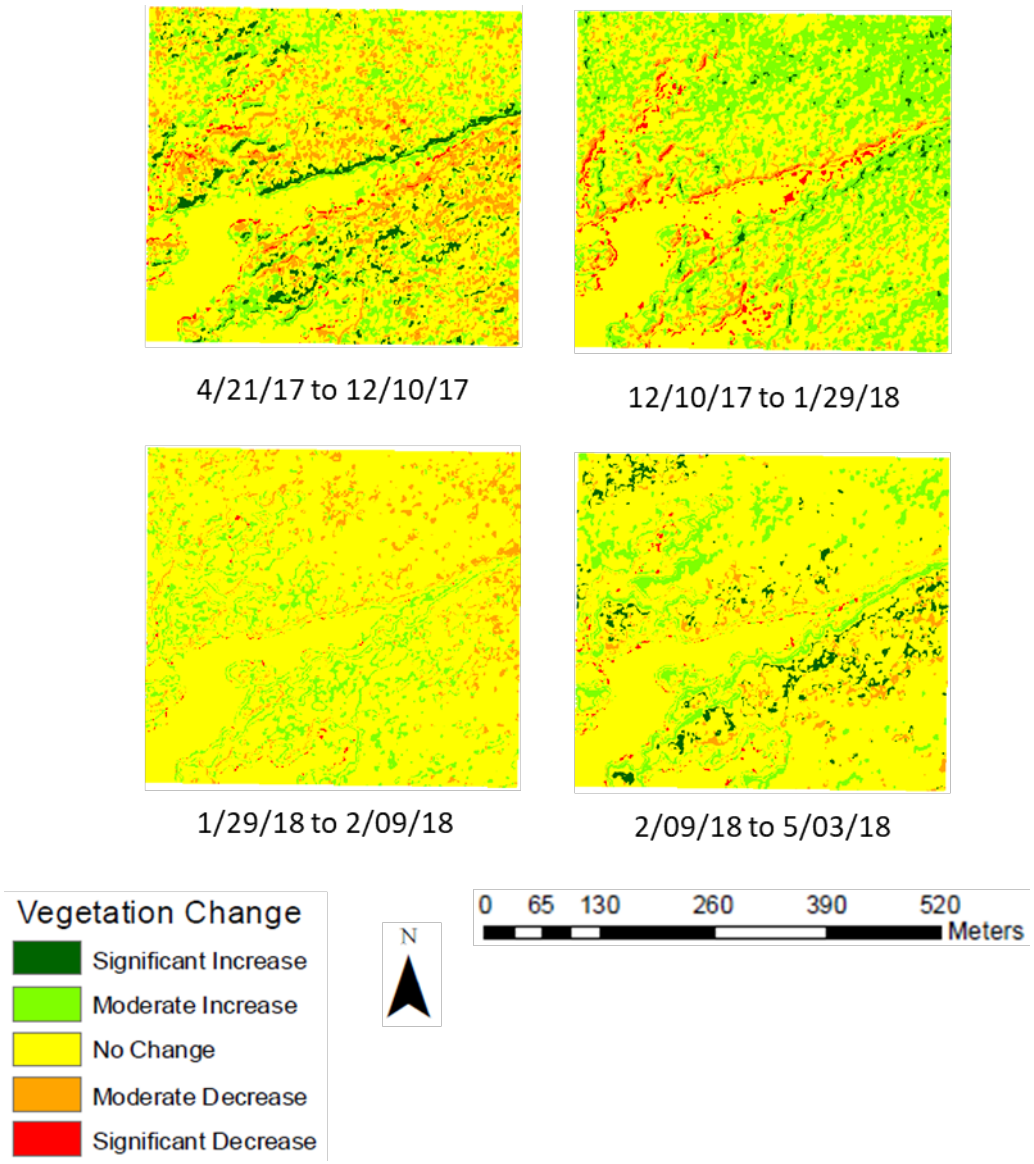

Figure 25: Map of vegetation change from April 2017 to May 2018 for Area 7.

5 Analysis and Discussion

There are a number of factors that can affect vegetation health: air temperature, precipitation, soil temperature and acidity, and soil composition, though the most probable of these is changes in precipitation and temperature [Andronico et. al., 2005; Aiuppa et. al, 2007; Shinohara, 2008]. Invasive species and disease can also affect vegetation health; since 2010 the most common fungal pathogen affecting Hawaii today is the fungus *Ceratocystis*, more commonly known as Rapid Ohia Death (ROD) [Asner et. al., 2018]. While the fungus has primarily invaded the outer edges of the Big Island of Hawaii, the fungus has spread inland since 2015 affecting regions near Areas 3, 4, and 6 of this study [ROD, 2019]. Though there have been confirmed locations of ROD within the ERZ since 2017, the presumed associated vegetation health decline is not prevalent throughout the study areas. In fact, the opposite effect is seen, thus leading to the exploration of other environmental factors to explain a change in vegetation health such as temperature and precipitation.

5.1 Temperature and Precipitation

Weather data was obtained from the Weather Underground (Wunderground) website (https://www.wunderground.com) for the year leading up to the 2018 eruption. Data were obtained from this organization instead of nationally-recognized weather organizations because Wunderground incorporates citizen science stations into its database, which increases the number of weather stations available for study. Due to these additional stations, Wunderground has a more complete weather record at numerous stations compared to the one regional national organization weather station. This was important to

ensure that we were capturing data from an area as close to the study locations as possible given the high variability in local weather patterns. Temperature and precipitation measurements were obtained from the Volcano Village weather station, which is located nearest to the Kilauea summit and Area 4.

Average precipitation between April and September 2017 was on the lower end for precipitation in the year leading up to the eruption (between 5.0 and 20.0 cm per month). The average precipitation for this time period was 23.0 cm in 2016, but only 10.6 cm in 2017. Precipitation increased in October and November 2017, to roughly 44.0 and 61.4 cm, respectively. Precipitation values then decreased overall between January and May 2018, with notable increases in February and April 2018 (46.6 and 39.8 cm, respectively (Figure 26)).

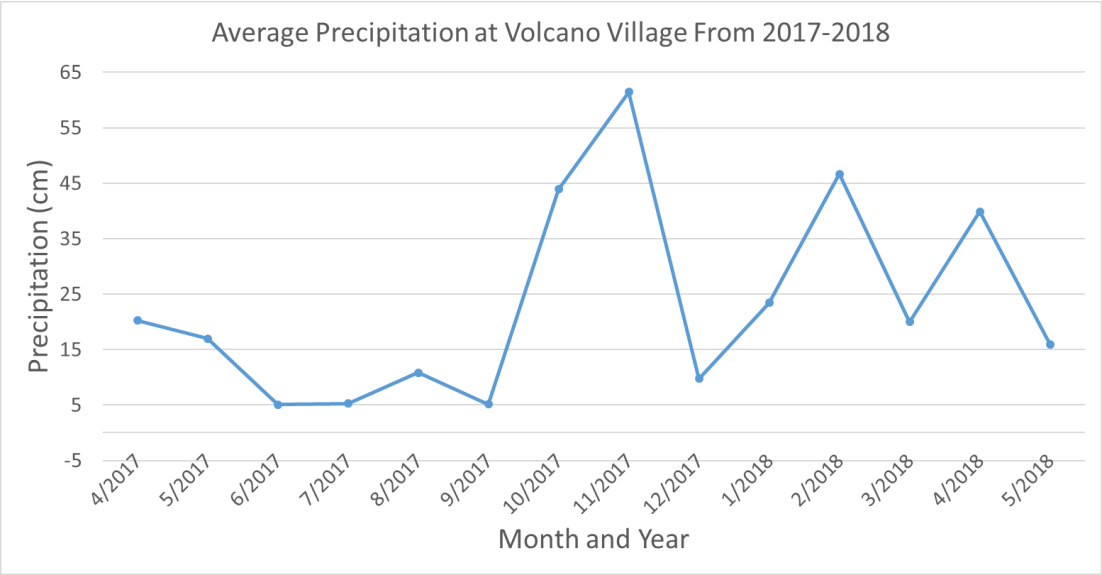

Figure 26: 2017-2018 Precipitation monthly average at Volcano Village weather station.

Temperatures for the year prior to the eruption averaged between 14.0°C and 17.8°C (Figure 27). During April and October 2017, the average temperature deviated very little, remaining between 16.3°C and 17.2°C. For November and December 2017, temperatures declined, averaging 15.4°C and 14.0°C, respectively. Temperatures began to steadily increase from January 2018, with an exception of March 2018, which averaged 14.4°C.

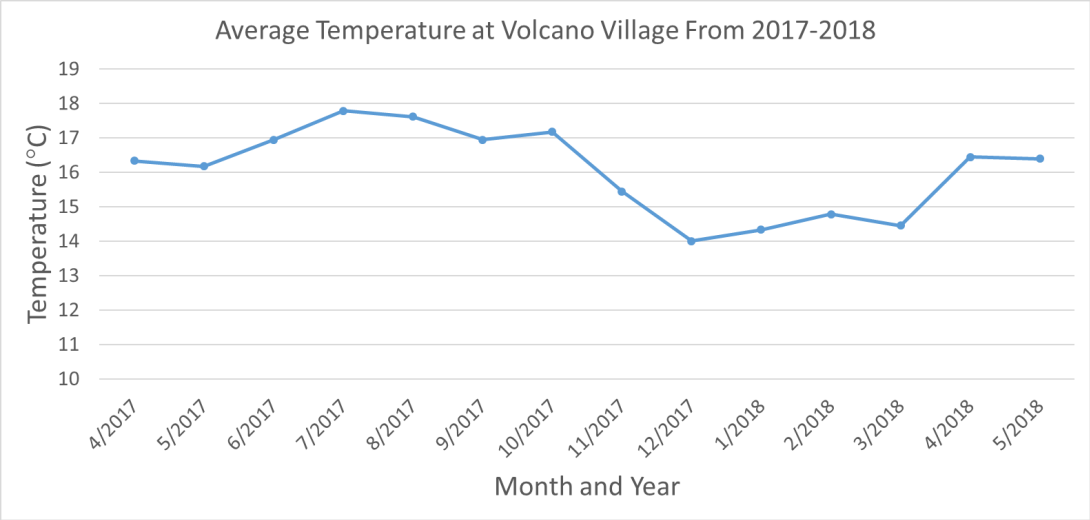

Figure 27: 2017-2018 Temperature monthly average at Volcano Village weather station.

Neither temperature nor precipitation appear to be correlated with vegetation health. Though April to September 2017 have higher temperatures, and November 2017 to February 2018 experience lower temperatures, there is no apparent correlation with change in vegetation health for all study areas during these time periods. There also doesn't appear to be a correlation between the amount of precipitation and changes in the extent of vegetation change across all study areas.

5.2 Analysis of Areas 1, 2, and 3

There does not appear to be a significant change in vegetation extent in Areas 1, 2, and 3 during the year prior to the 2018 Kilauea eruption based on the NDVI vegetation class derived area and the change detection images (Figures 28-76). The largest vegetation change seen in Areas 1 and 2 was a flux between the non vegetation and sparse vegetation classes. This is interpreted to be due largely to misclassification by the NDVI algorithm of a region primarily consisting of lava flows. However, there are a few shrubs that reside on the lava flows, and their spectral response can cause the NDVI algorithm to misclassify the pixel area from non-vegetation to sparse vegetation. This variable class designation is most commonly seen in the change detection images, where alternating decreases and increases in vegetation follow the known lava field delineations.

Within Area 3, dense and non-vegetation percentages remain relatively stable, while the greatest vegetation is within the moderate vegetation class. However, this area was a geothermal area of interest in previous degassing work (pers. comm., C. Deering). It is interesting that Area 3 displays a potential geothermal feature within the central to southwestern portion of study area. Though surrounding vegetation does not appear to trend towards the positive or negative, this small region of non to sparse vegetation maintains its shape integrity and profile for the duration of the study period.

5.3 Analysis of Areas 4 and 5

Due to past known correlation with summit activity and intrusive events, the Puhimau feature was targeted as an important study area for this research. It has been previously

described as a potential "window into the ERZ," both due to its close proximity to Kilauea's summit and degassing activity that coincides with intrusive events, as discussed earlier [McGee et. al, 2006]. Therefore, it was hypothesized that there might be a strong elevated NDVI signature in this study area prior to the eruption.

A significant change was indeed seen in Areas 4 and 5 in the year leading up to the 2018 eruption. Comparison of the Puhimau feature and surrounding vegetation (Area 4) between 4/17 and 5/18 shows a stark change from predominantly moderate to high vegetation to predominantly high to dense vegetation a year later (Appendix A: Figures 52 and 60). Area 5 displays this same "greening up" effect and is most obvious when comparing images from 4/17 and 4/18 (Appendix A: Figures 61 and 65). The roughly one-year difference in both of these study areas cannot be attributed to seasonal variation or climate factors, such as temperature and precipitation. Previous studies have also ruled out temperature and precipitation as factors for changing NDVI signatures [Seiler, 2017].

5.3.1 Area 4 (Puhimau) Analysis

There are a few key features of interest within the Puhimau geothermal area. The first is the apparent growth and shrinking patterns of the Puhimau feature. As discussed earlier, there is an "inner" feature of Puhimau, denoted by the non-vegetation class (colored red), as well as an "outer" feature, denoted by the sparse vegetation class (orange). This fluctuation can be seen in nearly all NDVI generated images for the duration of images analyzed for this study.

Two distinct “horns” appear in the outer Puhimau feature over the duration of the study in the top northwest and northeastern sides of the feature. Both of these micro features are due to declining vegetation health, and thus the growth of the outermost Puhimau feature. Additionally, the continued eastward migration of sparse vegetation land cover across the Chain of Craters Road was seen on the eastern side of the entire feature; this growth was described as “probable” in previous work [McGee et. al., 2006], but is certainly seen within this study.

Previous studies of the Puhimau feature have hypothesized that there are cryptic structural faults underlying the Puhimau feature based on degassing measurements. The known flux of CO_2 and H_2S can be interpreted as a NE-SW trending fault/fracture (due to CO_2 flux) and two roughly N-S trending faults/fractures (due to H_2S flux) [Torres, 2019]. Though degassing measurements were not obtained for this study, the fluctuation in the innermost and outer Puhimau feature support the hypothesis of cryptic structural faults at this location. Additionally, the alternating decrease and increase of vegetation health seen in the 1/18-2/18 and 2/18-3/18 change detection images (Figure 22) suggest that there is directional degassing occurring in the Puhimau feature along these potential faults during early 2018, directly prior to the eruption. There also appears to be an additional fault/fracture on the western edge of the Puhimau feature that also trends roughly N-S. These directional changes lead us to believe that gases are being exsolved at shallow depths from new potential cryptic structural faults that lie below the Puhimau geothermal feature.

5.3.2 Area 5 (Leilani Estates) Analysis

Leilani Estates (Area 5) also has a few key areas of interest within the year leading up to the eruption. As mentioned previously, analysis of the NDVI land cover classifications for April 2017 and April 2018 shows a dramatic difference in one year for healthy vegetation. This change is predominantly seen in what is known to be Ohia forest. Vegetation occupying the central portion of the study area experiences a marked increase to dense vegetation in the months prior to the 2018 eruption. Increased vegetation health is first seen in January 2018, with increasing coverage until April 2018.

The second notable feature within Area 5 is a small area along the upper northeastern portion of the eruption fissure. In contrast to the vegetation health increase in the central portion of the study area, this is a localized area of moderate to sparse vegetation. This area maintains its size and dimensions from September 2017 onward; from January to April 2018, however, the extent of moderate vegetation cover within this small feature decreases and sparse vegetation becomes more prominent. What is truly interesting is that the spatial extent of the increasing sparse vegetation is perpendicular to the eruption fissure at this location, and is the location of a wider fissure eruption (Fissure 12: https://volcanoes.usgs.gov/volcanoes/kilauea/multimedia_maps.html) during the May-August 2018 eruption.

5.4 Analysis of Areas 6 and 7

As discussed previously, Areas 6 and 7 do not experience significant vegetation change in terms of eruption predictor behavior. The change in vegetation health and extent can, however, be explained by environmental factors. Area 6 is located fairly close to areas that

were identified in 2017 to be affected by Rapid Ohia Death (ROD), a fungal infection that is affecting the Ohia forest on all Hawaiian Islands, effectively killing large portions of the Ohia forest.

Area 7 experienced vegetation fluctuation primarily around the lava field boundaries. Vegetation health and decline in these regions of the study area are likely related to vegetation rebound and retreat around lava field boundaries. We propose that vegetation can resurge along lava field boundaries, but also be quickly killed off due to the amount of heat emanating from the lava field. Lava fields can also act as a trench for water after rainfall events, which can enhance the spectral signature seen in the data imagery (pers. comm., C. Deering).

6 General Discussion

Seven study areas (including two control areas) were analyzed using ArcGIS and ERDAS Imagine to ascertain if the NDVI and land cover change detection can aid in identifying pre-eruptive behavior through the study of vegetation spectral signatures. Environmental factors such as temperature, precipitation, seasonal vegetation variability, and ROD were assessed and eliminated as possible reasons for the observed enhanced spectral response in vegetation. These findings direct us to investigating magmatic/volcanic factors that might instead explain vegetation change.

Of the five comparison study areas analyzed (excluding the two control areas) for the year leading up to the May-August 2018 Kilauea eruption, two (Areas 4 and 5) show changes in their spectral response beginning in January 2018 and the ensuing months leading up to the eruption that are attributed to pre-eruptive volcanic behavior changes. These two areas are therefore most likely to aid in determining pre-eruptive behavior for active, vegetated volcanic regions due to their enhanced spectral response just prior to the eruption, and are the focus of this general discussion.

It is known that plant growth, health, and extent are directly affected by CO_2 flux, and past experiments have shown plant response to elevated CO_2 flux [Drake et. al., 1997; Norby et. al., 2016]. These findings support the CO_2 fertilization hypothesis that rising CO_2 will have a positive effect on plant growth in response to increased carbon availability [Huang et. al., 2007; Zhu et al., 2016]. A NDVI study on passive degassing on Mammoth Mountain, however, found the opposite: that there is an observed decrease in NDVI with elevated CO_2 availability [Rouse et. al., 2010; Cawse-Nicholson et. al., 2018]. The

observed NDVI increase can be due to a number of factors, such as oxygen deprivation in soil pore space, inhibited root respiration, and soil acidification [Farrar et. al., 1995; McGee and Gerlach, 1998; Qi et. al., 1994].

Though these factors warrant further study in order to ascertain factors attributing to changing NDVI vegetation signatures, they are beyond the scope of this study. While we did not analyze these factors here, these previous studies can inform our working hypothesis on why we see a marked NDVI change prior to the eruption. We propose that there is a threshold (unquantified at this point) below which CO_2 flux from degassing magma enhances vegetation growth. Above this threshold, it begins to choke out vegetation and thus kills vegetation, yielding a decrease in the vegetation health and extent.

This hypothesis is supported by our analysis of imagery from Area 4 and 5. Most of the Puhimau study area (Area 4) shows increased vegetation health in April 2018 (with the exception of the actual geothermal feature itself). This is also seen for Leilani Estates (Area 5), with the exception of the vegetation surrounding the fissure eruption area. We propose that this elevated NDVI signature in both study areas is in response to magma movement in the months leading up to the eruption. Expanding on our working hypothesis, we theorize that the CO_2 threshold to kill off vegetation will be higher in densely vegetated areas than sparsely vegetated areas. Evidence for this is seen in the fact that Area 5 (dense Ohia forest) does not "green up" nearly as much as Area 4 (mixed vegetation) in response to what we theorize is increased CO_2 degassing in the region. We surmise that sparse to moderate vegetation should be more sensitive to geothermal flux due to lower vegetation amounts to begin with [McGee et. al., 2006]. Therefore, we should expect that the sparsely

vegetated Puhimau region would have a much more significant NDVI signature than a densely vegetated region such as Leilani Estates, because larger trees are able to tolerate higher CO_2 fluxes compared to shrubs and grasses.

The small region within Area 5 that experienced declining vegetation health directly surrounding the 2018 eruption fissure area supports the second half of our working hypothesis that CO_2 is only beneficial to vegetation health up to a certain point, but with one added detail. However, the observed declining vegetation is roughly aligned with the eruption fissure. Due to this observed directionality to the stressed NDVI signature, it is probable that the vegetation within this small area experienced higher CO_2 degassing flux through micro-faults than the surrounding vegetation.

This directional signature is most likely attributed to local faults and fractures, as well as preexisting lava flows. Additionally, the fluctuations of declining/increasing vegetation health in Area 5 for the year prior to the eruption can be attributed to possible pulses of magma moving into the LERZ. It is reasonable to conclude that the 2018 eruption fissures opened up under Leilani Estates due to the path of least resistance; there is a well-established fault system leading from the Upper ERZ to the LERZ [Cannon et. al., 2007], as well as preexisting lava flow boundaries, which essentially act as an impermeable seal for passive volcanic degassing. Therefore, we conclude that any pre-eruptive activity should follow existing fault structures and vegetated areas, as seen in Leilani Estates.

6.1 Direction of Future Work

It is clear that this area deserves further study in order to determine when the vegetation change began to occur and whether there is possible correlation with any other pre-eruptive activity. This is not only limited to consistent imagery dates across all study areas, but also acquiring higher temporal coverage of imagery dates rather than once a month. This study covered the April 2017 to May 2018 timeframe; however, it would also be beneficial to acquire imagery for all of 2017 and 2018 to determine any subtle background variations. As mentioned in the general discussion, there are numerous factors beyond the scope of this study that can affect the NDVI signature. There is almost certainly a temperature and precipitation correlation to vegetation change within the micro-climates of each study area, but the challenge lies in filtering out this background effect [Cawse-Nicholson, et. al., 2018].

It should also be mentioned that the NDVI only addresses the extent and the general health of each vegetation class, and not necessarily the health of individual plants themselves – a seemingly small distinction, but an important one. In this sense, the use of multi-spectral generated NDVI for monitoring soil gas emission changes is limited to only large changes that happen before the eruption occurs. Future studies could combine the use of multi-spectral and hyper-spectral data to allow detailed analysis of plant health.

This study shows that NDVI can be utilized in order to determine timing of pre-eruptive related events. Seismic data were not acquired for this study, but a change in vegetation class extent in correlation to other data sets can aid in the determination of magma movement within active rift zones. The change in vegetation extent is theorized to

potentially precede any other eruptive indicators such as seismic data, though this will need to be analyzed in future studies.

NDVI can be useful in identifying active or potentially active geothermal regions within an active rift zone. This is useful from a volcanic monitoring viewpoint, as it can help narrow down locations for field campaigns and deployment of monitoring equipment.

7 Conclusions

This exploratory study on the May-August 2018 Kilauea eruption utilized high-resolution multispectral data and image processing software and techniques to ascertain if there was a change in vegetation health and extent in correlation with pre-eruptive volcanic activity prior to the eruption. We have shown that NDVI has the potential to be used as a potential indicator of pre-eruptive unrest in active, vegetated volcanic regions in combination with other datasets. An important result from this study is an established method for analyzing large vegetation imagery datasets. However, future studies should acquire consistent imagery across all study areas for improved analysis and results. The results of this work have implications for the utilization of NDVI in assessing vegetation and general vegetation health and class extent changes.

8 Works Cited

Andronico D, Branca S, Calvari S, Burton M, Caltabiano T, Corsaro RA, et al. A multi-disciplinary study of the 2002-03 Etna eruption: insights into a complex plumbing system. Bull Volcanol 2005; 67:314-330.

Aiuppa A, Moretti R, Federico C, Giudice G, Gurrieri S, Liuzzo M, et al. Forecasting Etna eruptions by real-time observation of volcanic gas composition. Geology 2007; 35:1115-1118.

Asner, G.P.; Martin, R.E.; Keith, L.M.; Heller, W.P.; Hughes, M.A.; Vaughn, N.R.; Hughes, R.F.; Balzotti, C. A Spectral Mapping Signature for the Rapid Ohia Death (ROD) Pathogen in Hawaiian Forests. *Remote Sens.* 2018, *10*, 404.

Bateson, L. & Vellico, Michela & Beaubien, S.E. & Pearce, Jonathan & Annunziatellis, A. & Ciotoli, Giancarlo & Coren, Franco & Lombardi, Salvatore & Marsh, Stuart. (2008). The application of remote-sensing techniques to monitor CO2-storage sites for surface leakage: Method development and testing at Latera (Italy) where naturally produced CO2 is leaking to the atmosphere. International Journal of Greenhouse Gas Control. 2. 388-400. 10.1016/j.ijggc.2007.12.005.

Burns, B. (1997), Vegetation change along a geothermal stress gradient at the Te Kopia steamfield, Journal of the Royal Society of New Zealand, 27:2, 279-293, DOI: 10.1080/03014223.1997.9517539

Cannon, E.C., Bürgmann, R., Crone, A.J., Machette, M.N., and Dart, R.L., 2007, Map and data for Quaternary faults and fault systems on the Island of Hawai'i: U.S. Geological Survey Open-File Report 2007-1284, 81 p., 1 plate.

Cawse-Nicholson, K., Fisher, J. B., Famiglietti, C. A., Braverman, A., Schwandner, F. M., Lewicki, J. L., Townsend, P. A., Schimel, D. S., Pavlick, R., Bormann, K. J., Ferraz, A., Kang, E. L., Ma, P., Bogue, R. R., Youmans, T., and Pieri, D. C.: Ecosystem responses to elevated CO_2 using airborne remote sensing at Mammoth Mountain, California, Biogeosciences, 15, 7403–7418, https://doi.org/10.5194/bg-15-7403-2018, 2018.

Congalton, R. G., 1957. Assessing the accuracy of remotely sensed data: principles and practices. Russell Congalton, Kass Green. ISBN 0-87371-986-7.

Decker, R.W. (1987), Dynamics of Hawaiian volcanoes: An overview. In Volcanism in Hawaii (Decker, R., Wright, T., and Stauffer, P. eds.), U.S. Geological Survey Professional Paper 1350, pp. 997–1018.

Demarée G.R., Ogilvie A.E.J. (2001) *Bons Baisers d'Islande*: Climatic, Environmental, and Human Dimensions Impacts of the *Lakagígar* Eruption (1783–1784) in Iceland. In: Jones P.D., Ogilvie A.E.J., Davies T.D., Briffa K.R. (eds) History and Climate. Springer, Boston, MA

Drake, B. G., Gonzàlez-Meler, M. A., and Long, S. P.: More Efficient Plants: A Consequence of Rising At- mospheric CO_2 ?, Annu. Rev. Plant Phys., 48, 609–639, https://doi.org/10.1146/annurev.arplant.48.1.609, 1997.

Farrar, C. D., Sorey, M. L., Evans, W. C., Howle, J. F., Kerr, B. D., Kennedy, B. M., and Southon, J. R.: Forest-killing diffuse CO_2 emission at Mammoth Mountain as a sign of magmatic unrest, Nature, 376, 675–678, https://doi.org/10.1038/376675a0, 1995.

Heute, A. R., 1988. A soil-adjusted vegetation index (SAVI). Remote Sens. Environ. 25 (3), 295-309.

Houlie, N, Komorowski, J. Cl, de Michele, M., Kasereka, M., Ciraba, H. Early detection of eruptive dykes revealed by normalized difference vegetation index (NDVI) on Mt. Etna and Mt. Nyiragongo. Earth Planet Sci Lett 2006; 246:231-240.

Jensen, J. R., 1986. Introductory Digital Image Processing: A Remote Sensing Perspective. Prentice-Hall, Englewood Cliffs, New Jersey.

Jensen, J. R., Remote Sensing of the Environment: An Earth Resource Perspective, Prentice Hall, 2000.

Hinkle, M.E. (1978), Helium, mercury, sulfur compounds, and carbon dioxide in soil gases of the Puhimau Thermal Area, Hawaii Volcanoes National Park, Hawaii, U. S. Geological Survey Open-File Report No. 78–246, 15 pp.

Huang, J.-G., Bergeron, Y., Denneler, B., Berninger, F., and Tardif, J.: Response of forest trees to increased at- mospheric CO_2 , Crit. Rev. Plant Sci., 26, 265–283, https://doi.org/10.1080/07352680701626978, 2007.

Lillesand, T.M., Kiefer, R,W., Chipman, J.W., 1987. Remote Sensing and Image Interpretation. John Wiley & Sons, New York, 2004.

McGee, K. A. and Gerlach, T. M.: Annual cycle of mag- matic CO_2 in a tree-kill soil at Mammoth Moun- tain, California: Implications for soil acidification, Geology, 26, 463–466, https://doi.org/10.1130/0091- 7613(1998)026<0463:ACOMCI>2.3.CO;2, 1998.

McGee, K. A., Sutton, A. J., Elias, T., Doukas, M. P., & Gerlach, T. M. 2006. Puhimau Thermal Area: A Window into the Upper East Rift Zone of Volcano, Hawaii? Pure and Applied Geophysics, 163(4), 837-851.

Norby, R. J., De Kauwe, M. G., Domingues, T. F., Duursma, R. A., Ellsworth, D. S., Goll, D. S., and Zaehle, S.: Model– data synthesis for the next generation of forest free-air CO_2 enrichment (FACE) experiments, New Phytol., 209, 17–28, https://doi.org/10.1111/nph.13593, 2016.

"ROD: The Disease Distribution." *College of Tropical Agriculture and Human Resources*, The University of Hawaii, 2019, cms.ctahr.hawaii.edu/rod/THE-DISEASE/DISTRIBUTION.

Planet Team (2017). Planet Application Program Interface: In Space for Life on Earth. San Francisco, CA. https://api.planet.com.

Qi, J., Marshall, J. D., and Mattson, K. G.: High soil carbon dioxide concentrations inhibit root respiration of Douglas fir, New Phy- tol., 128, 435–442, 1994.

Rouse, J. H., Shaw, J. A., Lawrence, R. L., Lewicki, J. L., Dobeck, L. M., Repasky, K. S., and Spangler, L. H.: Multi-spectral imaging of vegetation for detecting CO_2 leaking from underground, Environ. Earth Sci., 60, 313–323, 2010.

Scarpa R., Gasparini P. (1996) A Review of Volcano Geophysics and Volcano-Monitoring Methods. In: Monitoring and Mitigation of Volcano Hazards. Springer, Berlin, Heidelberg

Seiler, R, Kirchner, JW, Krusic PJ, Tognetti R, Houlié, N, Andronico D, et al. (2017). Insensitivity of Tree-Ring Growth to Temperature and Precipitation Sharpens the Puzzle of Enhanced Pre-Eruption NDVI on Mt. Etna (Italy). PLoS ONE 12(1): e0169297. Doi:10.1371/journal.pone.0169297

Seiler, R, et al (2017). Tree-ring width reveals the preparation of the 1974 Mt. Etna eruption. Sci. Rep. 7, 44019; doi: 10.1038/srep44019.

Shinohara, H. (2008), Excess degassing from volcanoes and its role on eruptive and intrusive activity, *Rev. Geophys*., 46, RG4005, doi: 10.2019/2007RG000244.

Tilling, R. I. The critical role of volcano monitoring in risk reduction. *Advances in Geosciences*, European Geosciences Union, 2008, 14, pp.3-11. ⟨hal-00297038⟩

Torres Rosa, Christie, "LINKING HISTORICAL, FIELD, AND SATELLITE DATA TO DETERMINE THE RELATIONSHIP BETWEEN GAS EMISSIONS AND VEGETATION CHANGE IN THE PUHIMAU GEOTHERMAL AREA EAST RIFT ZONE KILAUEA, HAWAII", Open Access Master's Thesis, Michigan Technological University, 2019.

Tortini, Riccardo & van Manen, Saskia & Parkes, Bethan & Carn, Simon. (2017). The impact of persistent volcanic degassing on vegetation: A case study at Turrialba volcano, Costa Rica. International Journal of Applied Earth Observation and Geoinformation. 59. 92-103. 10.1016/j.jag.2017.03.002.

U.S. Geological Survey., 2019. Kilauea 2018 lower East Rift Zone lava flow thicknesses: a PRELIMINARY MAP. Retrieved August 8, 2019, from https://volcanoes.usgs.gov/volcanoes/kilauea/multimedia_maps.html

U.S. Geological Survey., 2018. The May 1924 Explosive Eruption of Kīlauea. Retrieved June 21, 2019, from https://volcanoes.uSGS.gov/volcanoes/kilauea/geo_hist_1924_halemaumau.html

U.S. Geological Survey., 2019. The Pu‘u ‘Ō‘ō Eruption Lasted 35 Years. Retrieved June 18, 2019, from https://volcanoes.uSGS.gov/volcanoes/kilauea/geo_hist_1983.html

Zhu, Z., Piao, S., Myneni, R. B., Huang, M., Zeng, Z., Canadell, J. G., Ciais, P., Sitch, P., Friedlingstein, P., Arneth, A., Cao, C., Cheng, L., Kato, E., Koven, C., Li, Y., Lian, X., Liu, Y., Liu, R., Mao, J., Pan, Y., Peng, S., Peñuelas, J., Poulter, B., Pugh, T. A. M., Stocker, B. D., Viovy, N., Wang, X., Wang, Y., Xiao, Z., Yang, H., Zaehle, S., and Zeng, N.: Greening of the Earth and its drivers, Nat. Clim. Change, 6, 791–795, 2016.

A Appendix 1: NDVI Figures

A.1 Area 1 NDVI Figures

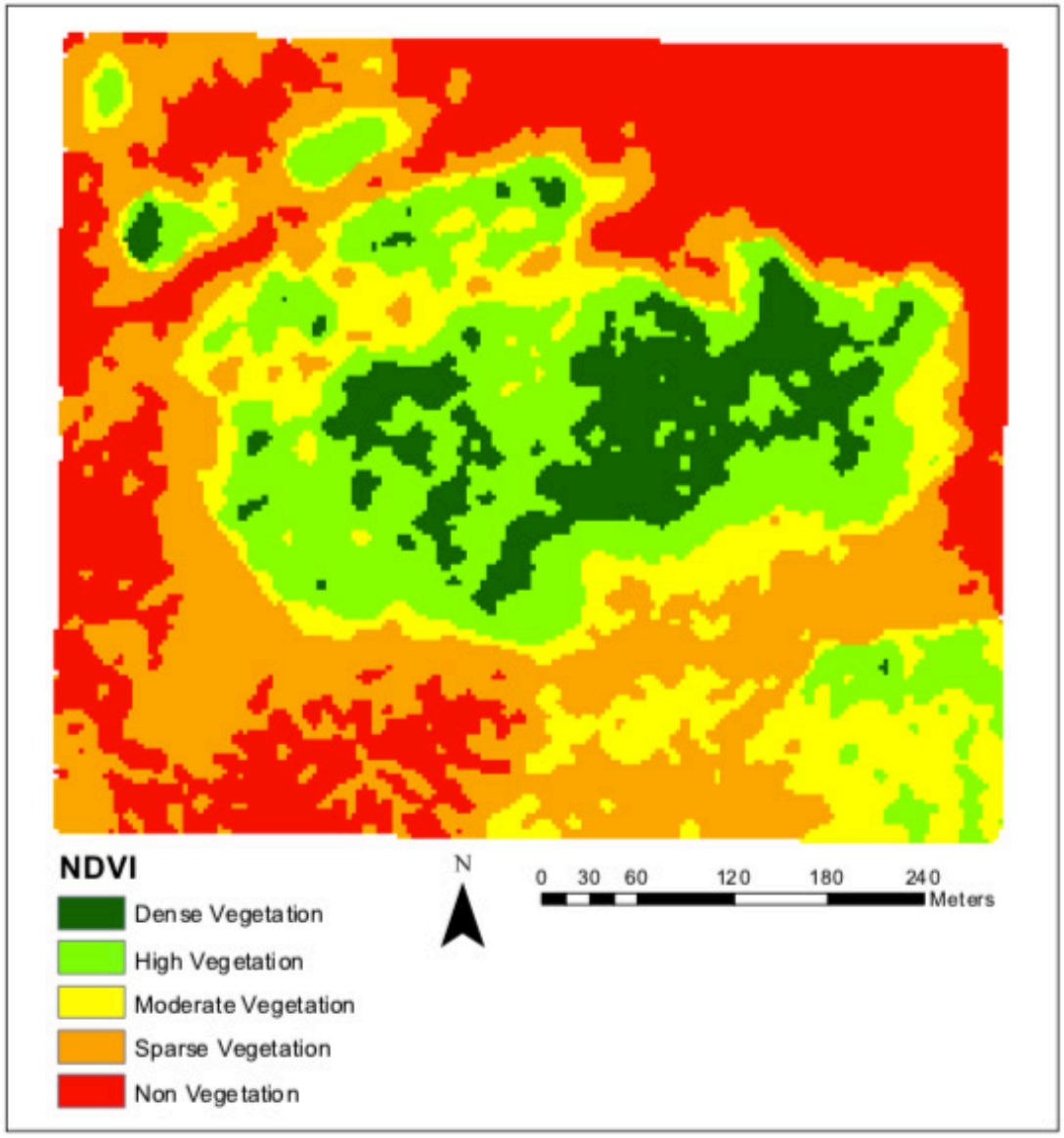

Figure 28: Area 1 NDVI Classification for April 2017.

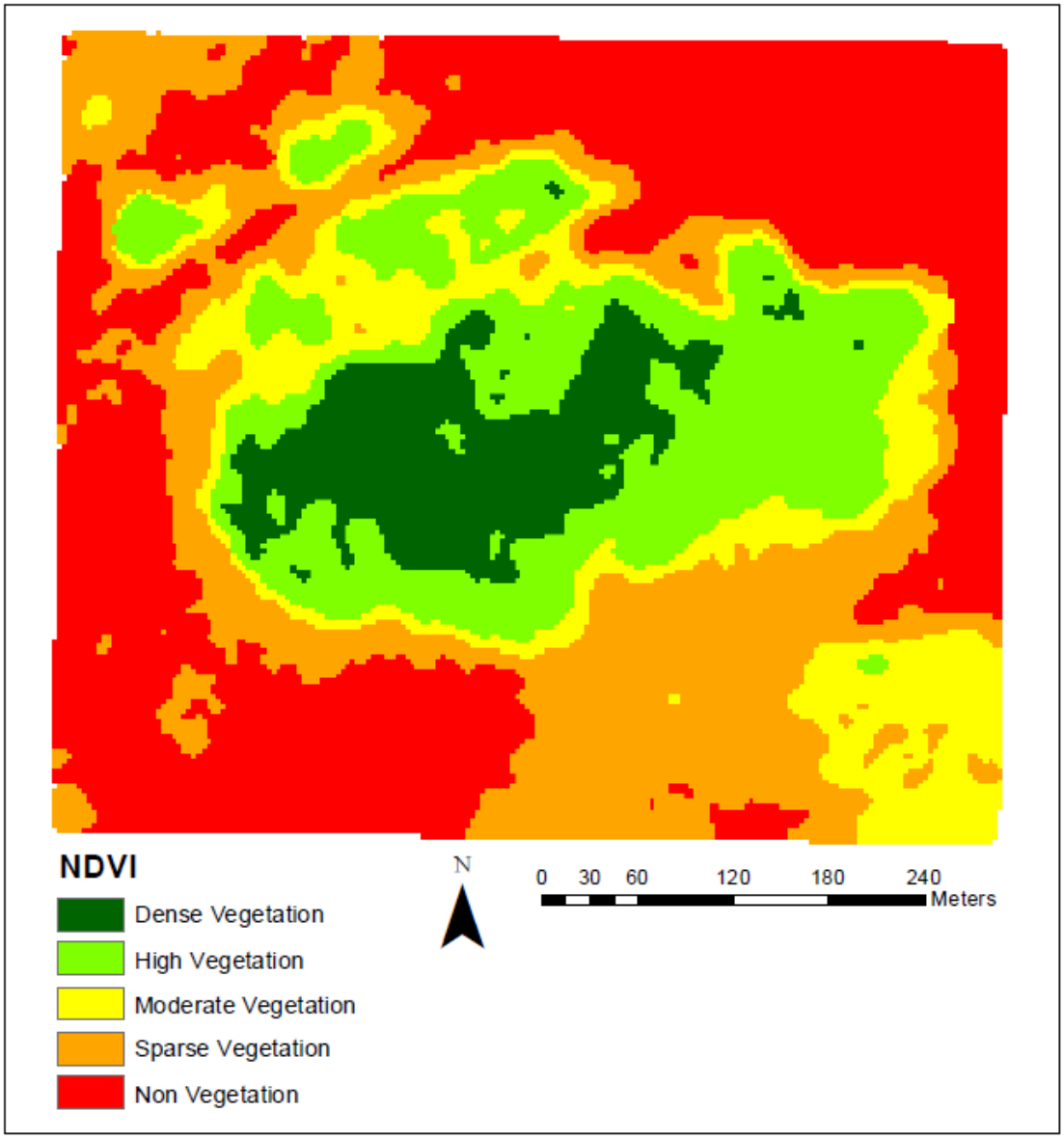

Figure 29: Area 1 NDVI Classification for June 2017.

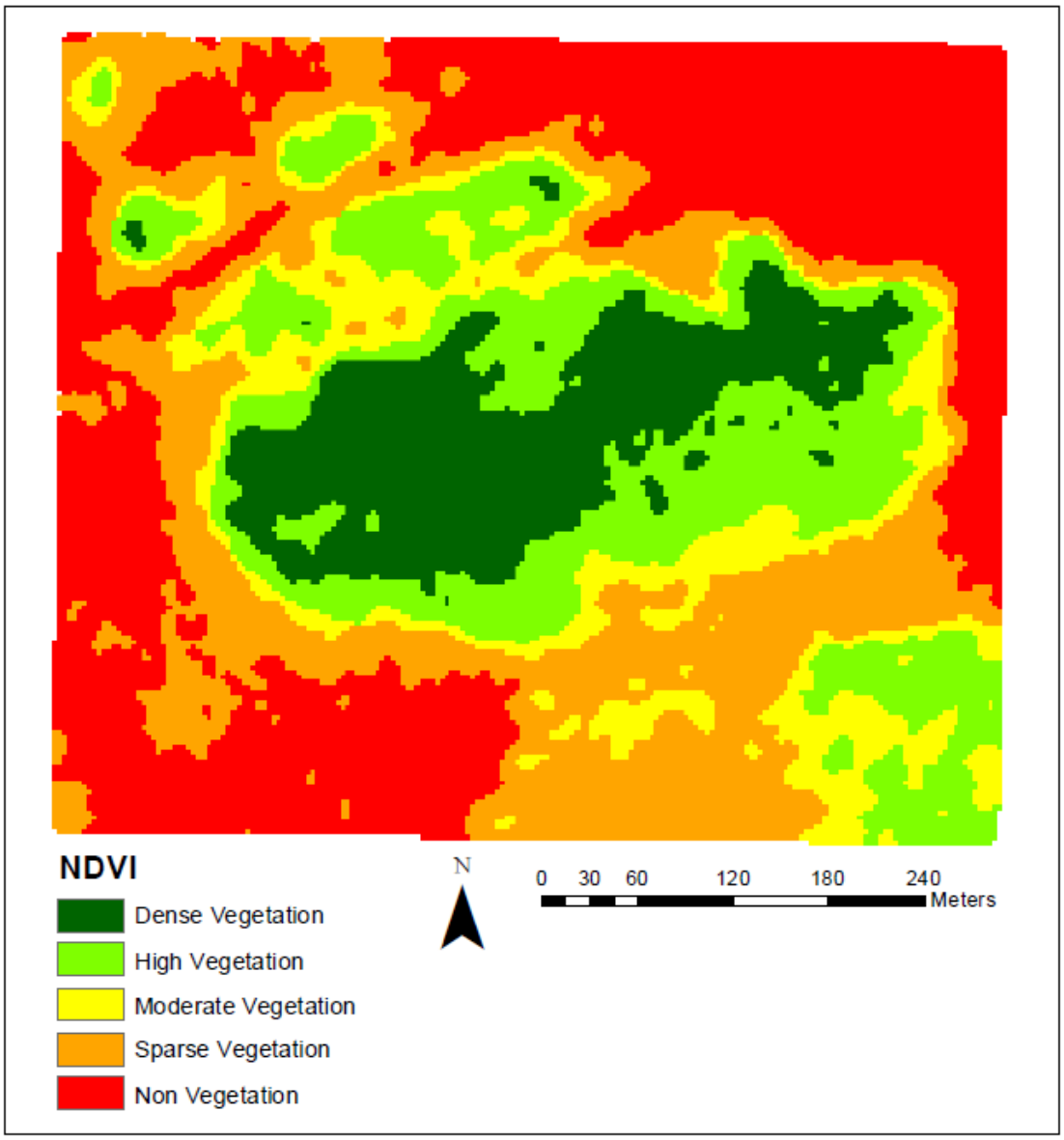

Figure 30: Area 1 NDVI Classification for August 2017.

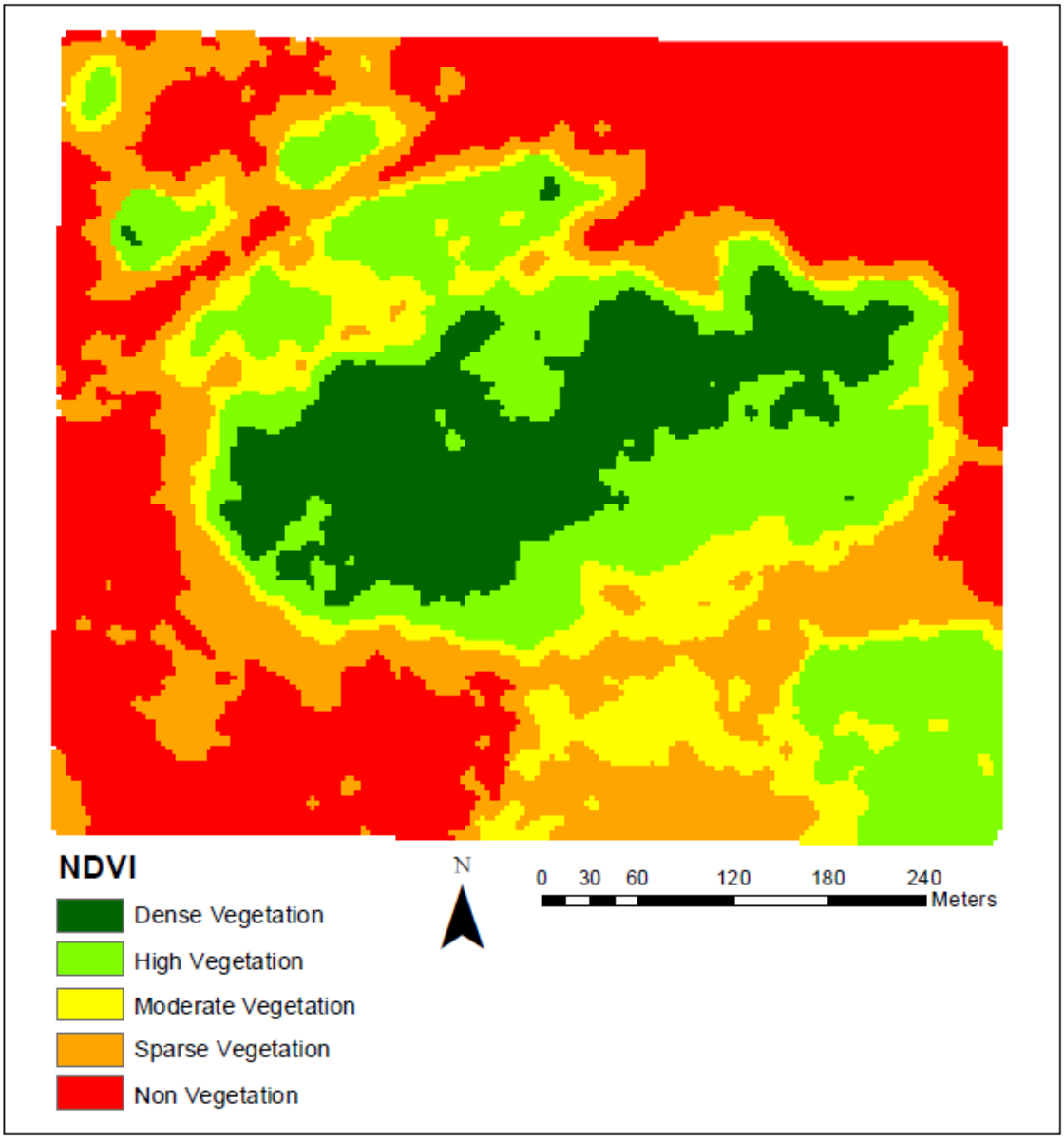

Figure 31: Area 1 NDVI Classification for September 2017.

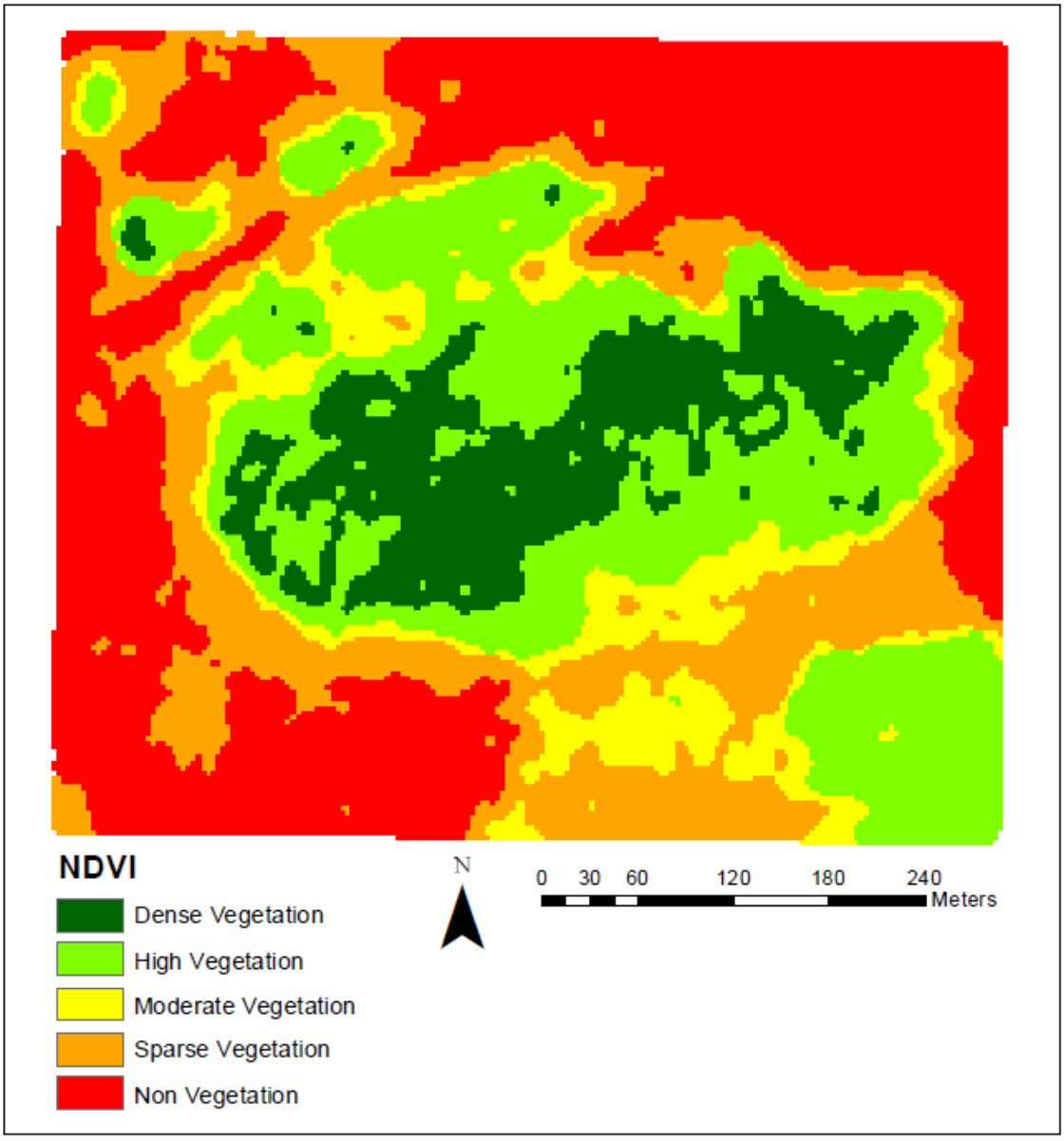

Figure 32: Area 1 NDVI Classification for December 2017.

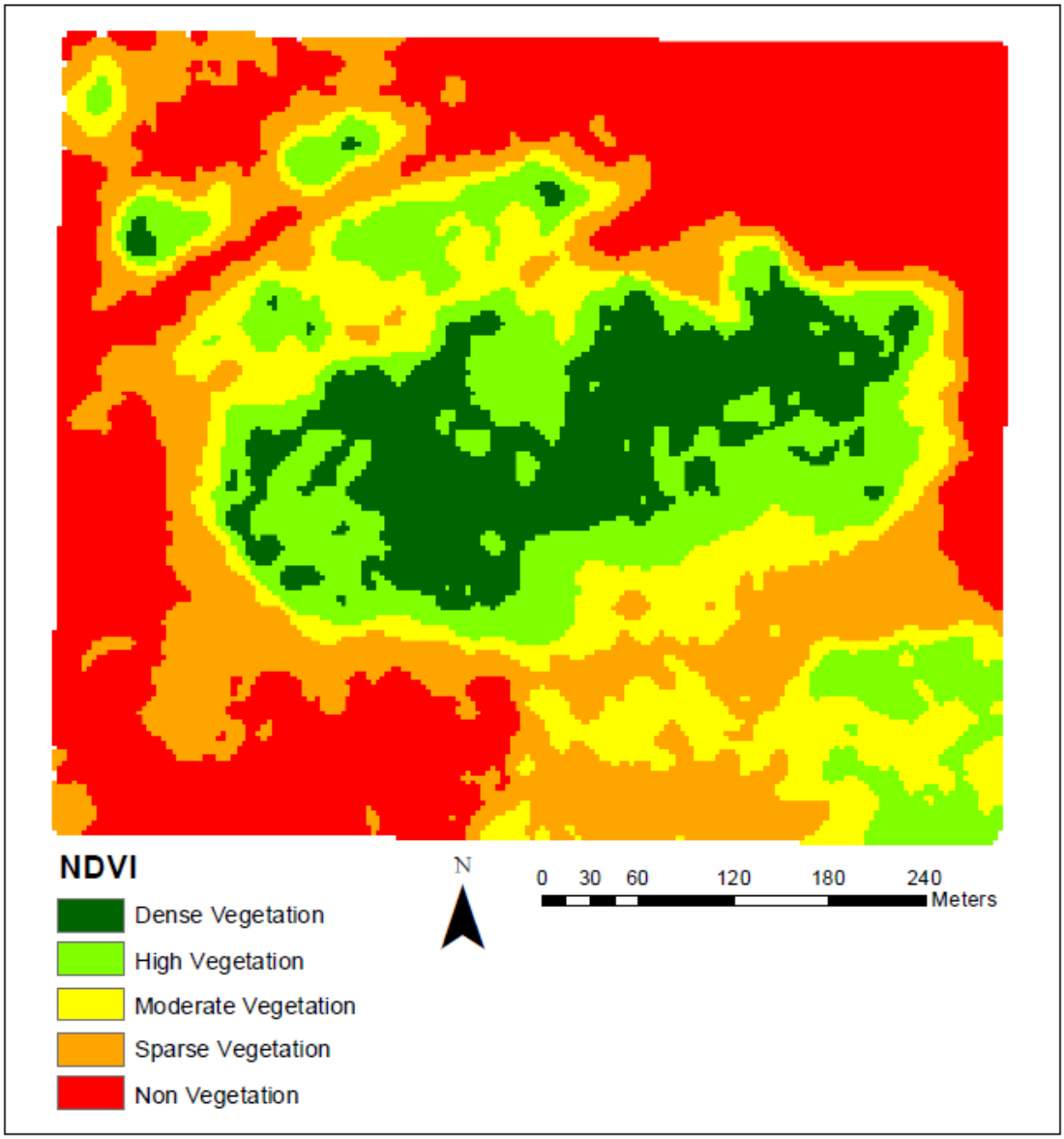

Figure 33: Area 1 NDVI Classification for January 2018.

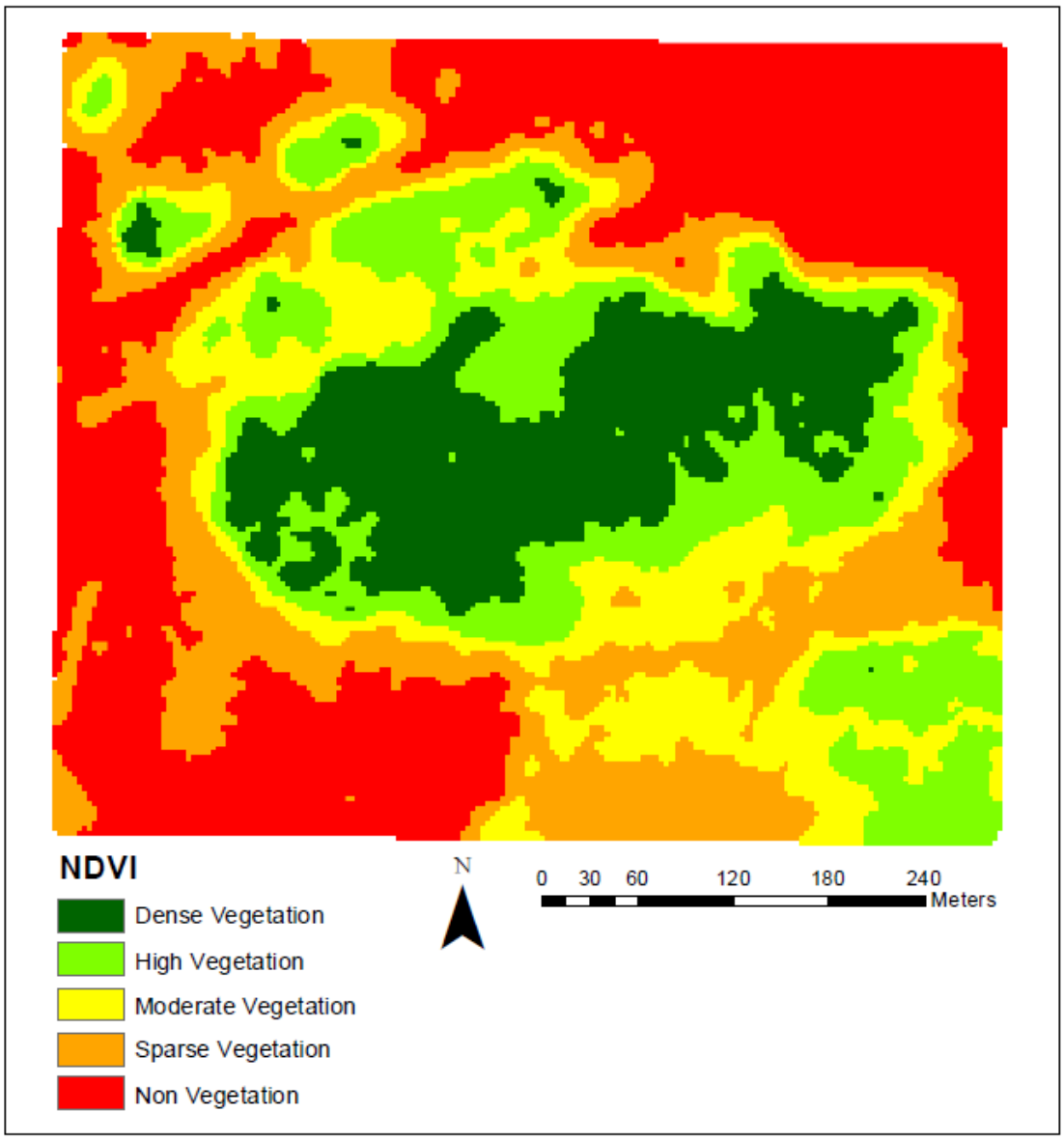

Figure 34: Area 1 NDVI Classification for February 2018.

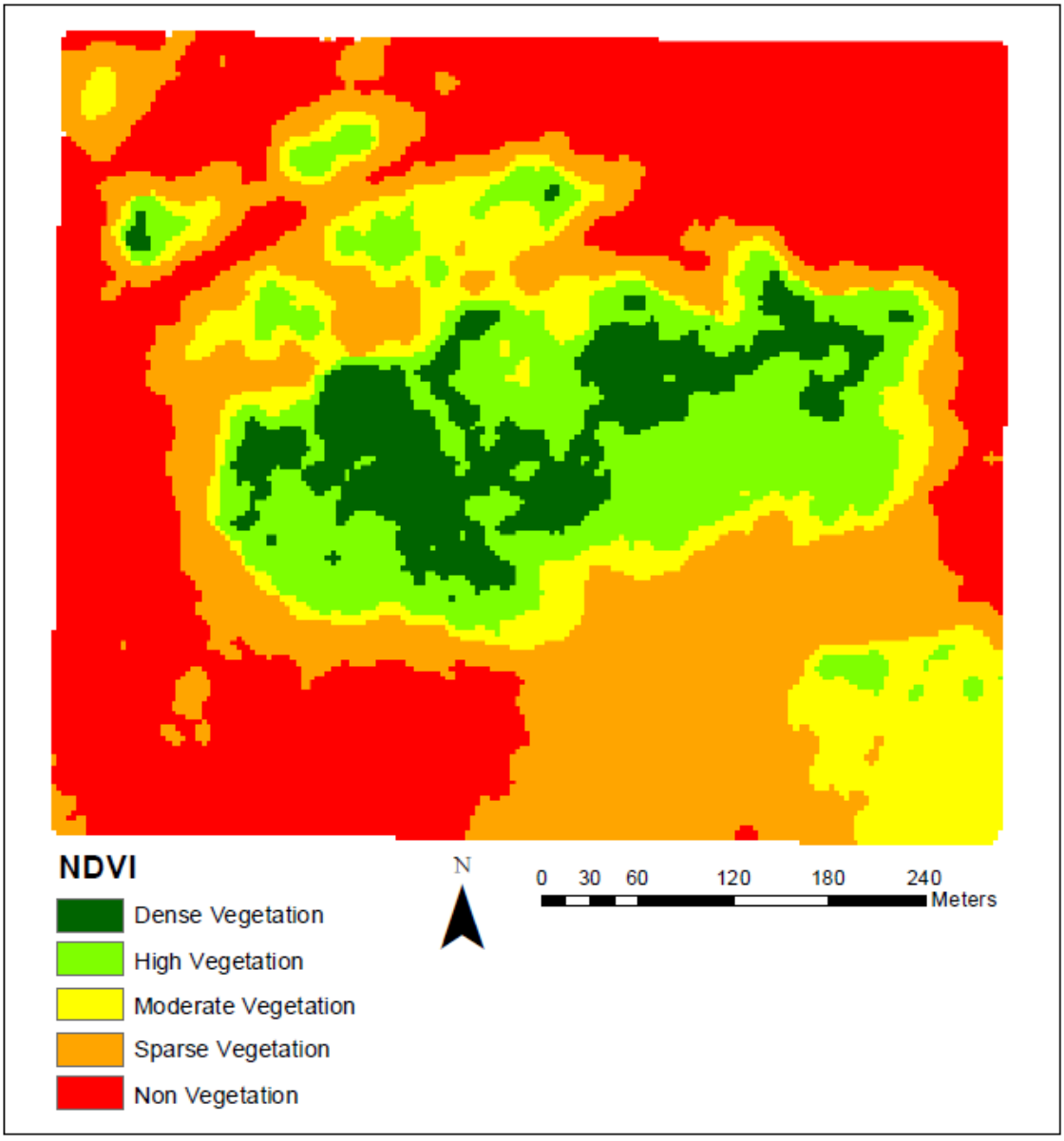

Figure 35: Area 1 NDVI Classification for March 2018.

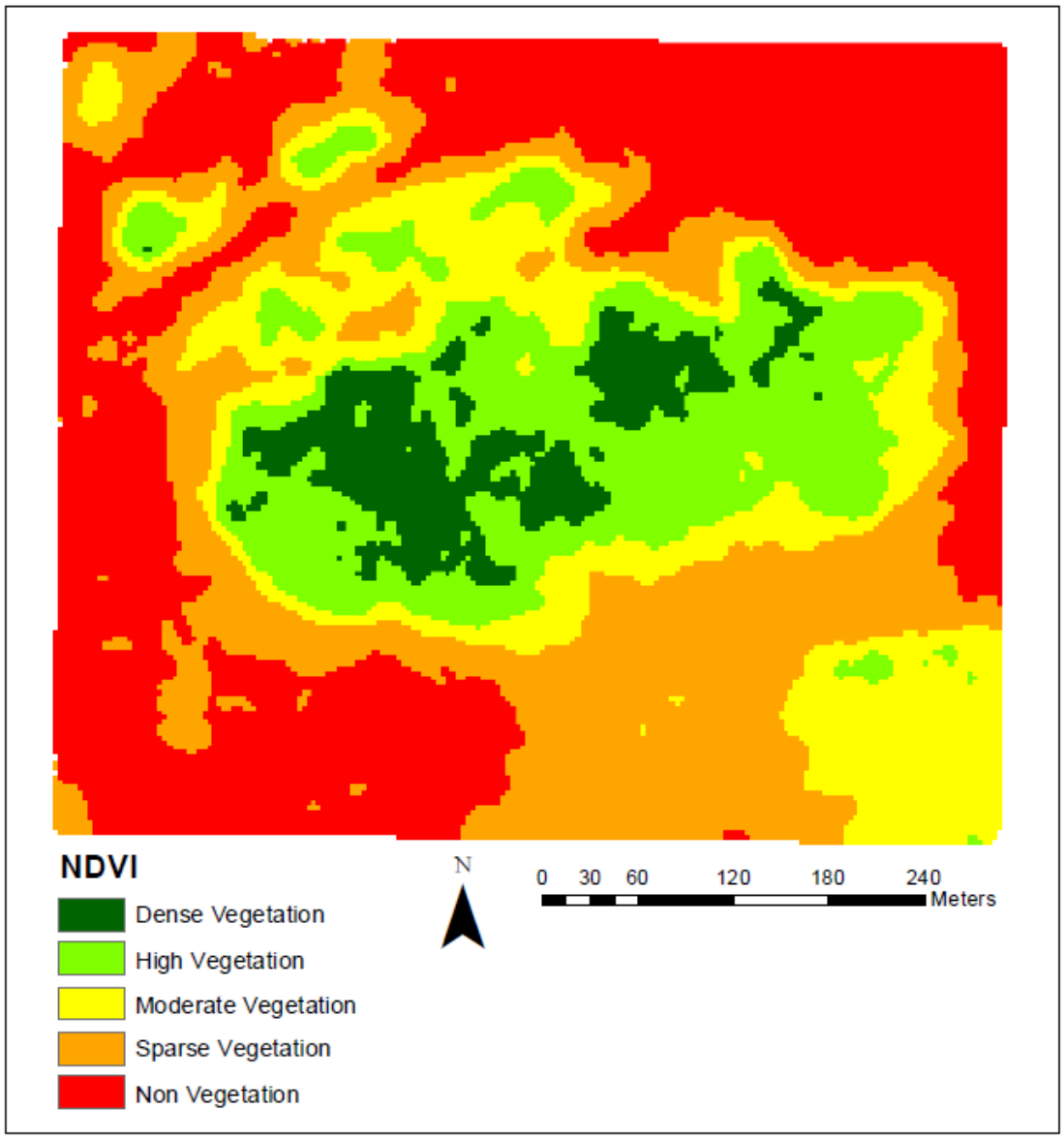

Figure 36: Area 1 NDVI Classification for May 2018.

A.2 Area 2 NDVI Figures

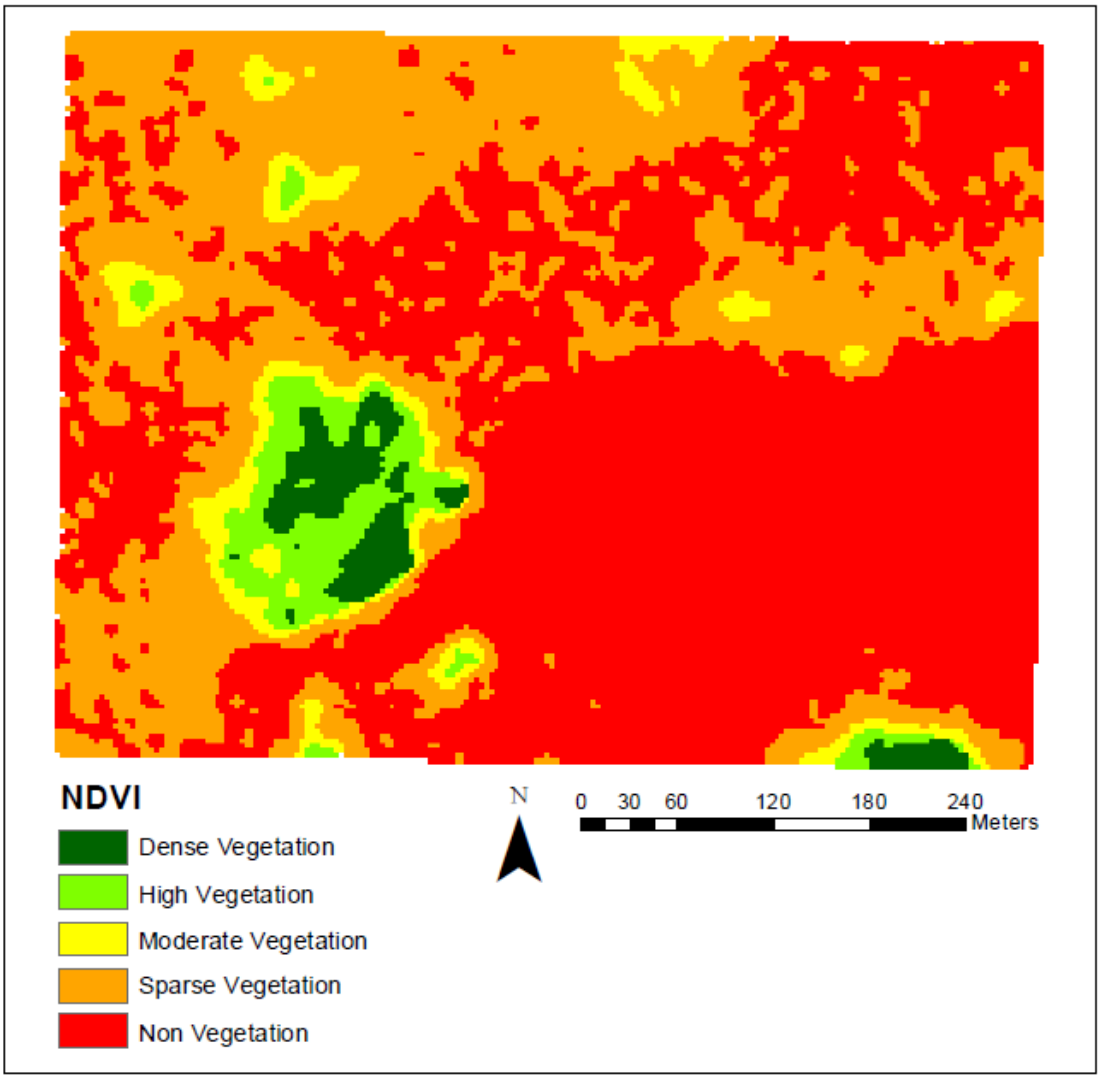

Figure 37: Area 2 NDVI Classification for April 2017.

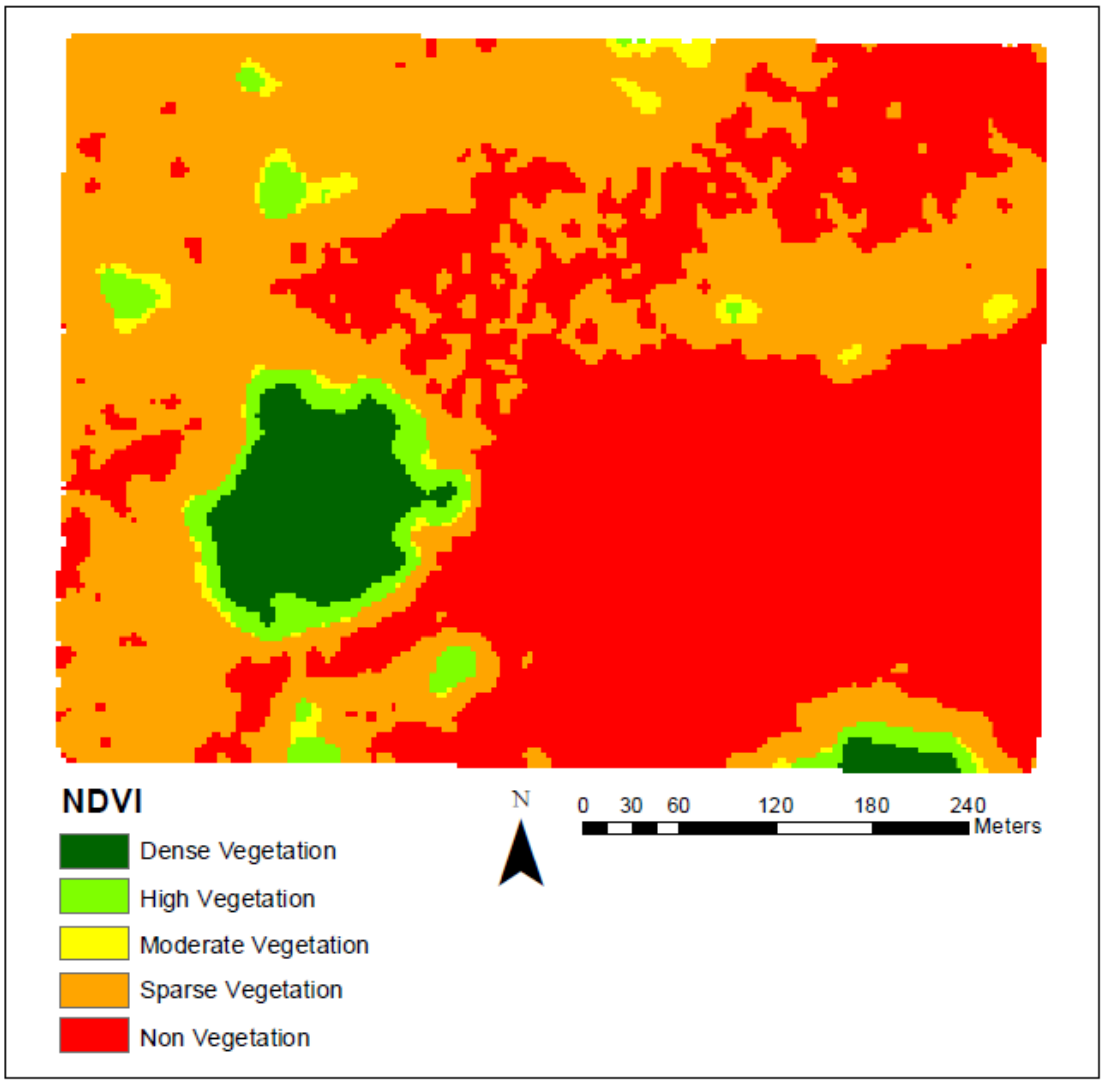

Figure 38: Area 2 NDVI Classification for June 2017.

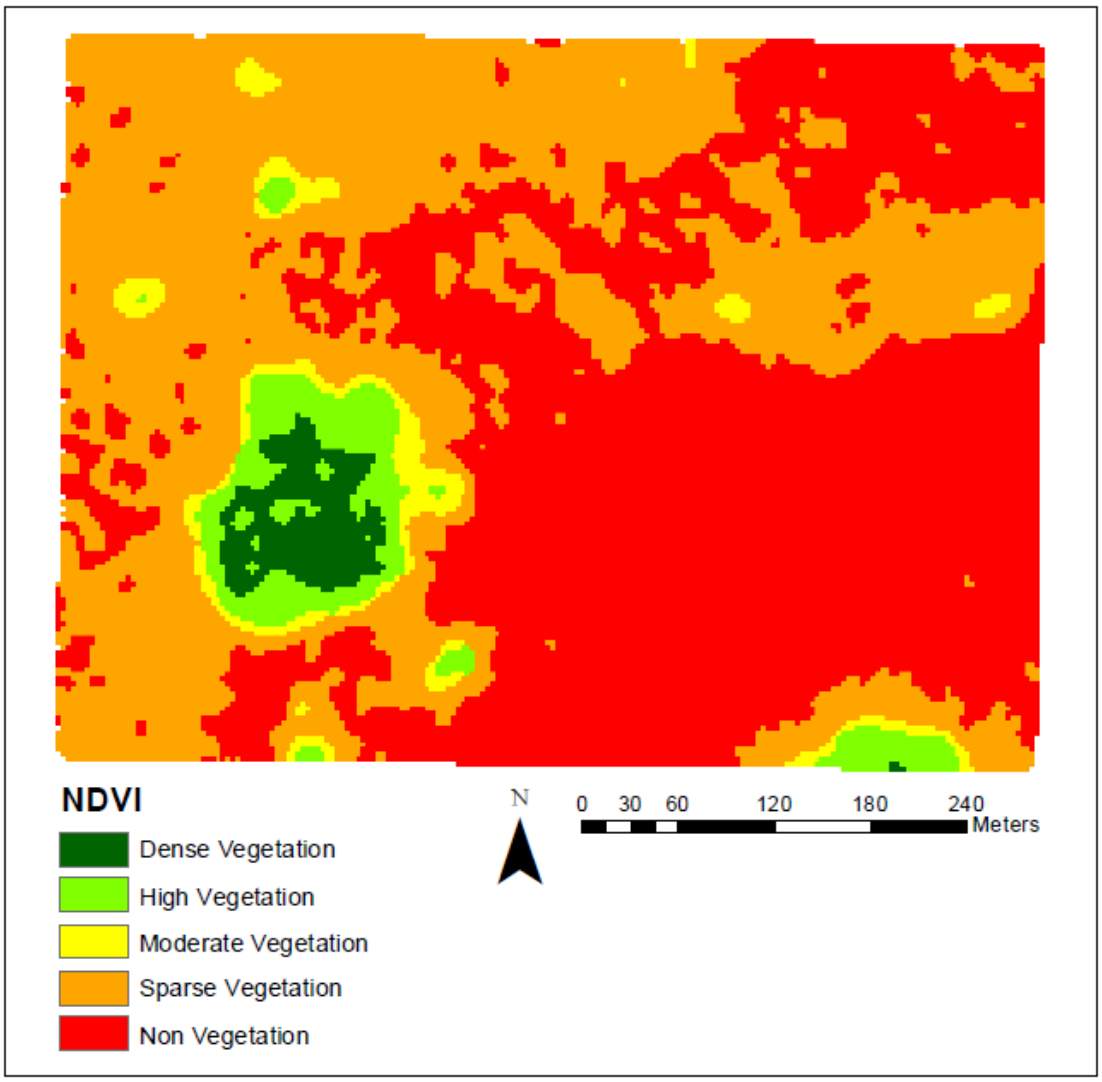

Figure 39: Area 2 NDVI Classification for August 2017.

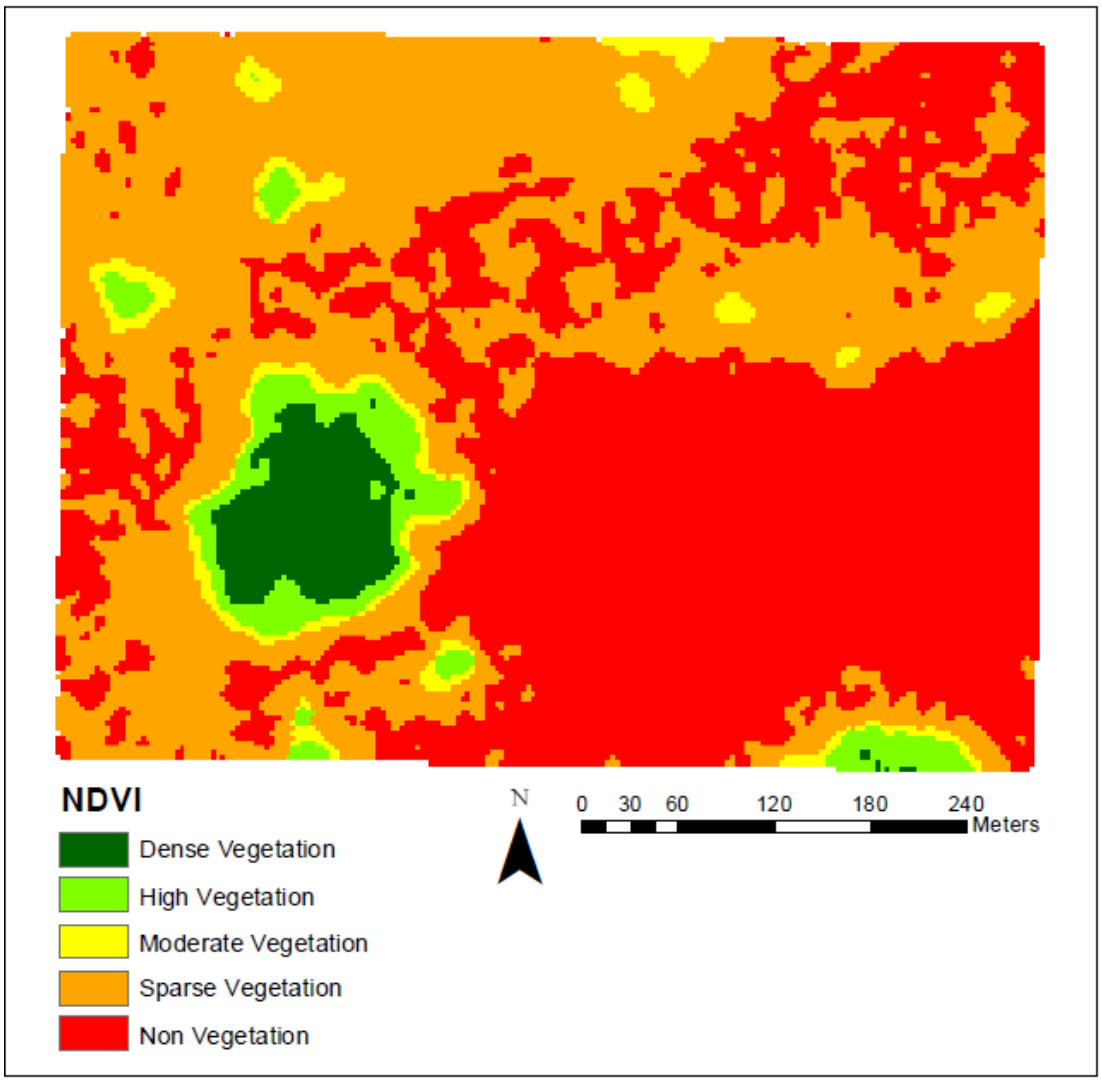

Figure 40: Area 2 NDVI Classification for September 2017.

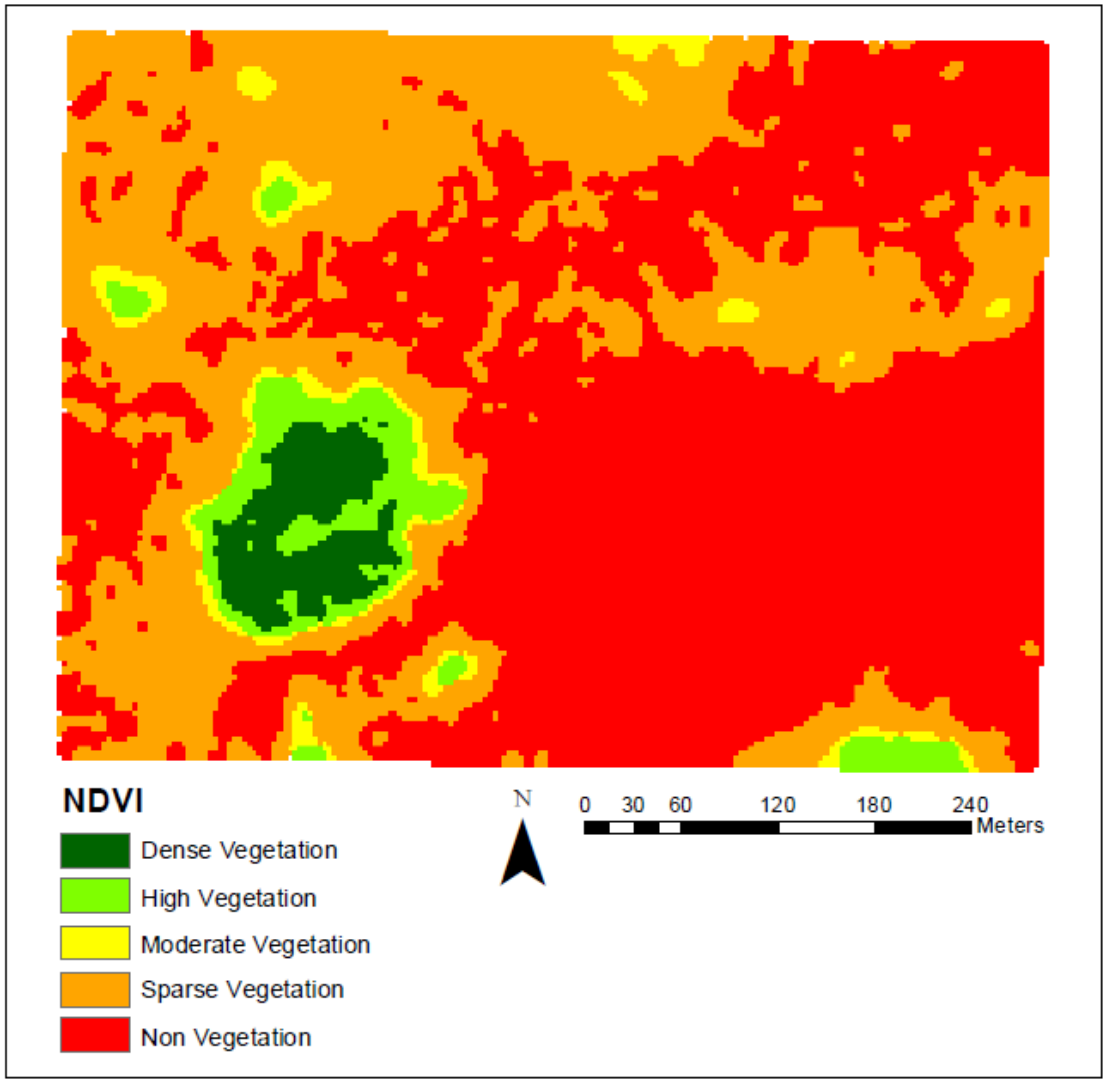

Figure 41: Area 2 NDVI Classification for December 2017.

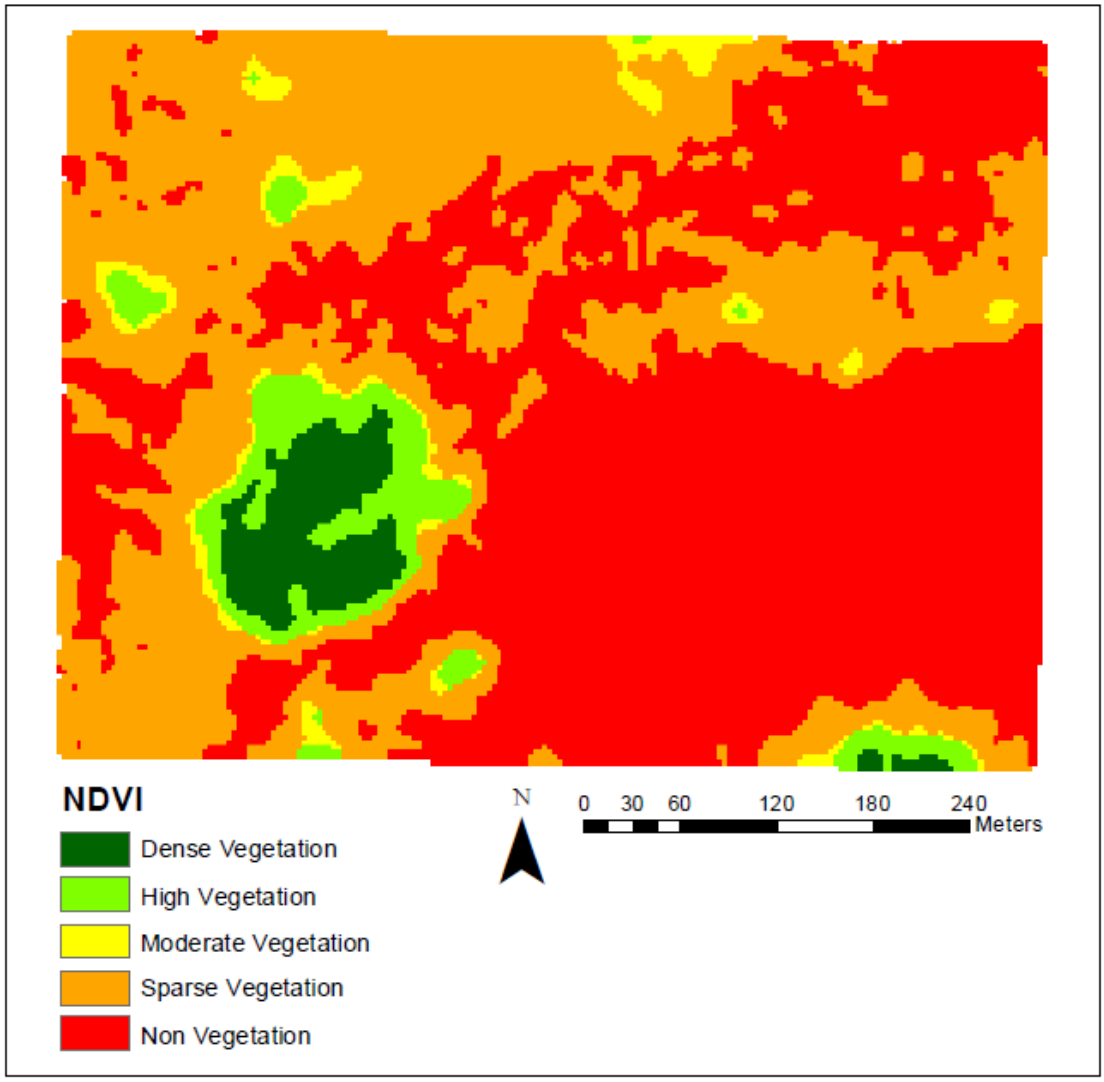

Figure 42: Area 2 NDVI Classification for January 2018.

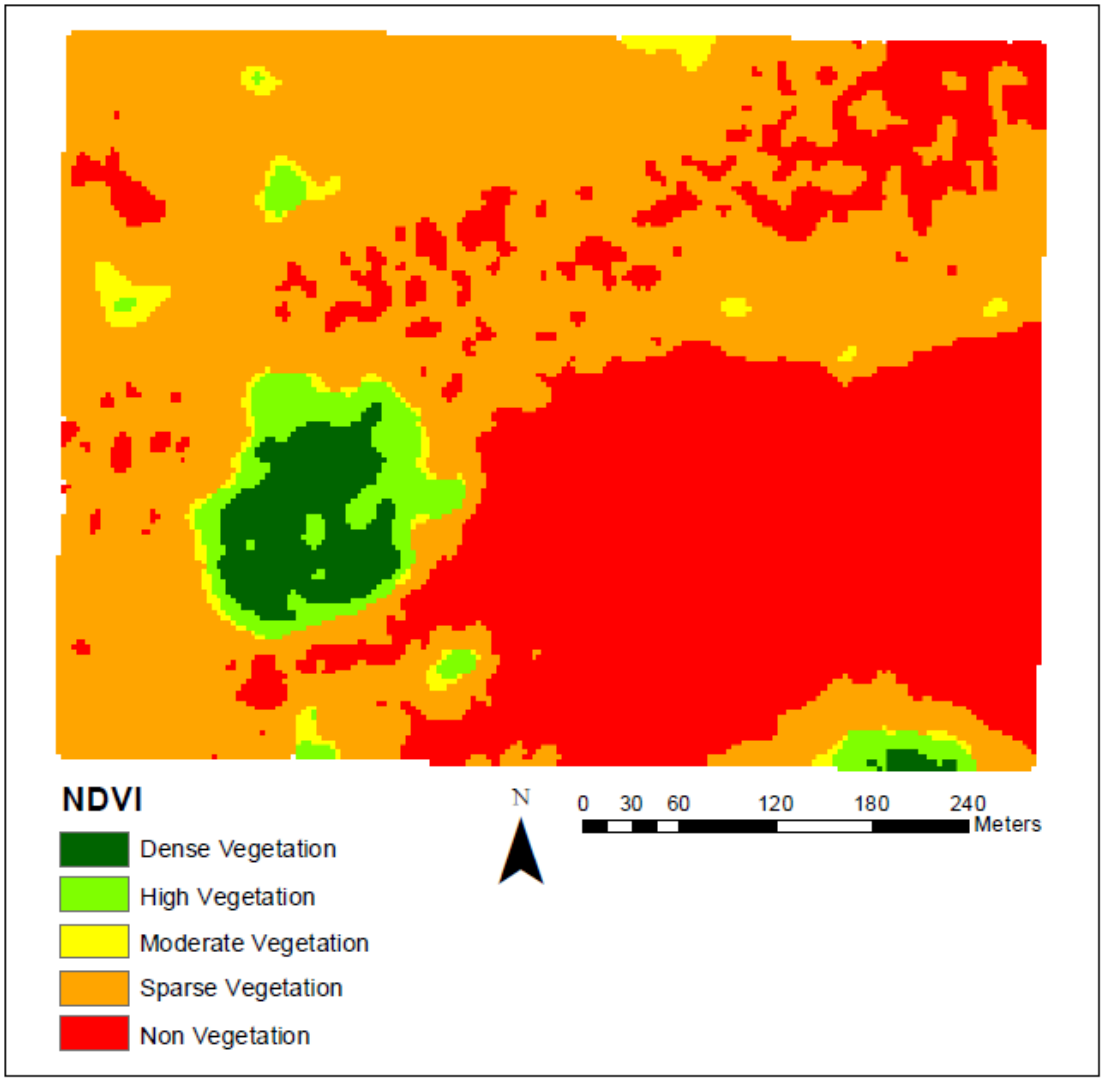

Figure 43: Area 2 NDVI Classification for February 2018.

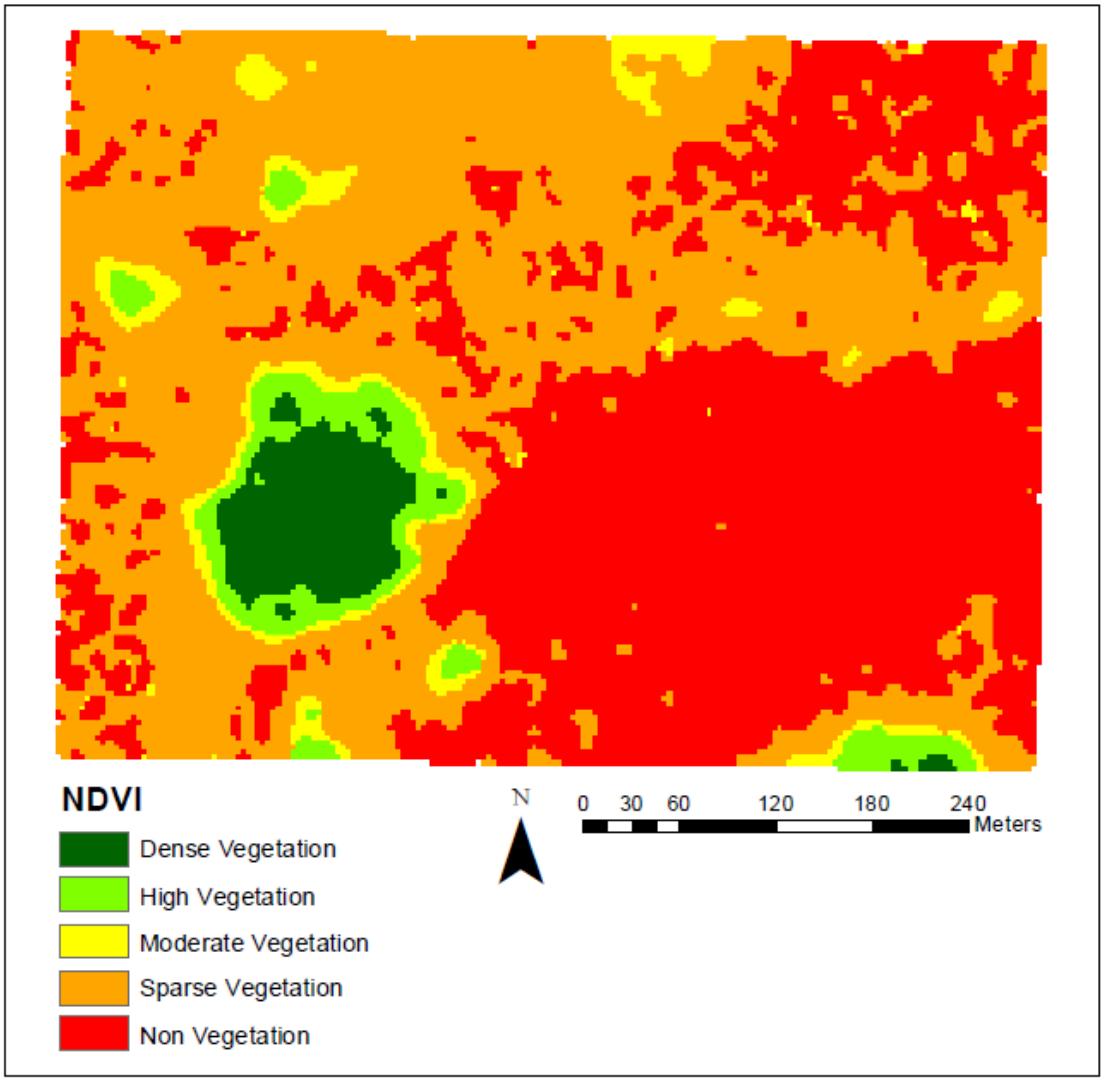

Figure 44: Area 2 NDVI Classification for May 2018.

A.3 Area 3 NDVI Figures

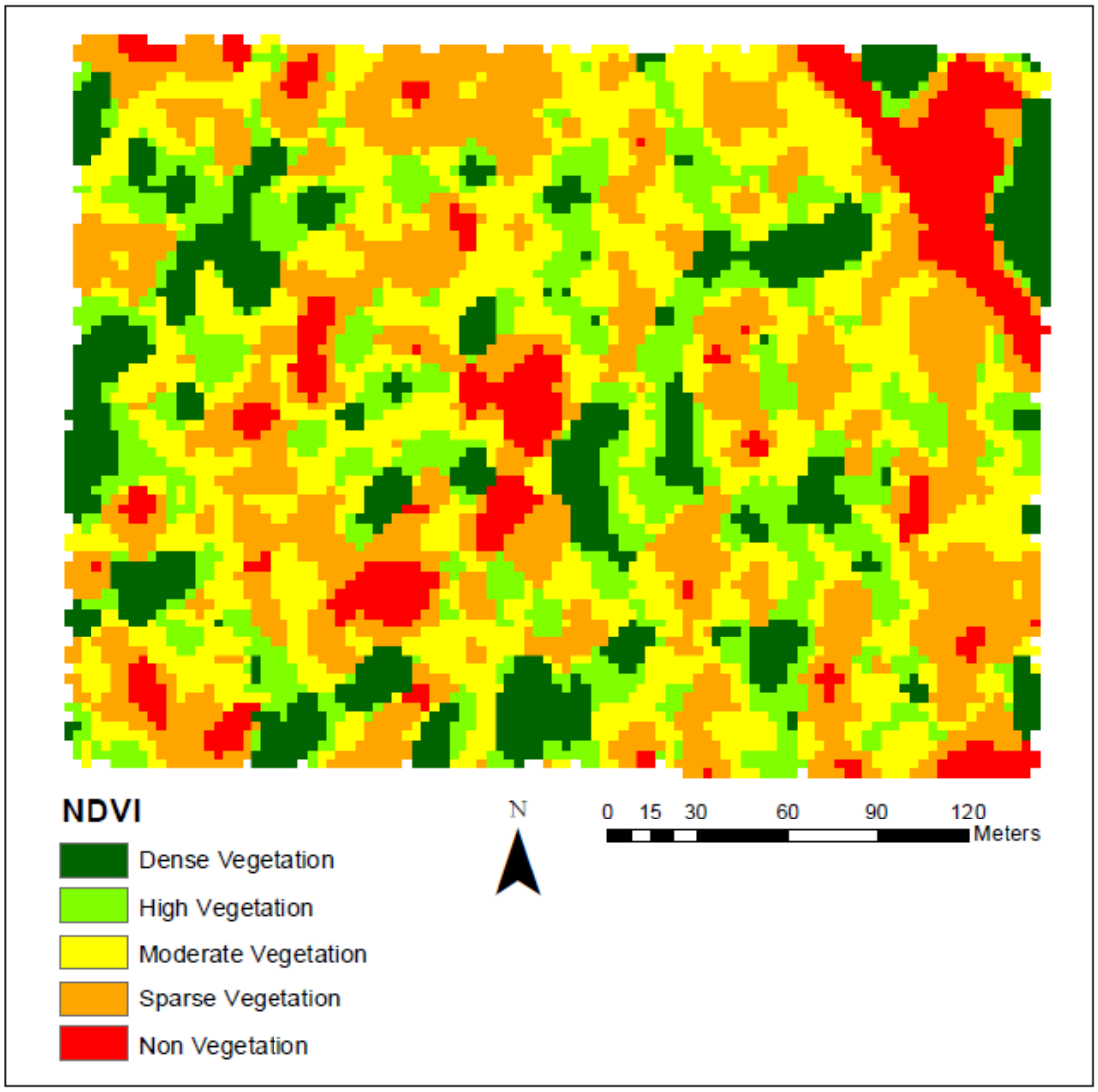

Figure 45: Area 3 NDVI Classification for April 2017.

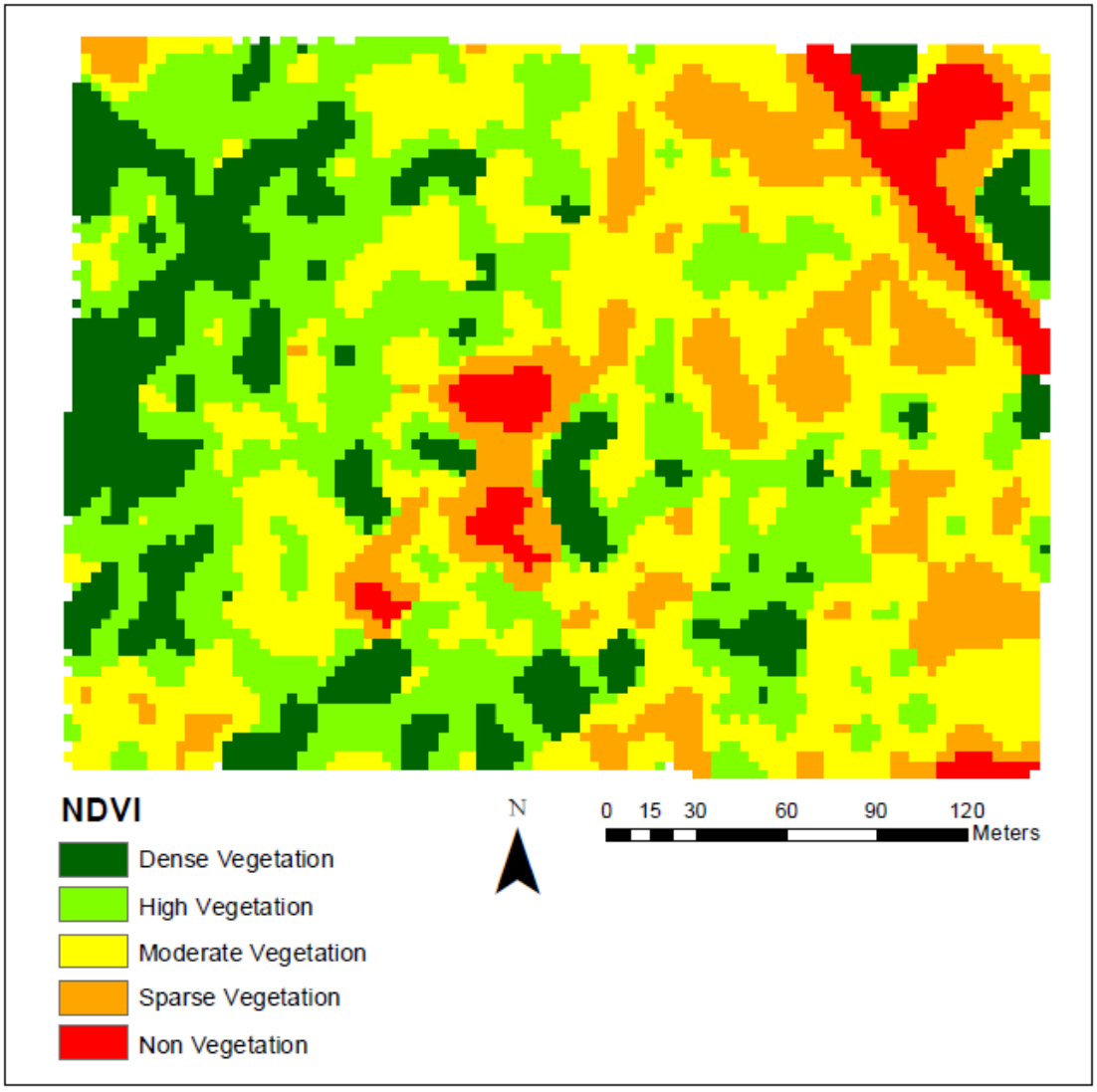

Figure 46: Area 3 NDVI Classification for June 2017.

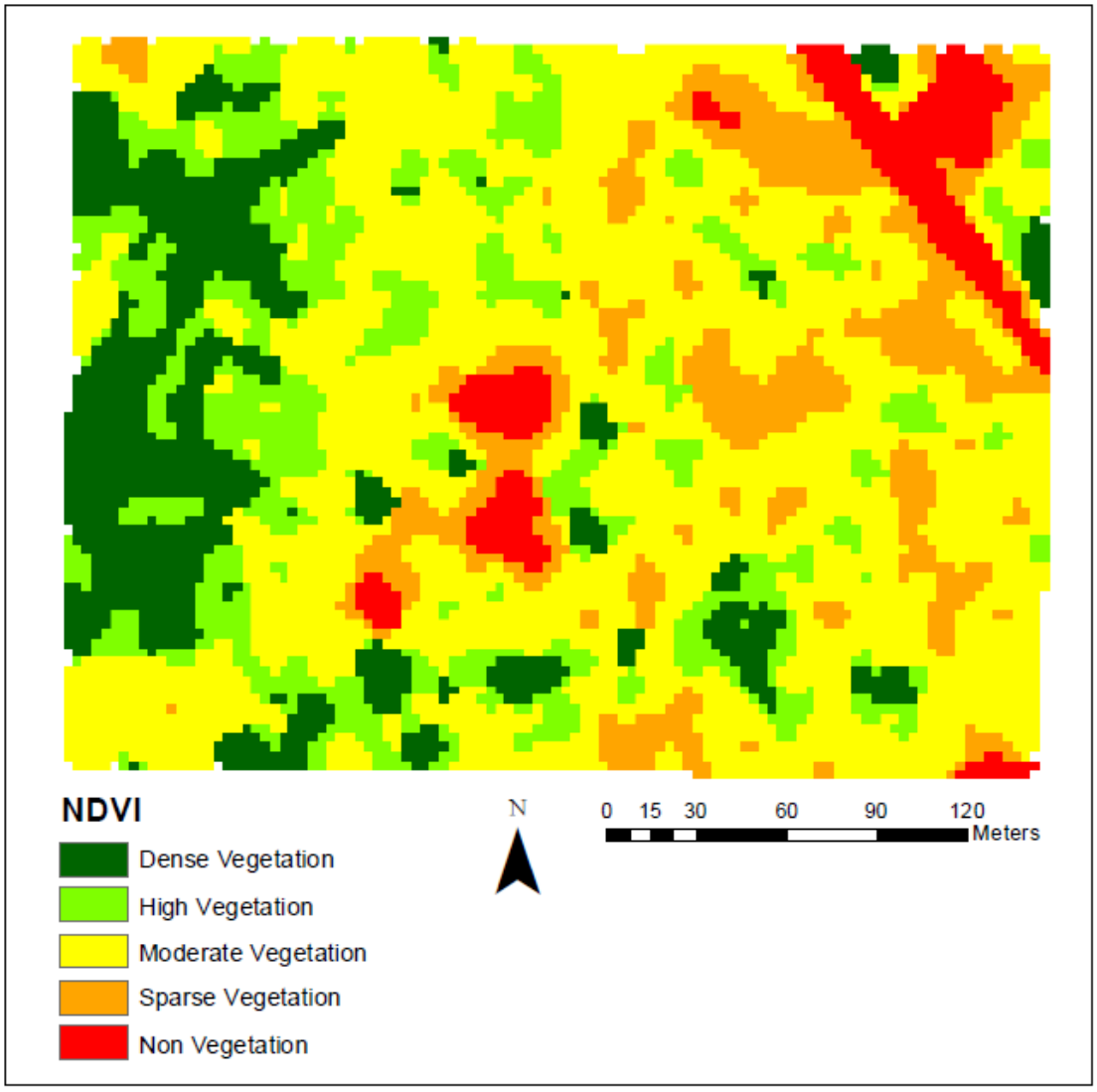

Figure 47: Area 3 NDVI Classification for August 2017.

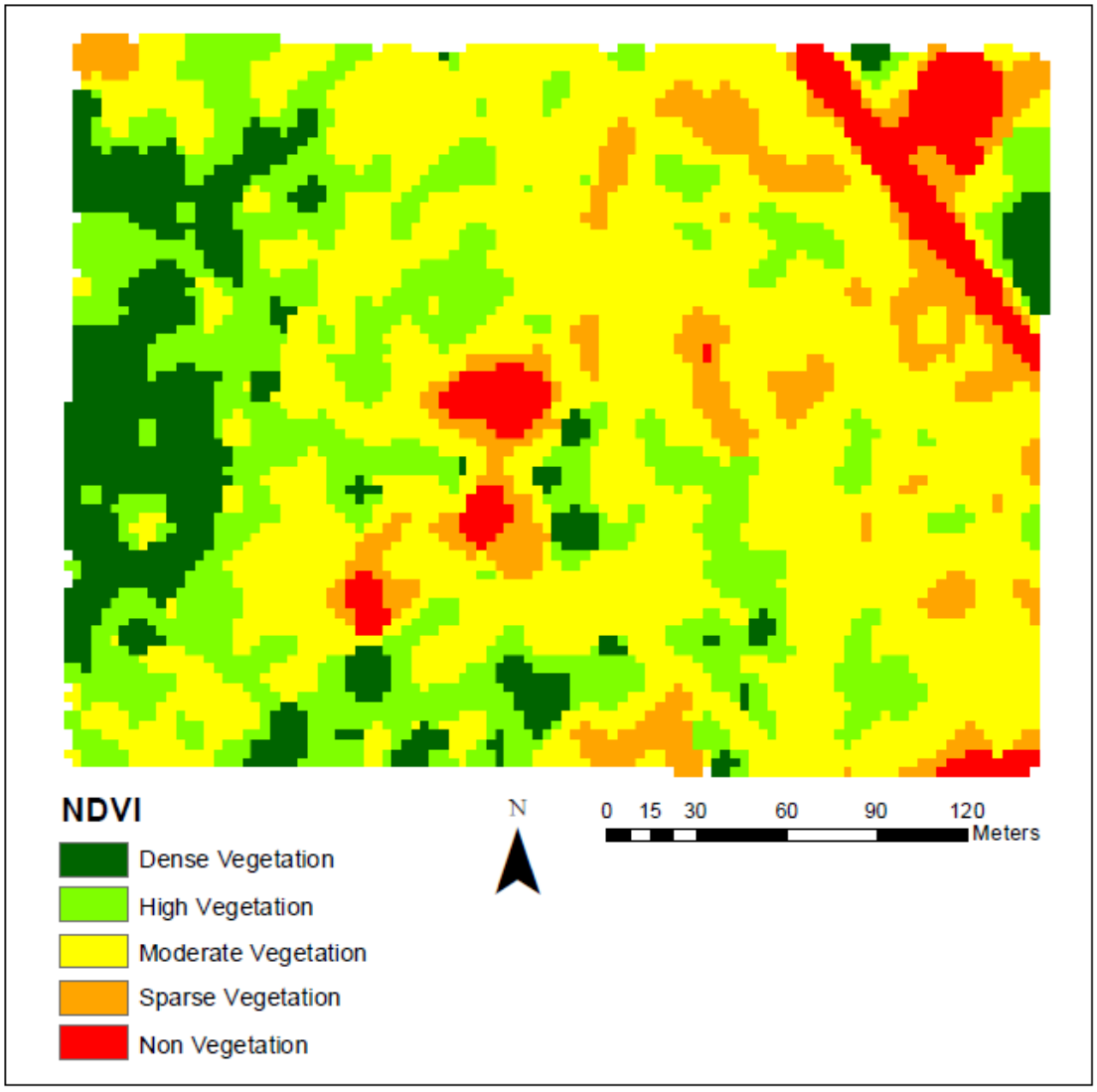

Figure 48: Area 3 NDVI Classification for September 2017.

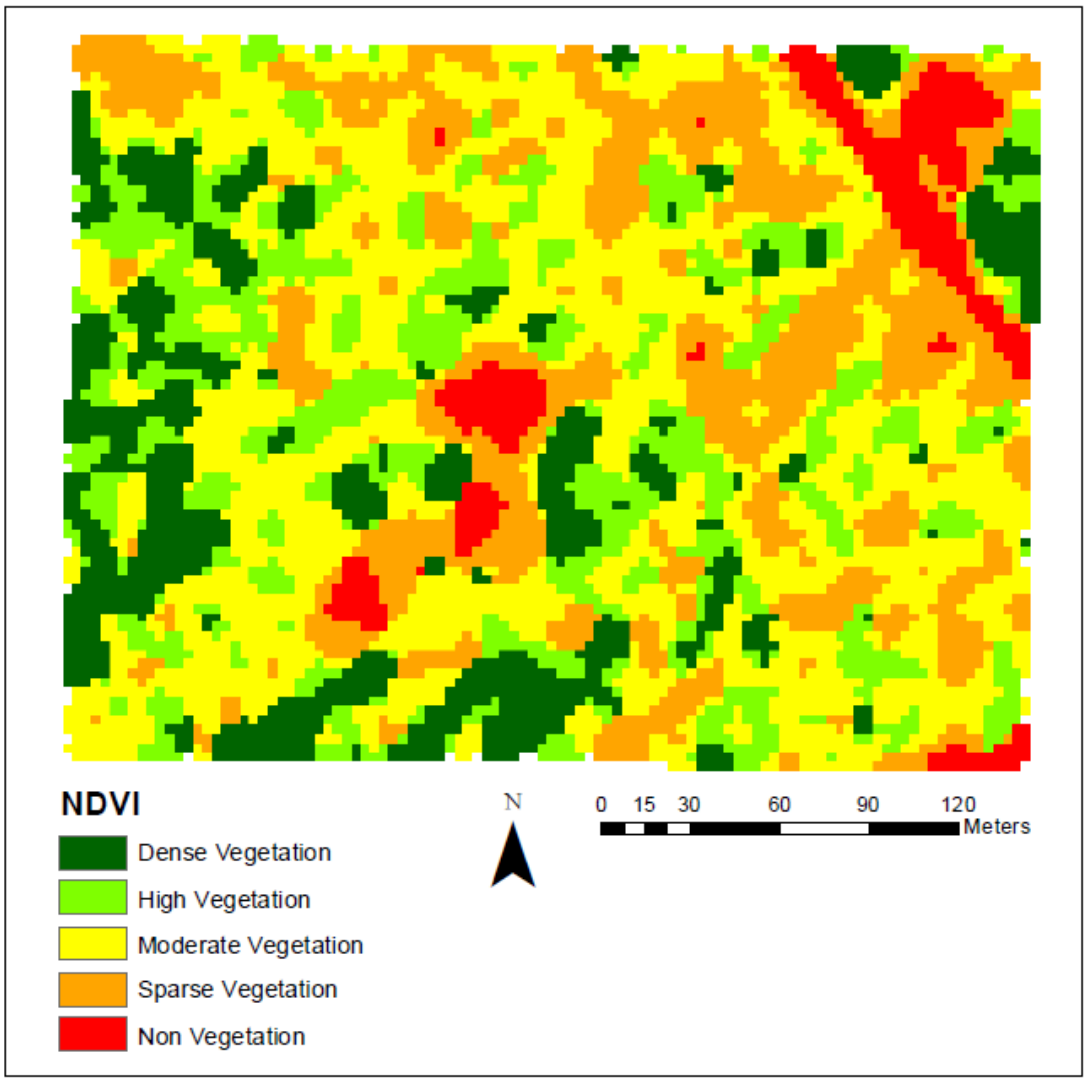

Figure 49: Area 3 NDVI Classification for December 2017.

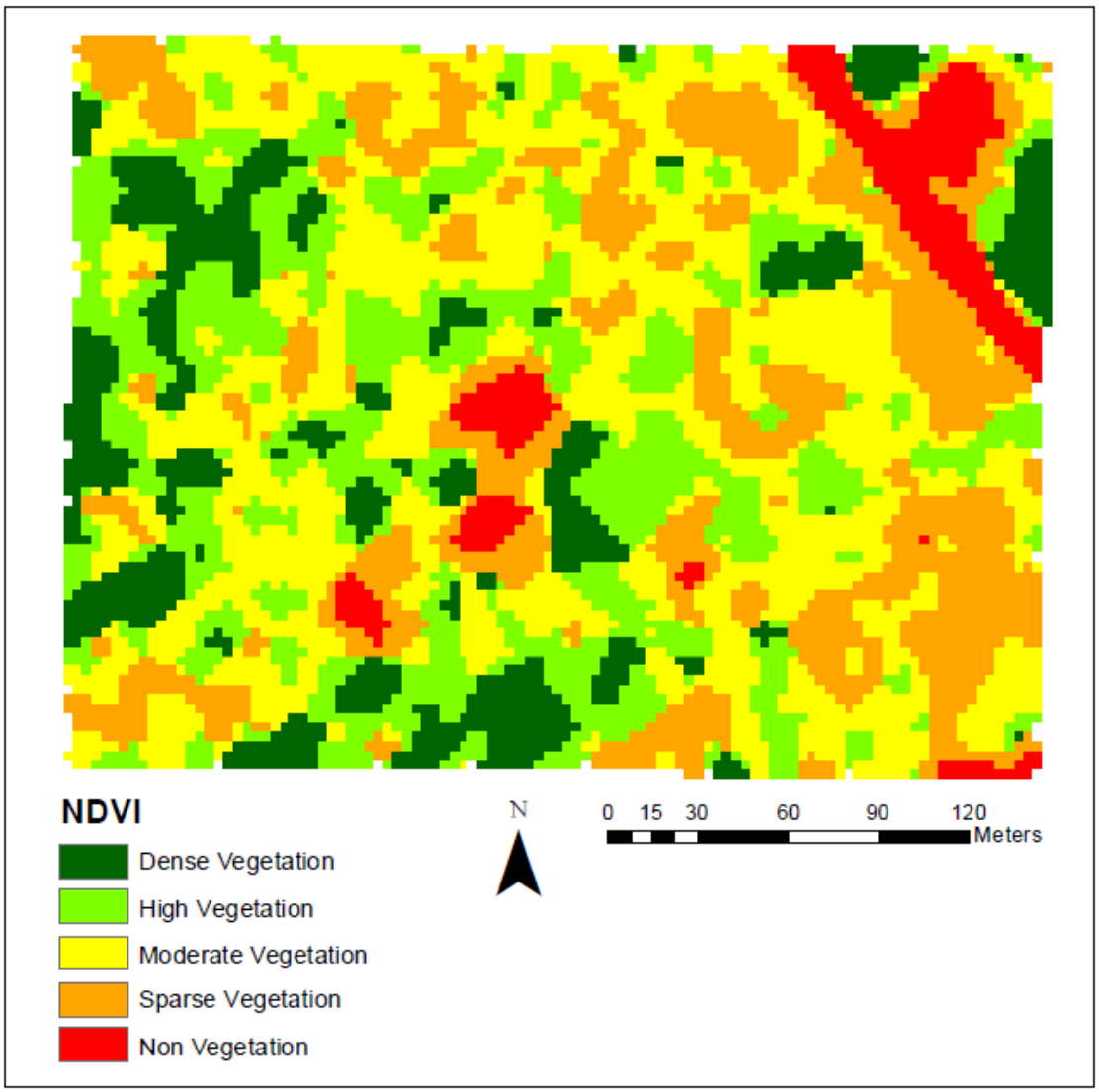

Figure 50: Area 3 NDVI Classification for January 2018.

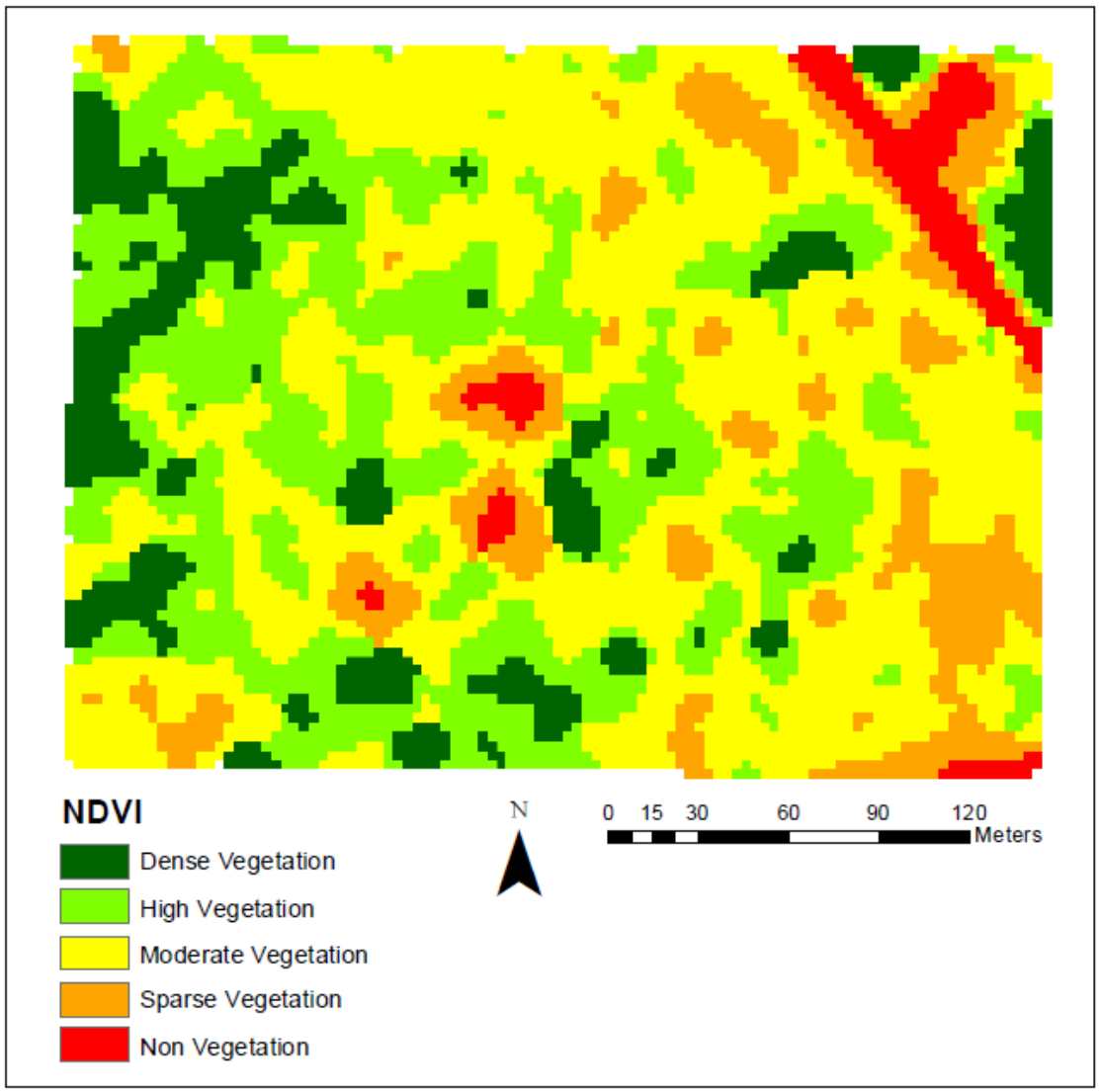

Figure 51: Area 3 NDVI Classification for May 2018.

A.4 Area 4 NDVI Figures

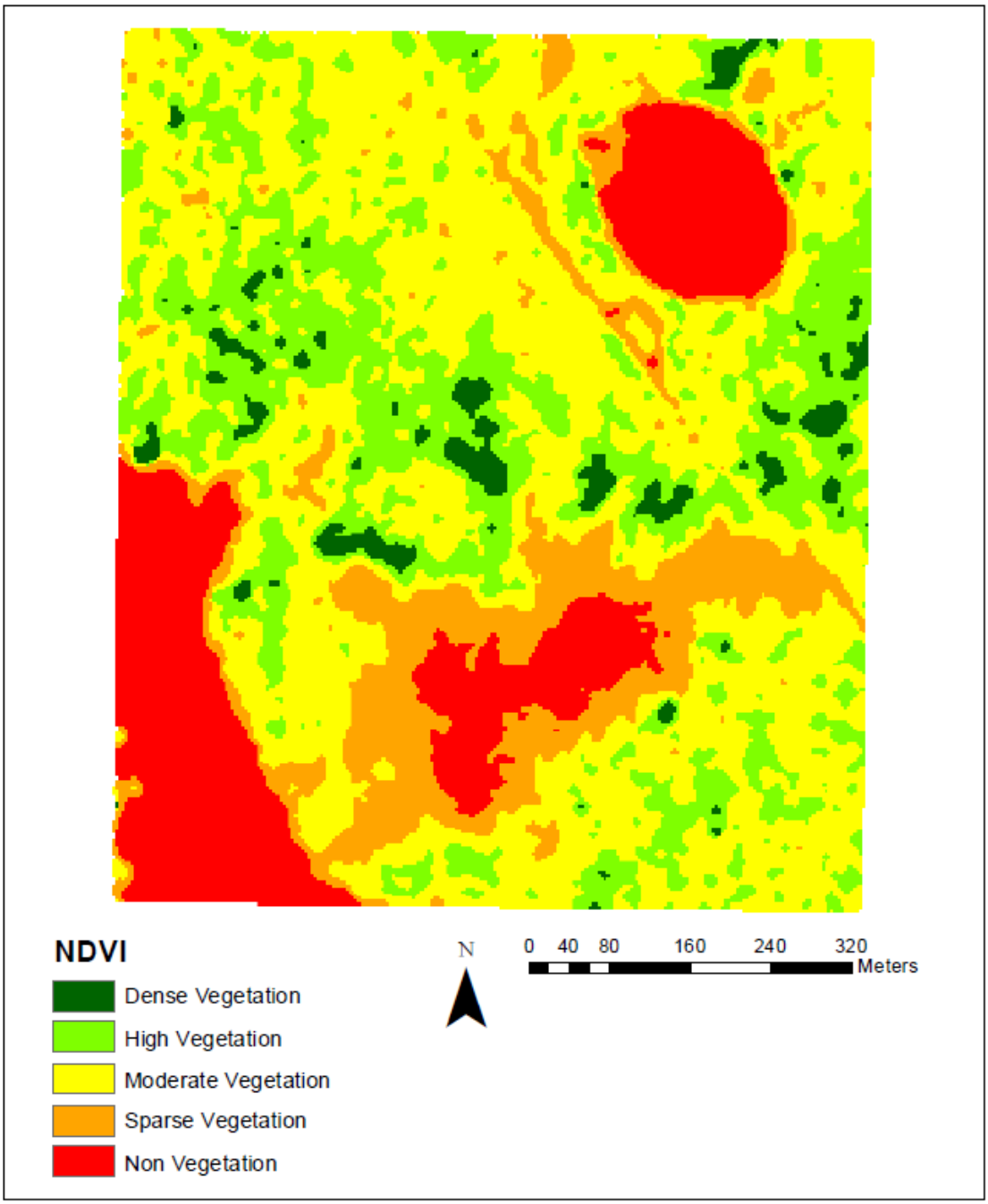

Figure 52: Area 4 NDVI Classification for April 2017.

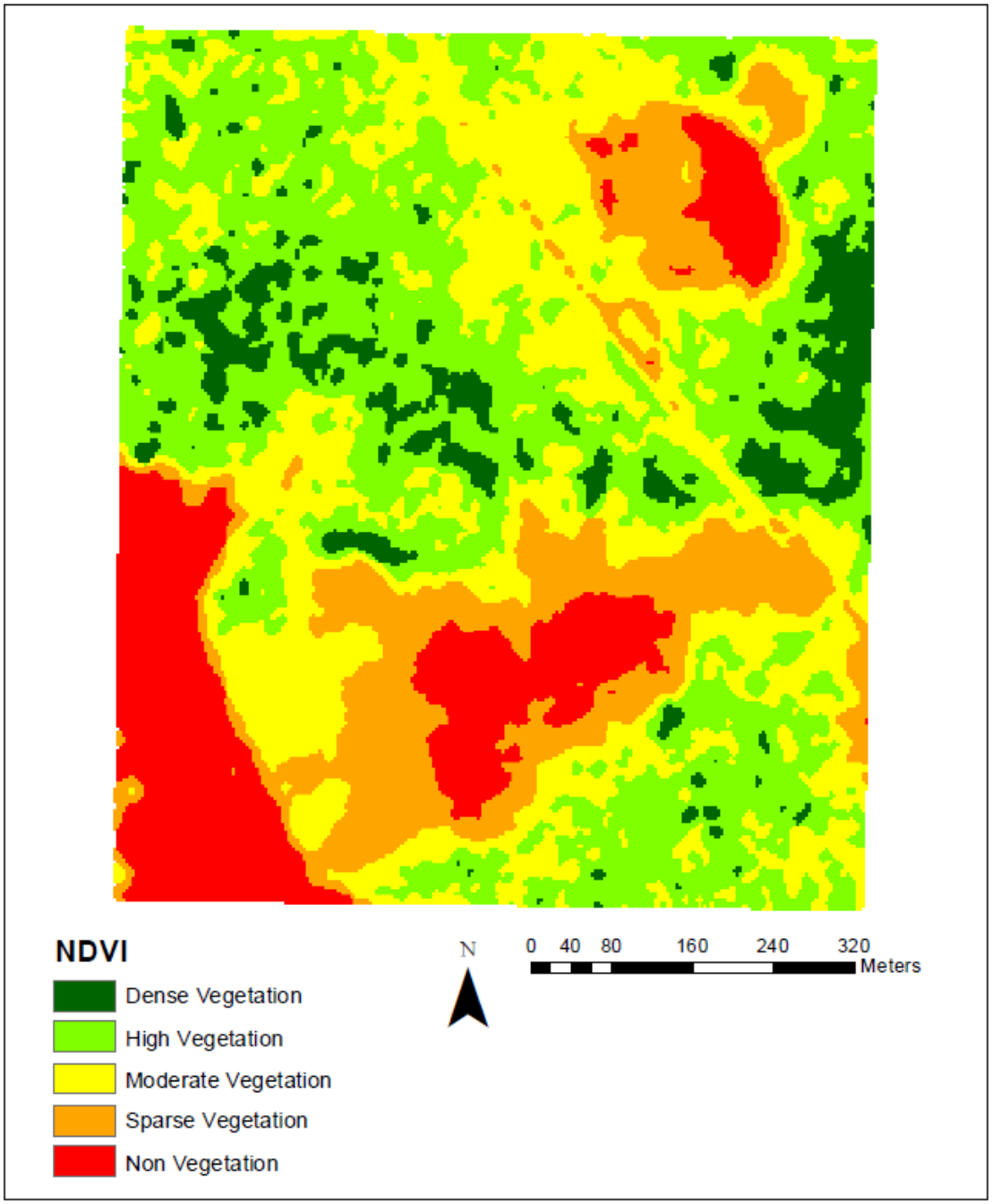

Figure 53: Area 4 NDVI Classification for June 2017.

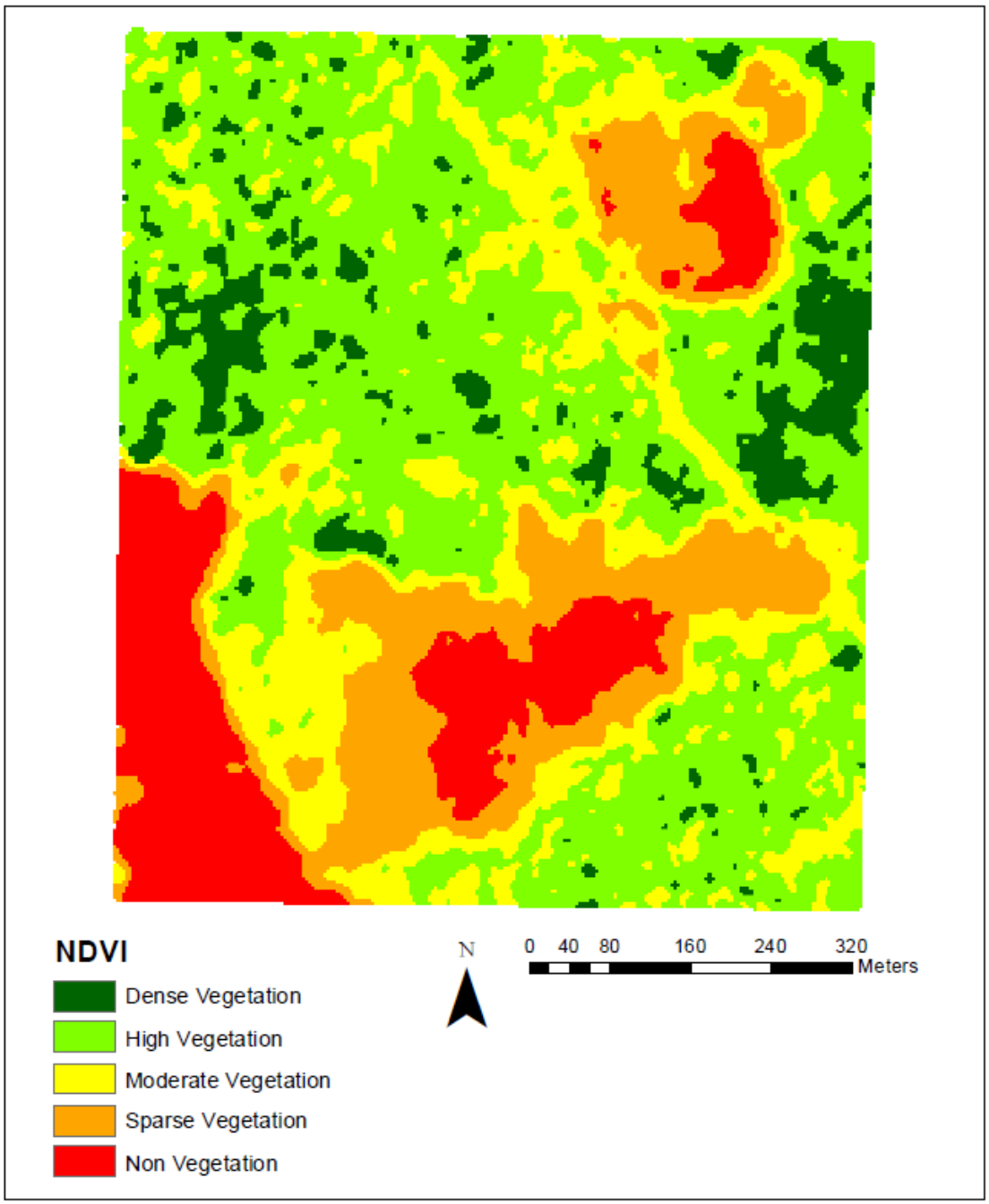

Figure 54: Area 4 NDVI Classification for August 2017.

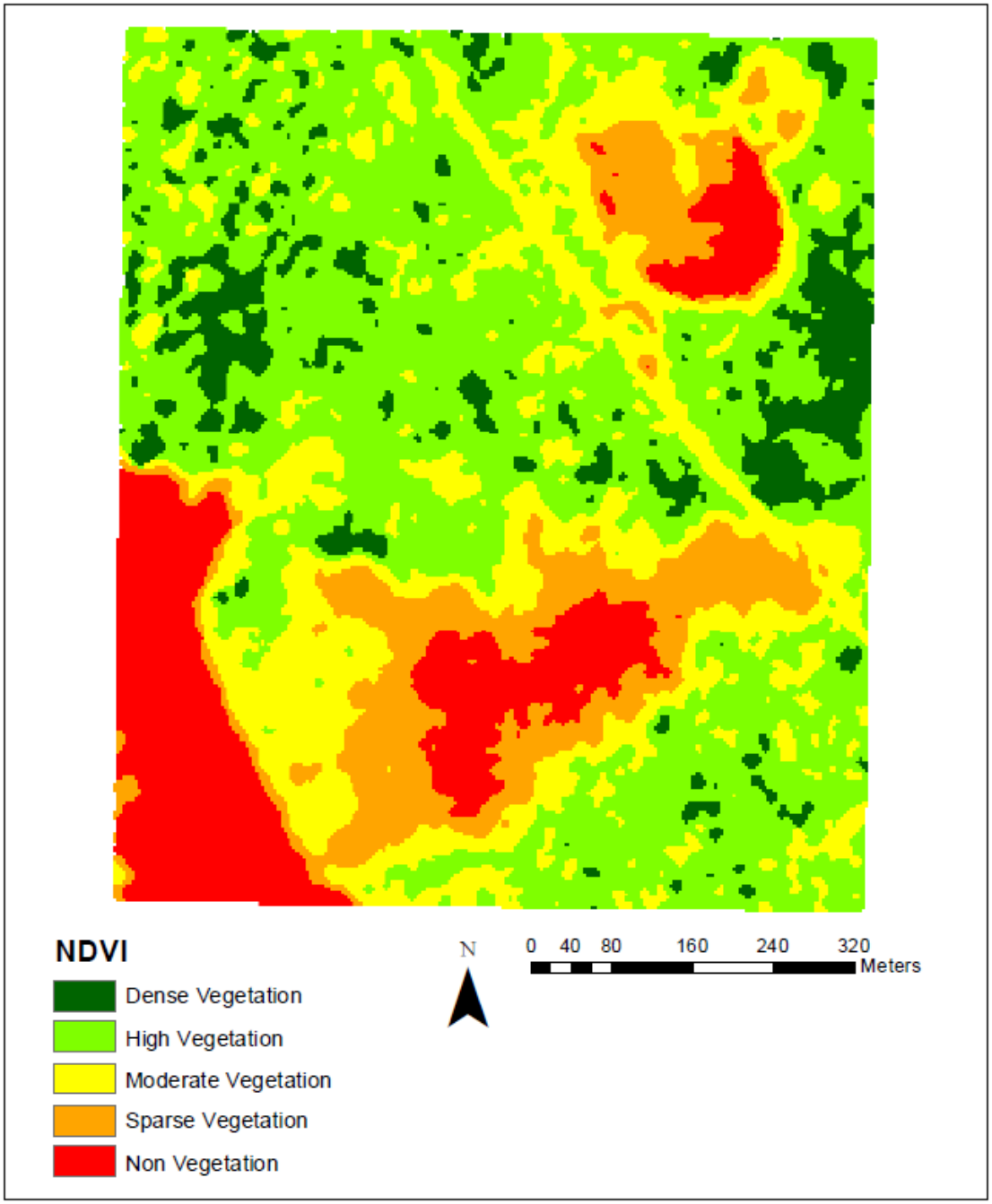

Figure 55: Area 4 NDVI Classification for September 2017.

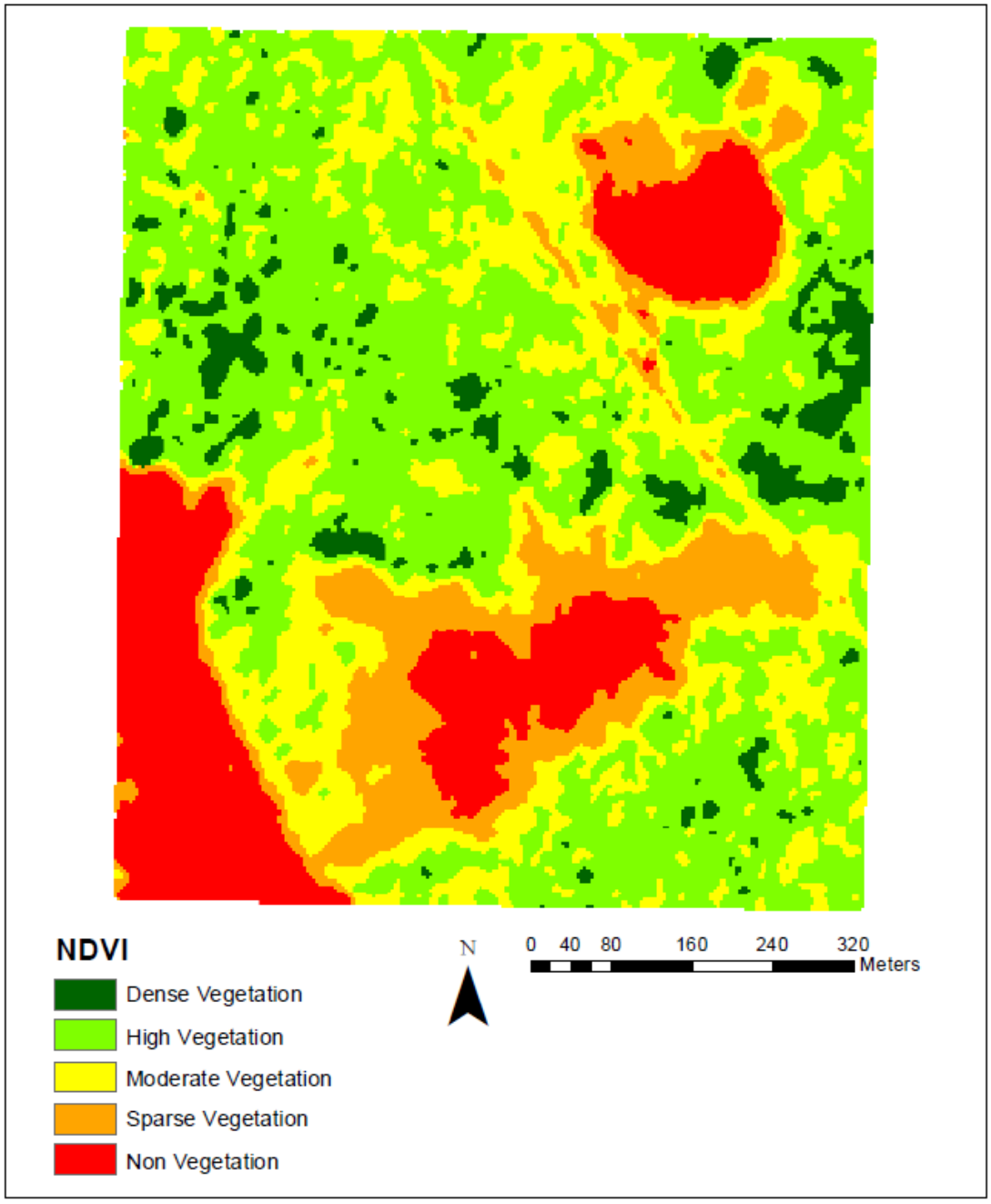

Figure 56: Area 4 NDVI Classification for December 2017.

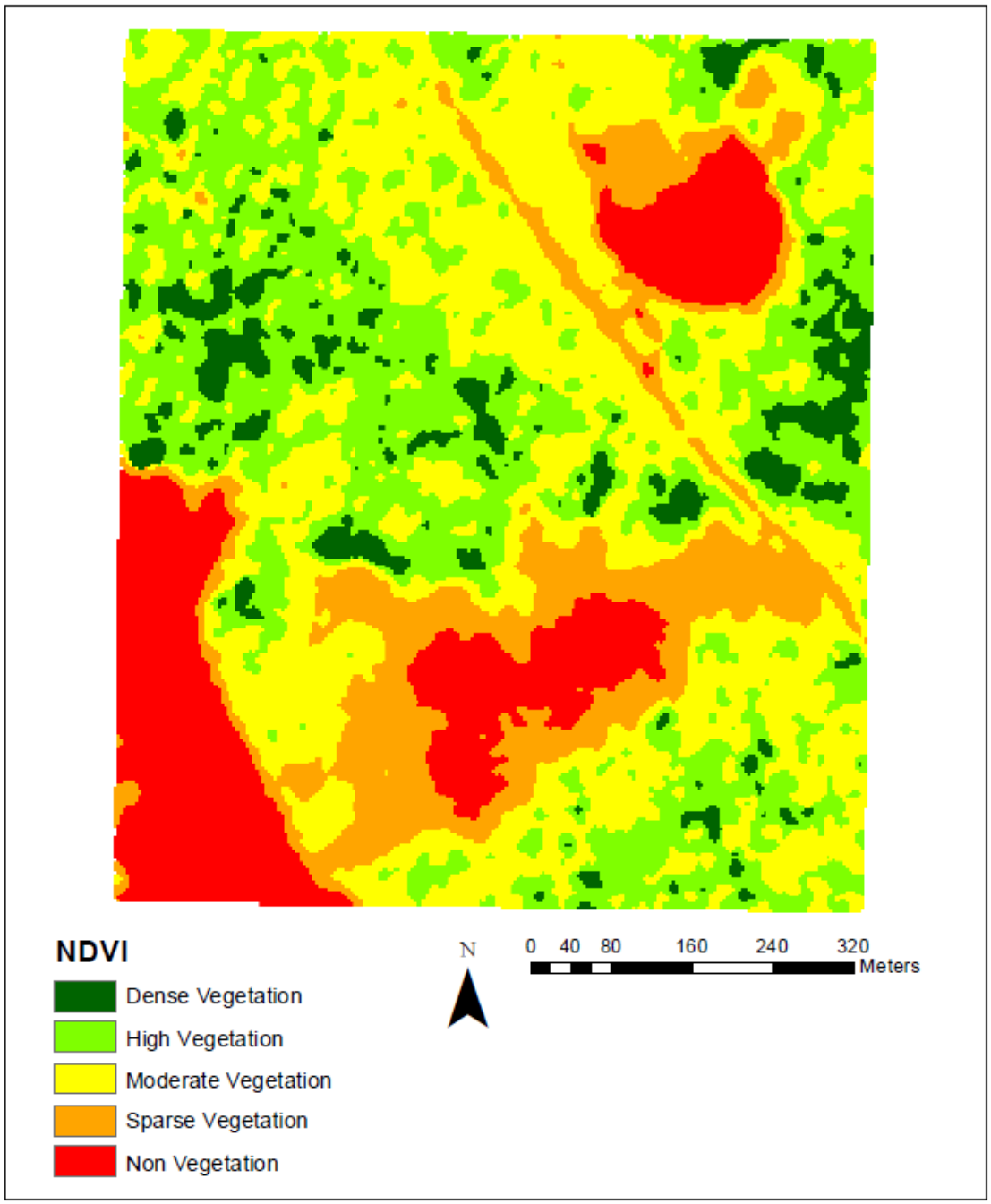

Figure 57: Area 4 NDVI Classification for January 2018.

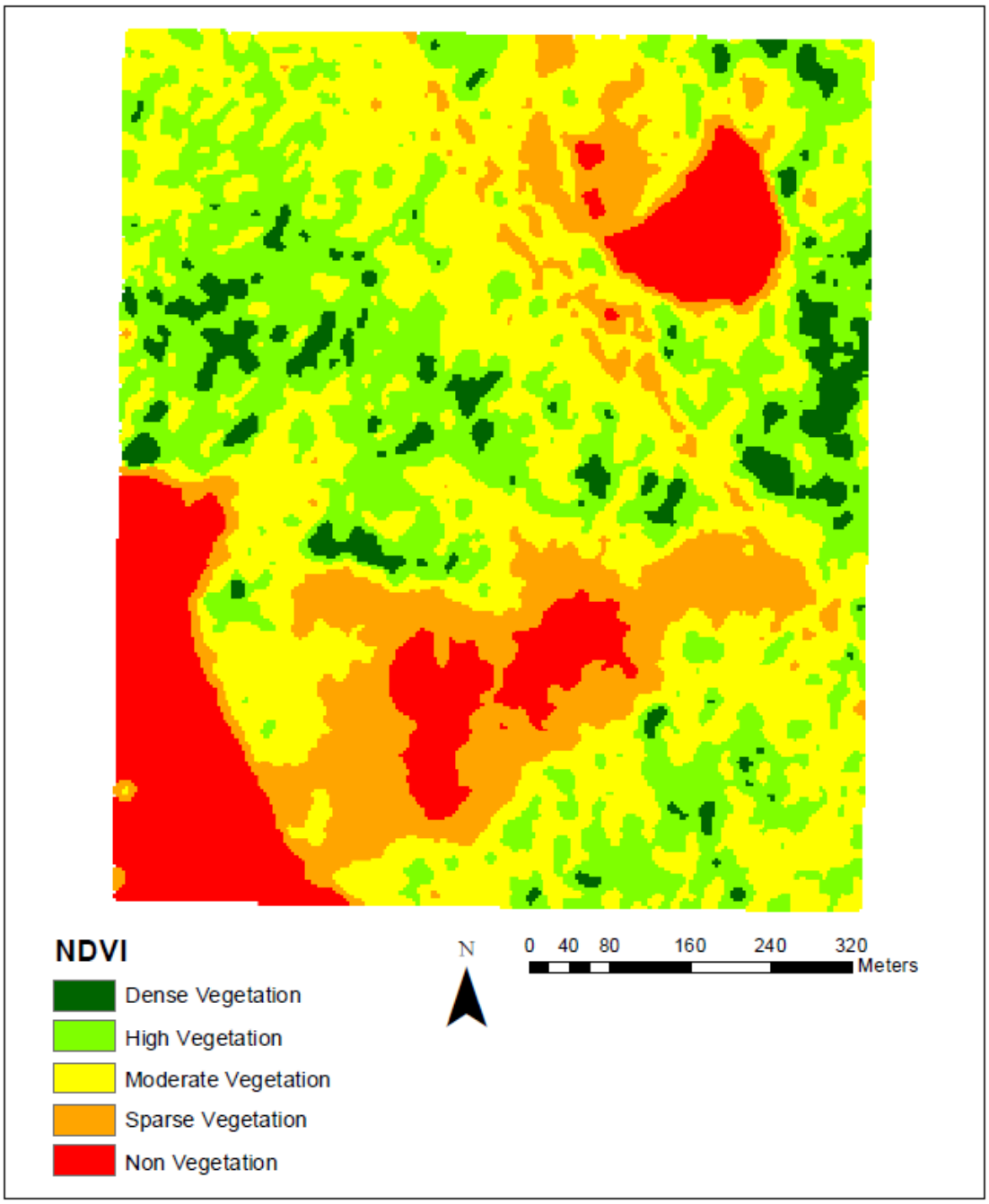

Figure 58: Area 4 NDVI Classification for February 2018.

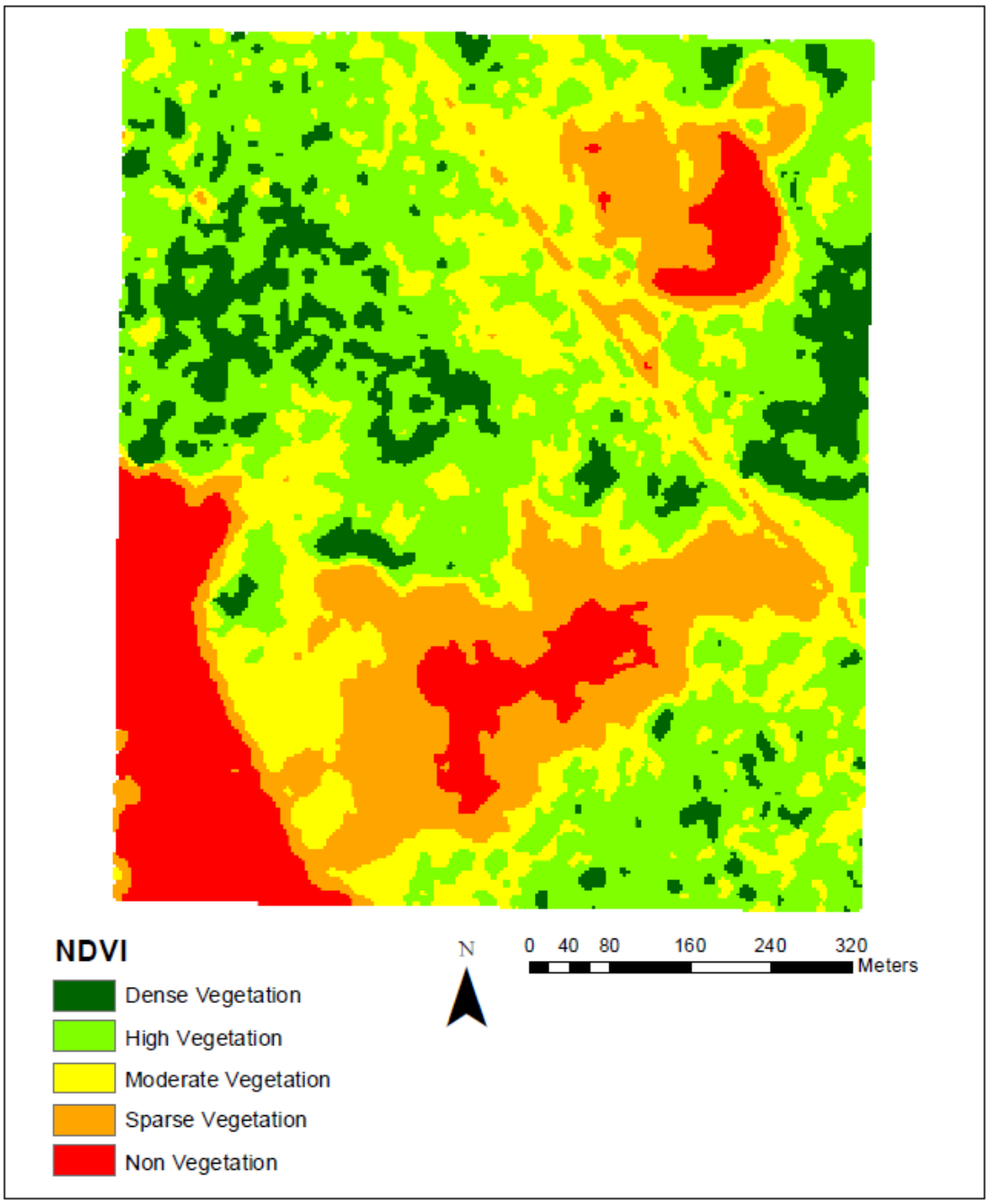

Figure 59: Area 4 NDVI Classification for March 2018.

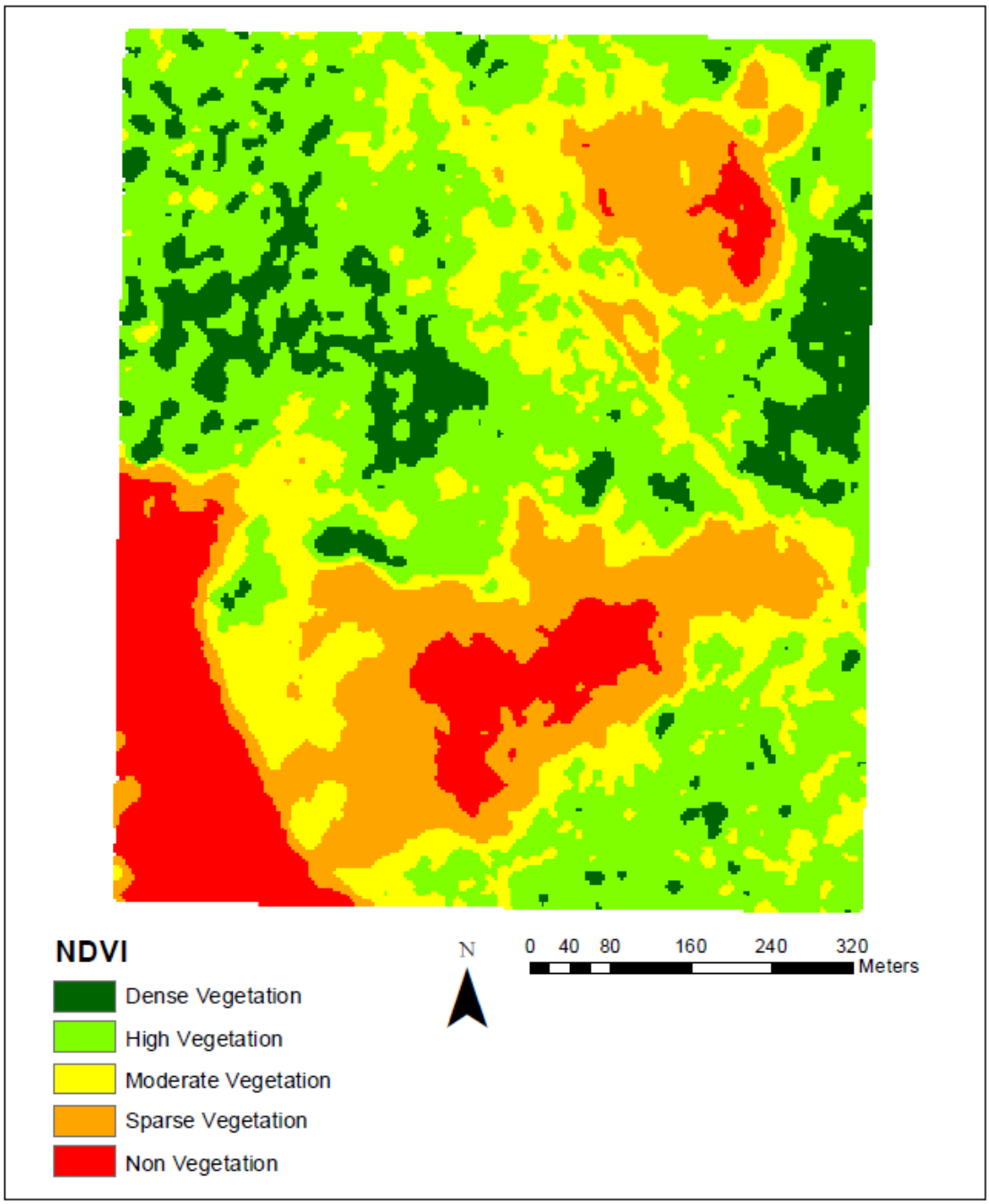

Figure 60: Area 4 NDVI Classification for May 2018.

A.5 Area 5 NDVI Figures

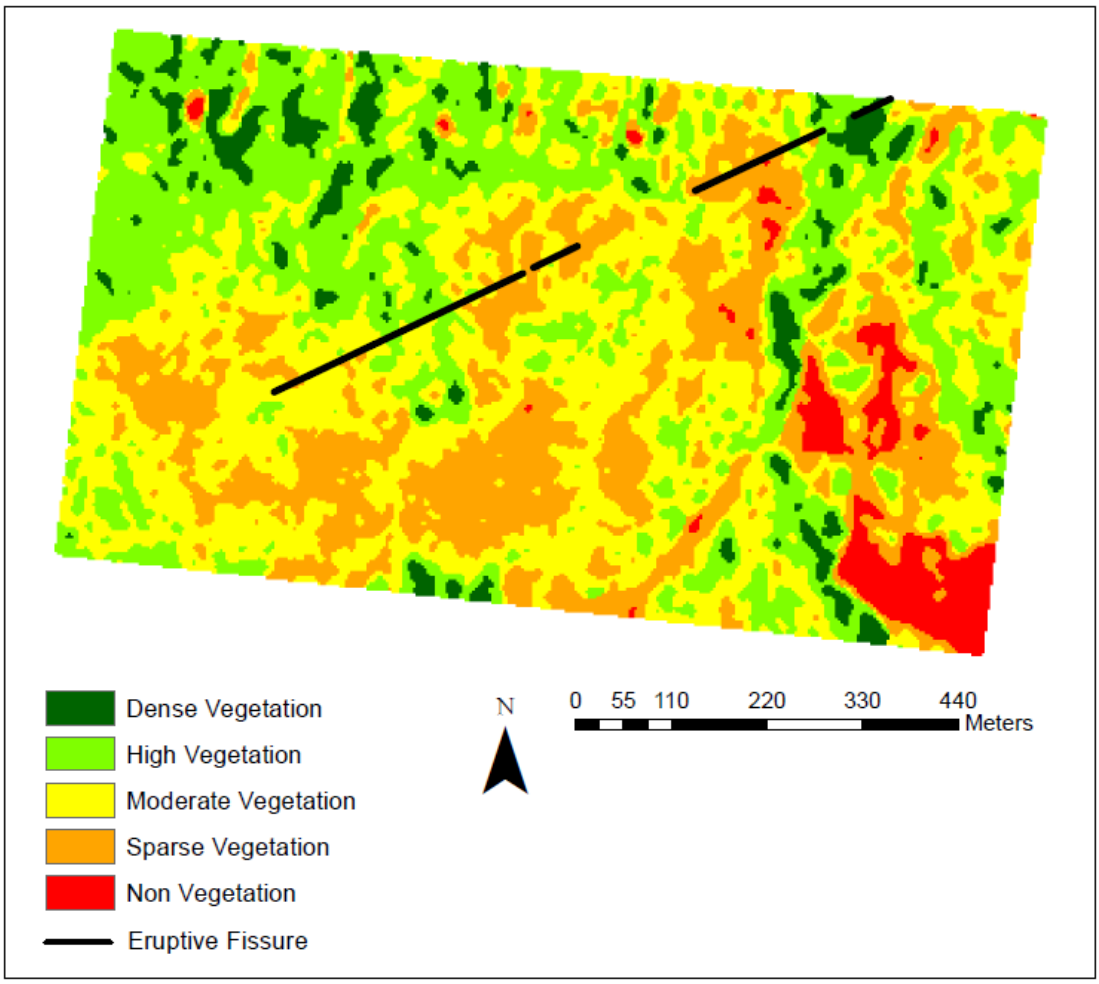

Figure 61: Area 5 NDVI Classification for April 2017.

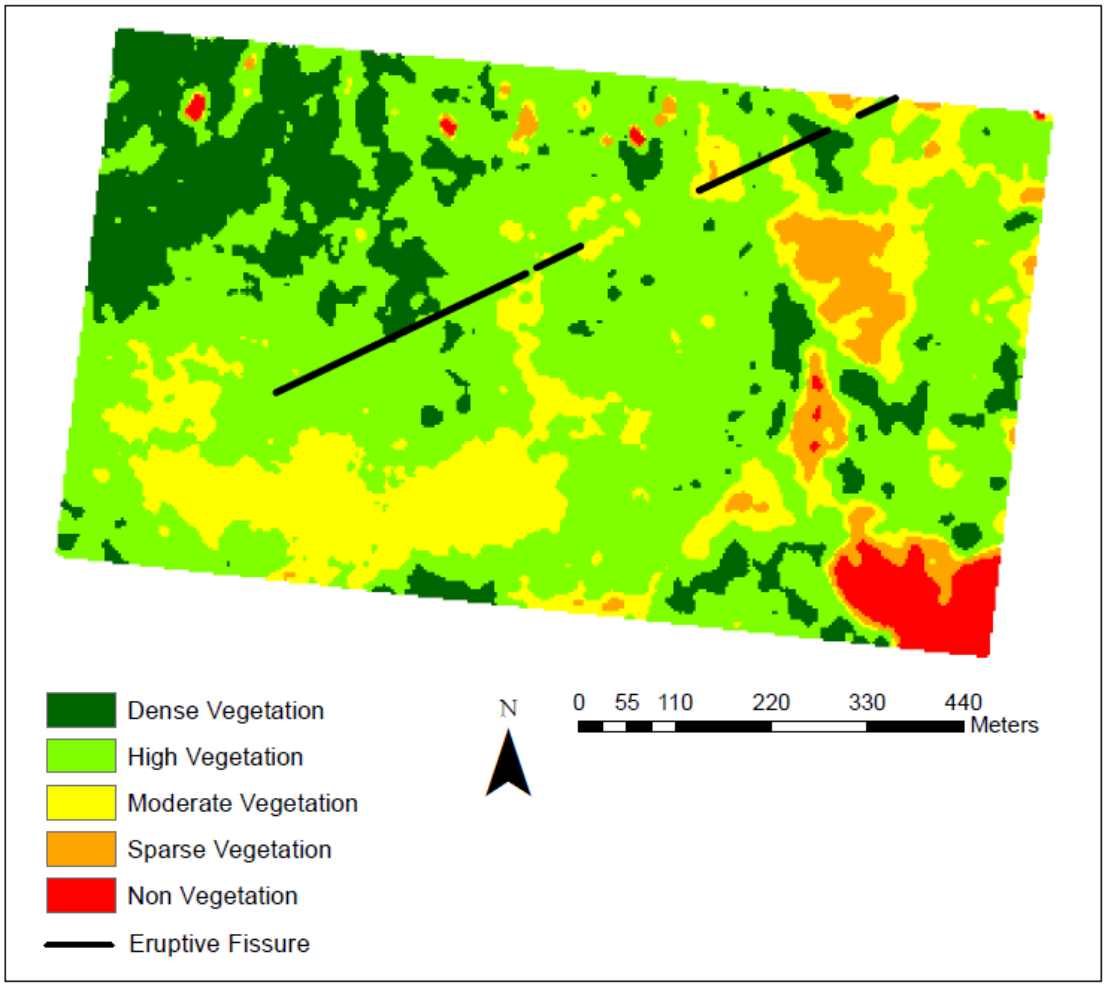

Figure 62: Area 5 NDVI Classification for September 2017.

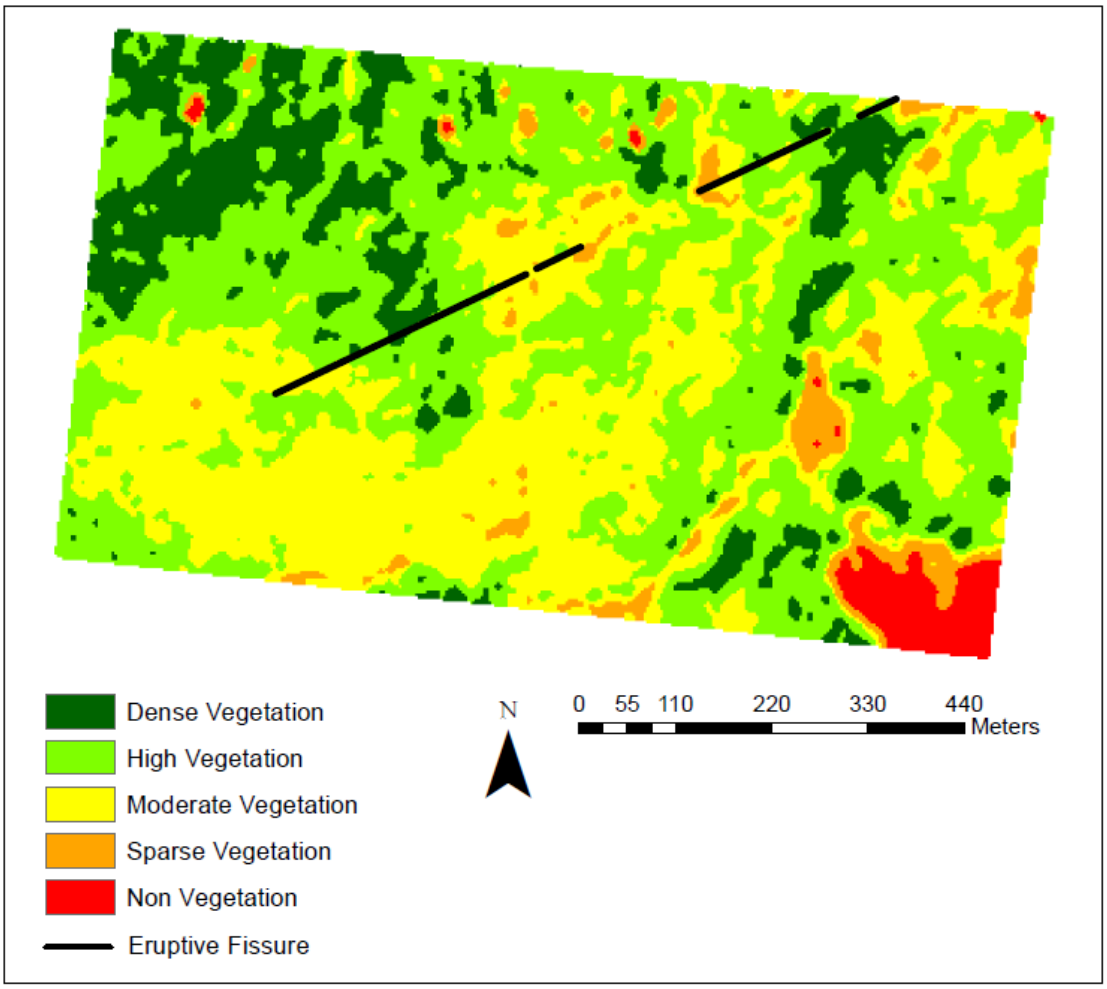

Figure 63: Area 5 NDVI Classification for January 2018.

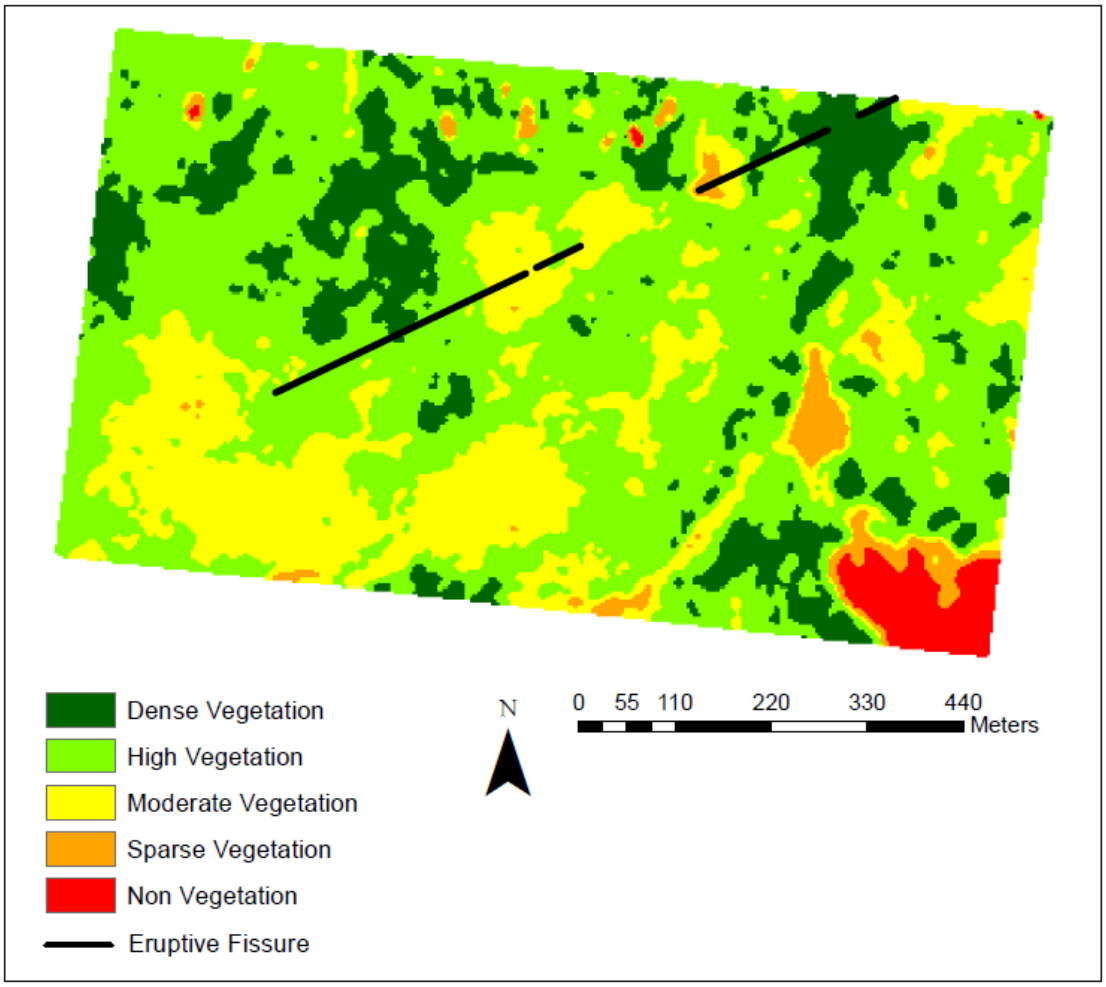

Figure 64: Area 5 NDVI Classification for February 2018.

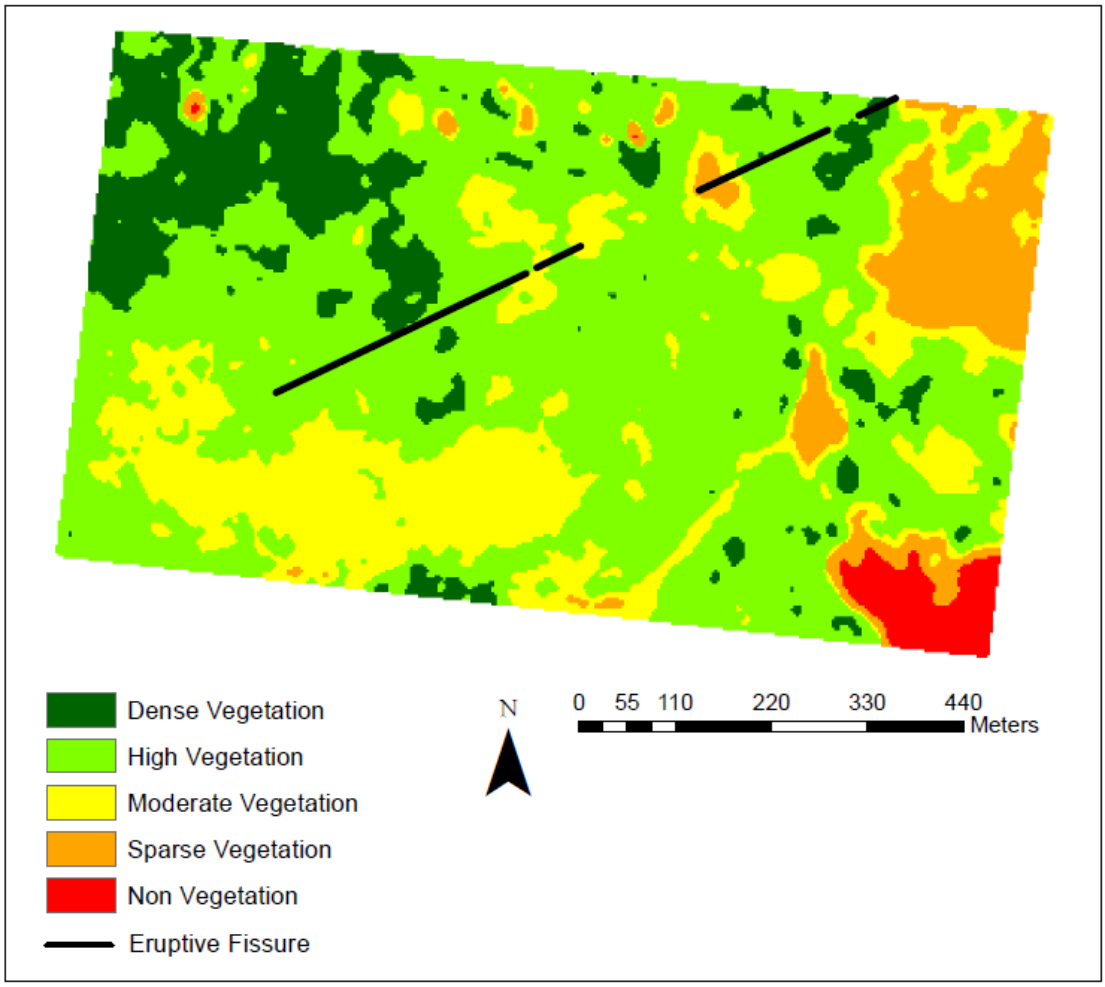

Figure 65: Area 5 NDVI Classification for April 2018.

A.6 Area 6 NDVI Figures

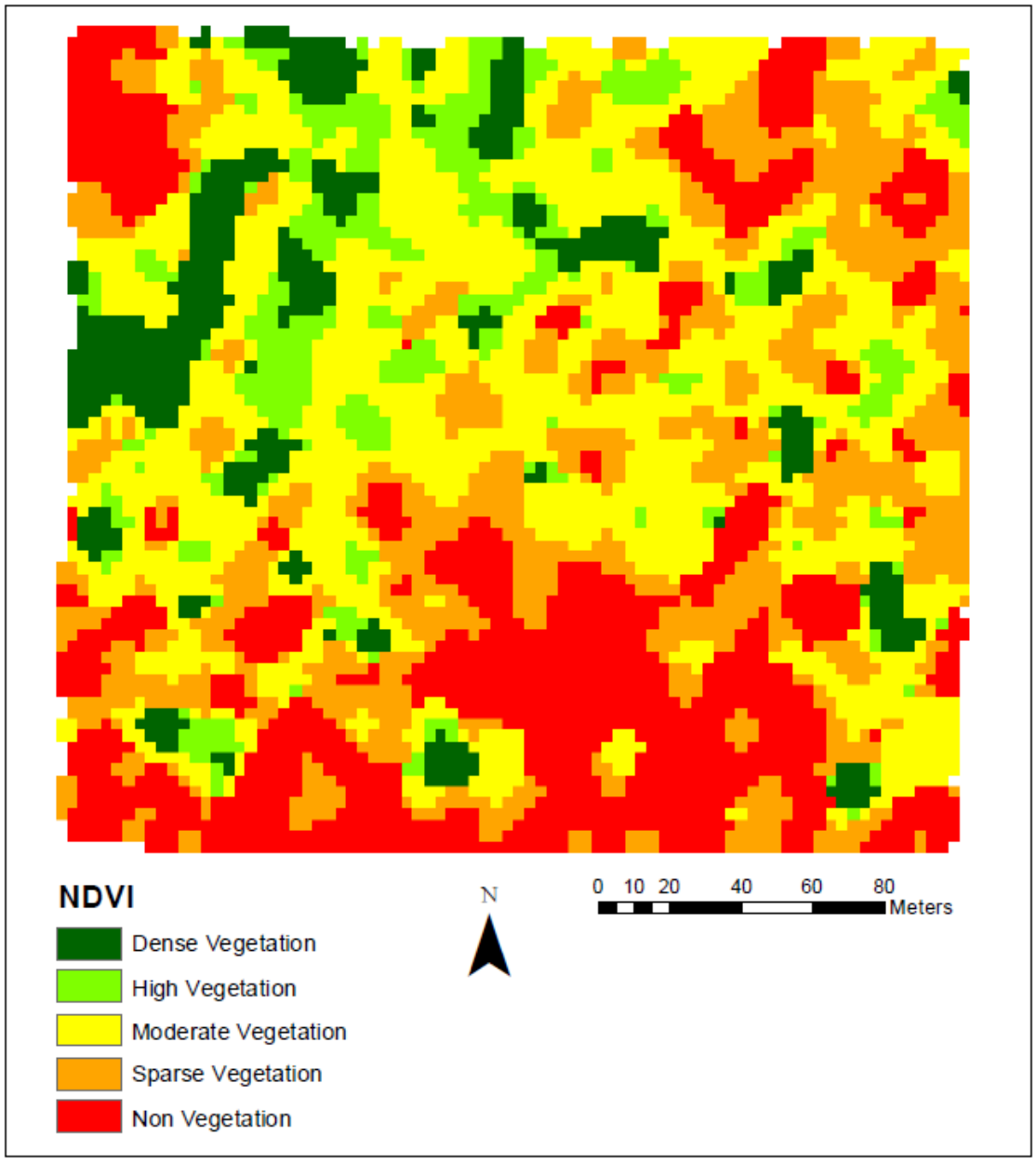

Figure 66: Area 6 NDVI Classification for April 2017.

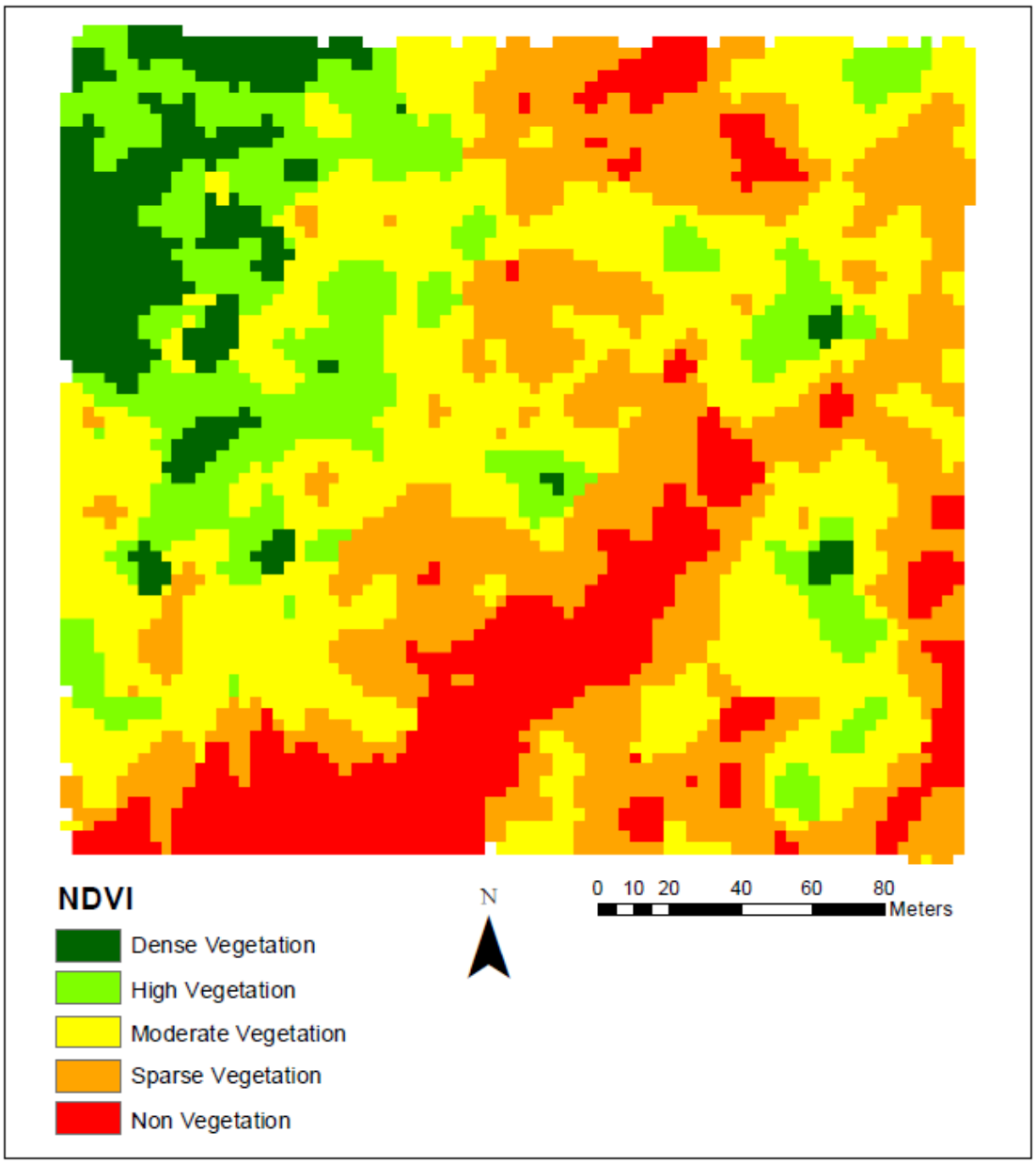

Figure 67: Area 6 NDVI Classification for September 2017.

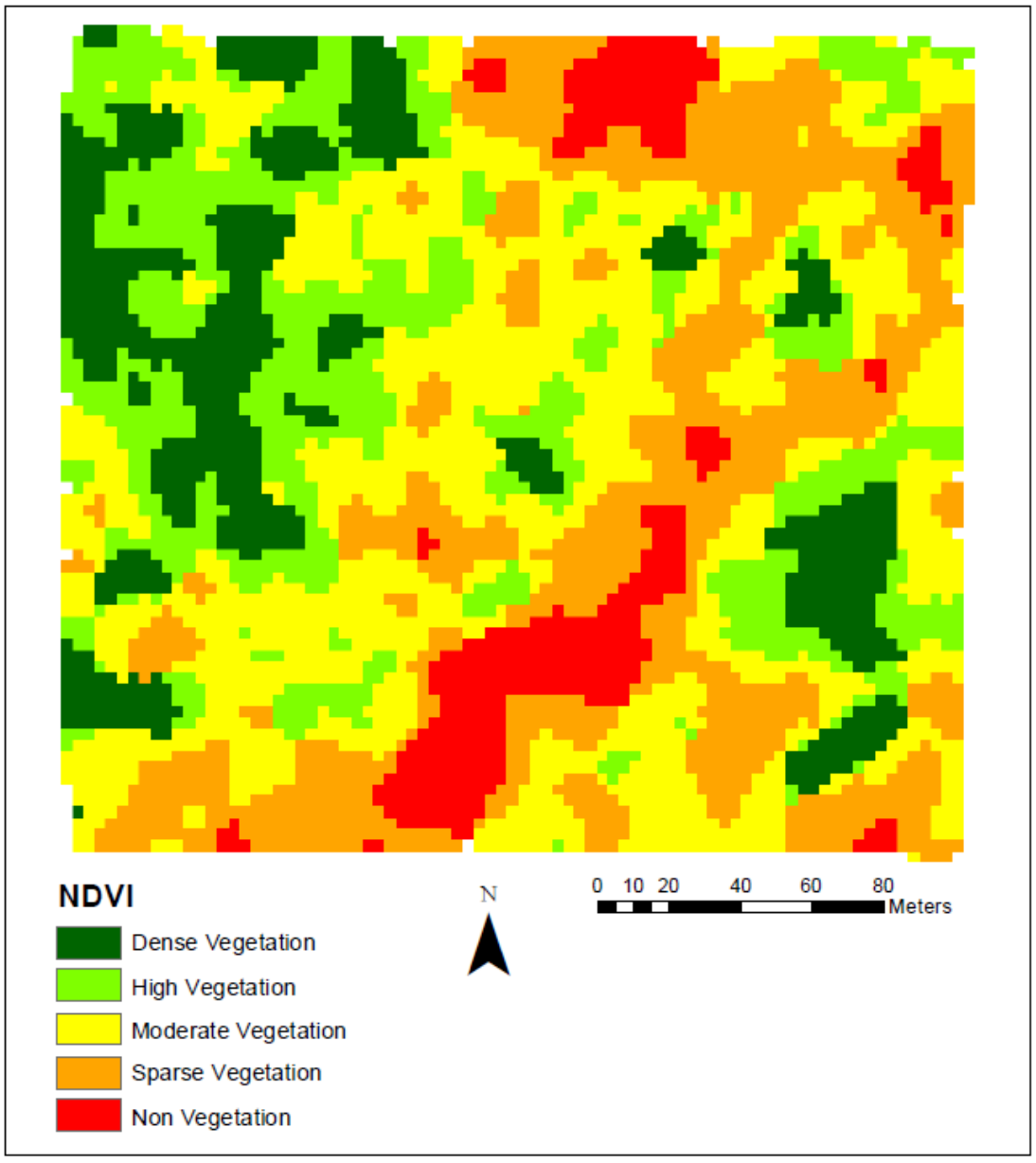

Figure 68: Area 6 NDVI Classification for December 2017.

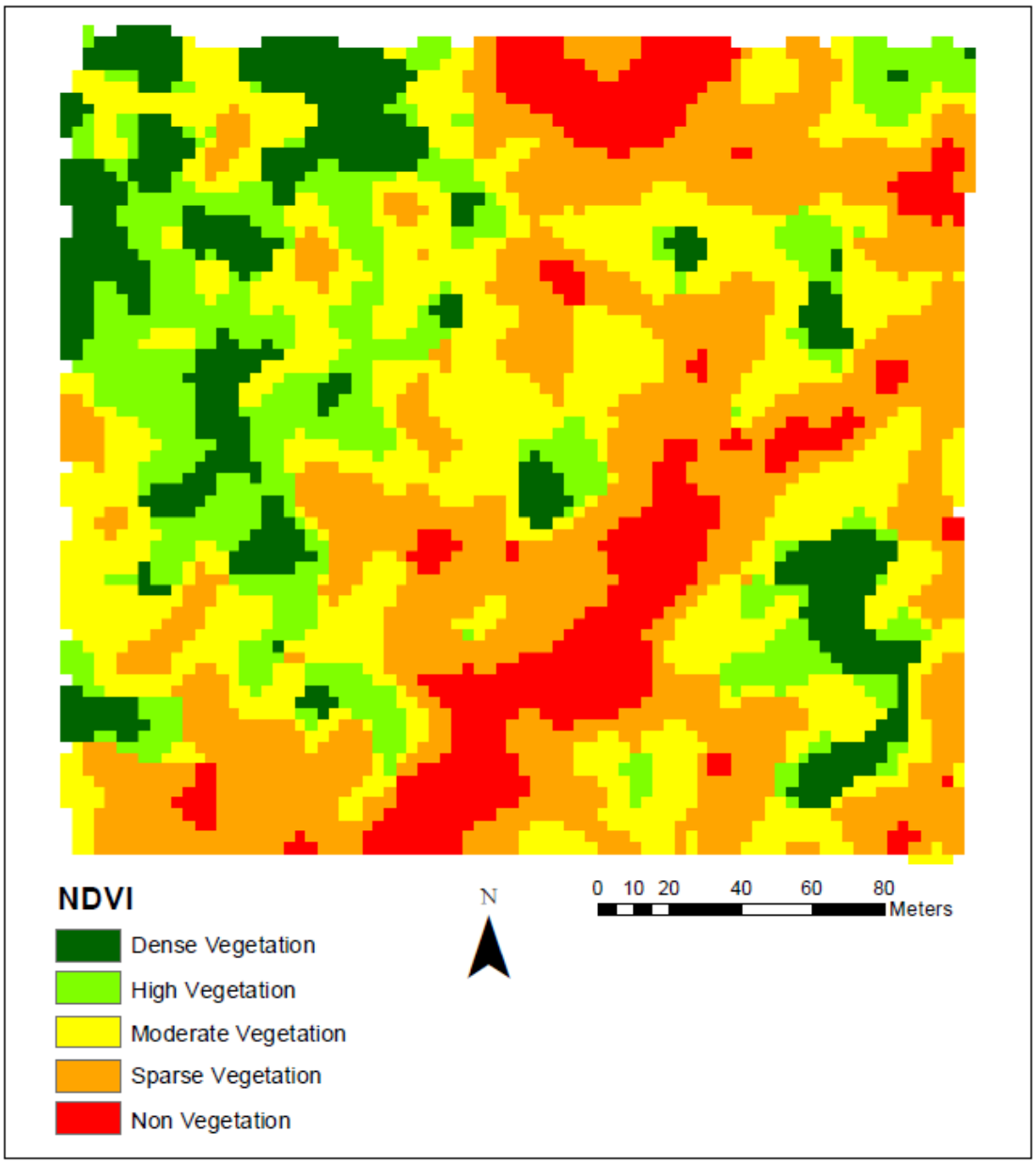

Figure 69: Area 6 NDVI Classification for January 2018.

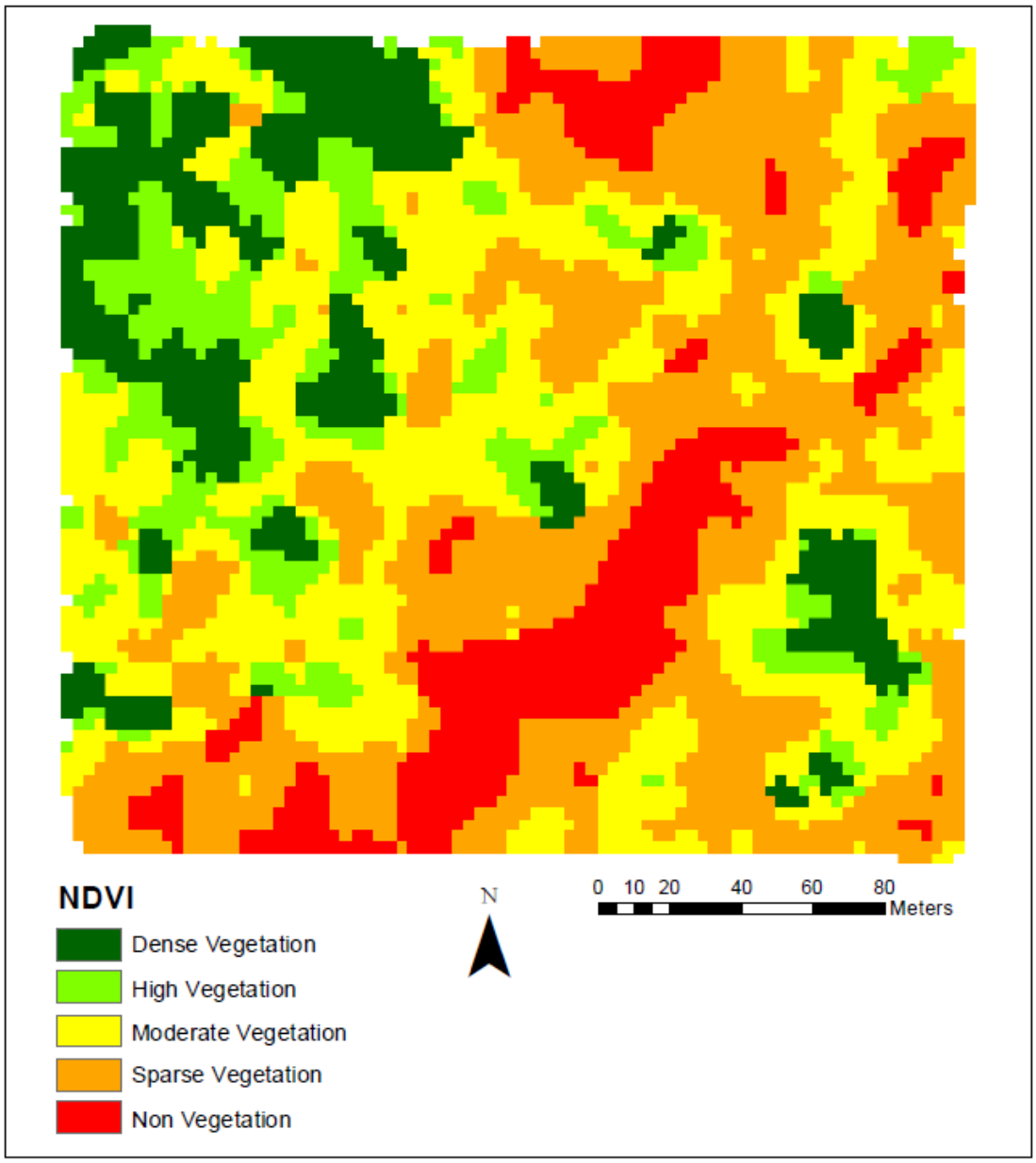

Figure 70: Area 6 NDVI Classification for February 2018.

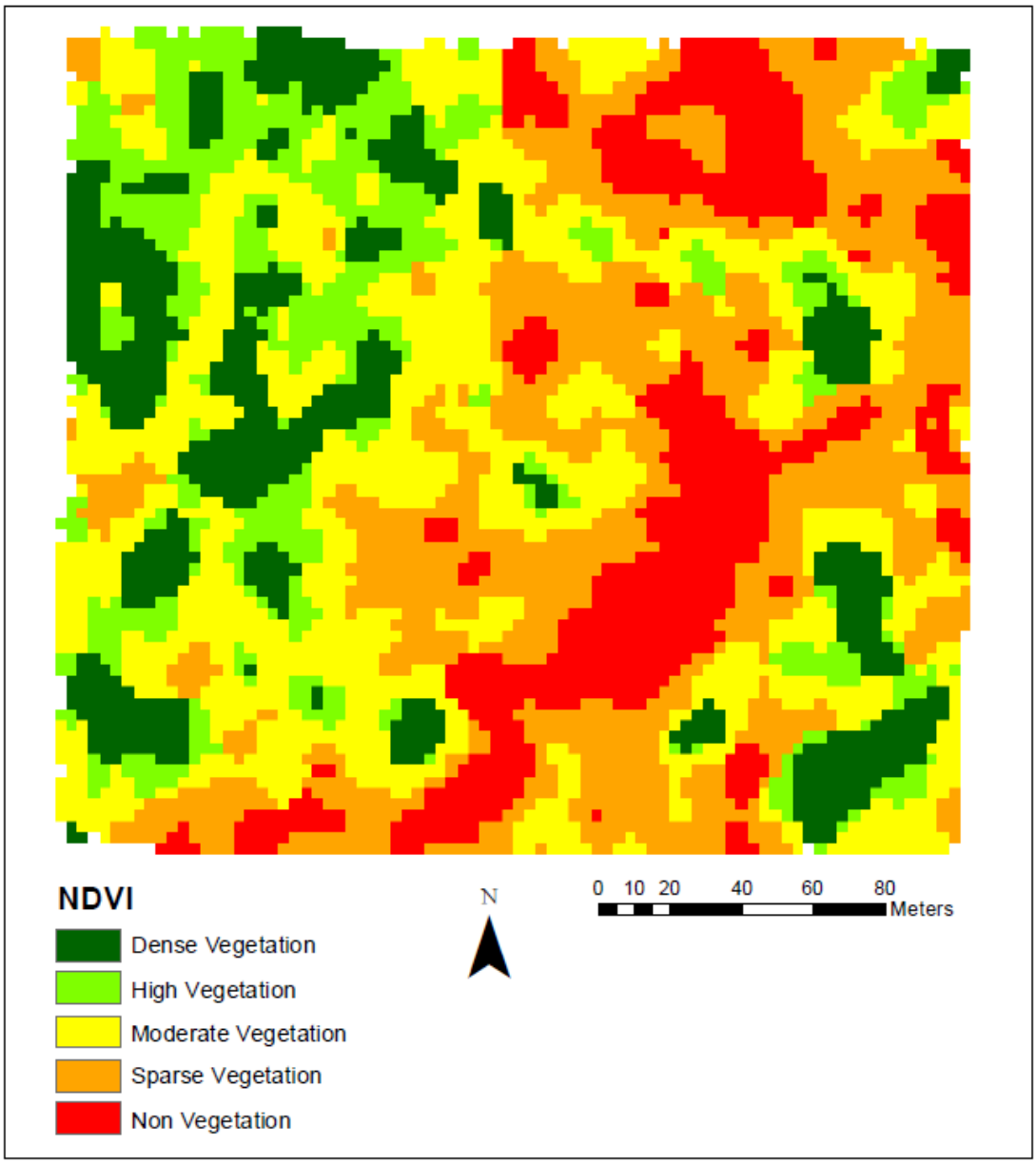

Figure 71: Area 6 NDVI Classification for May 2018.

A.7 Area 7 NDVI Figures

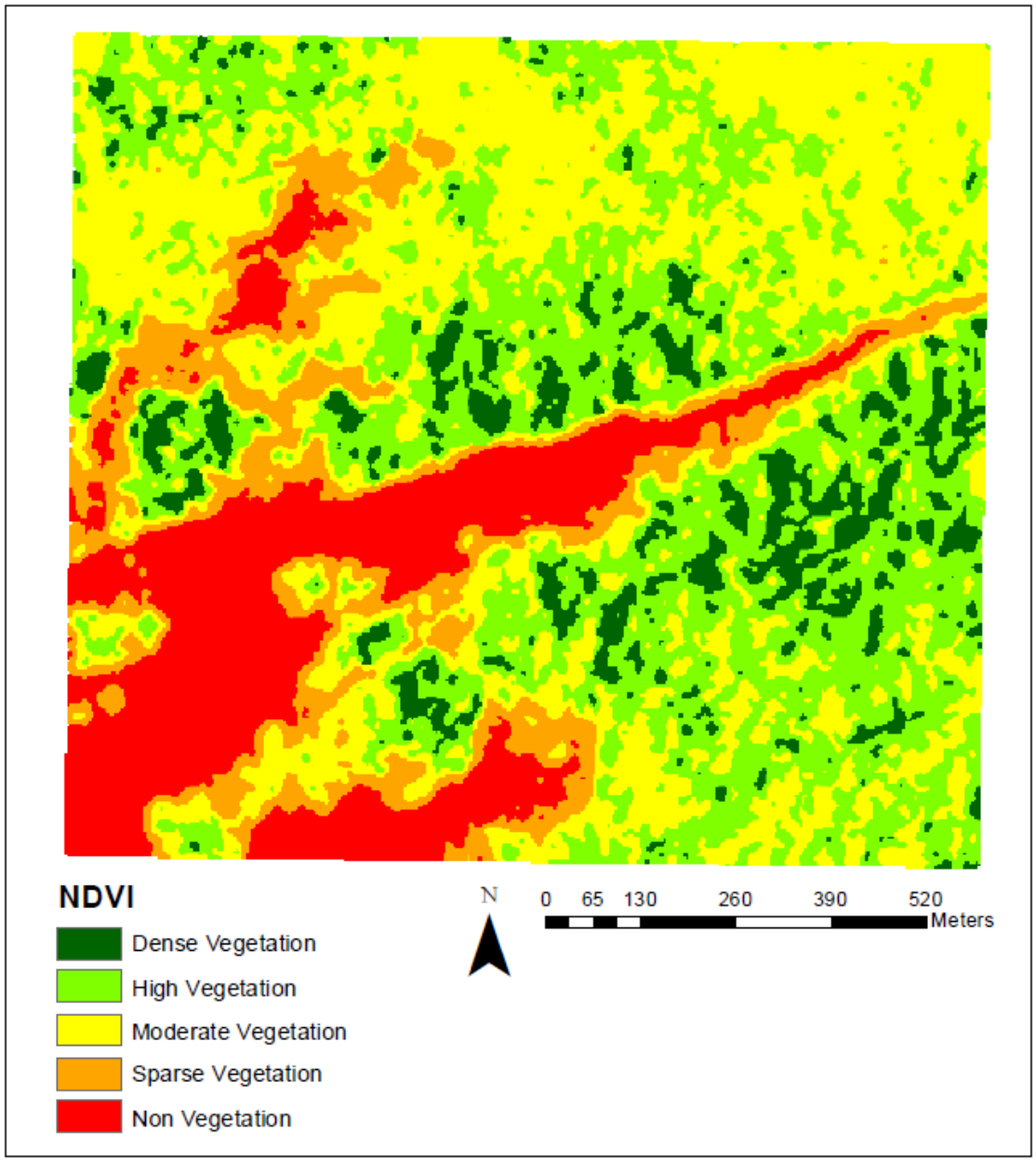

Figure 72: Area 7 NDVI Classification for April 2017.

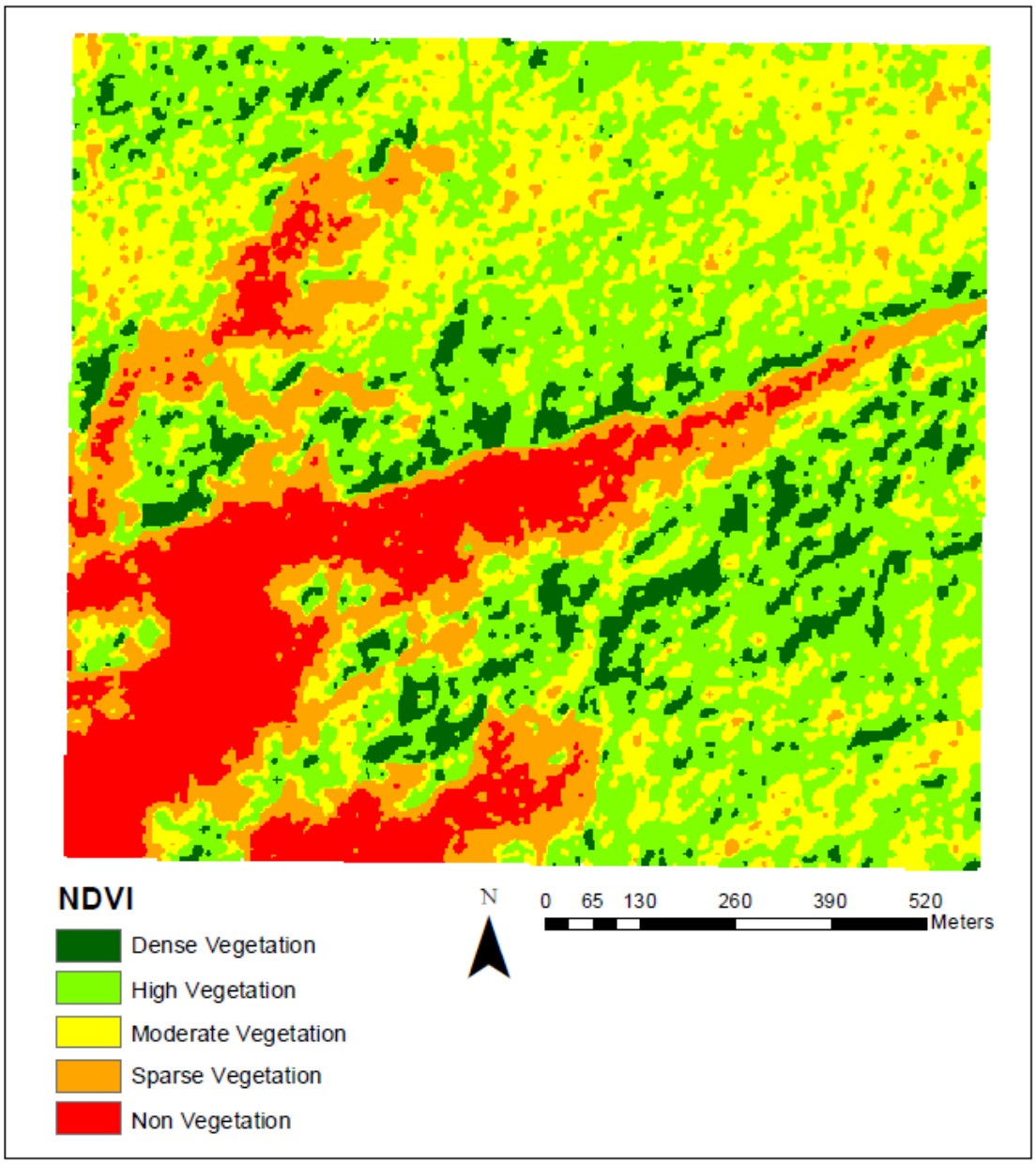

Figure 73: Area 7 NDVI Classification for December 2017.

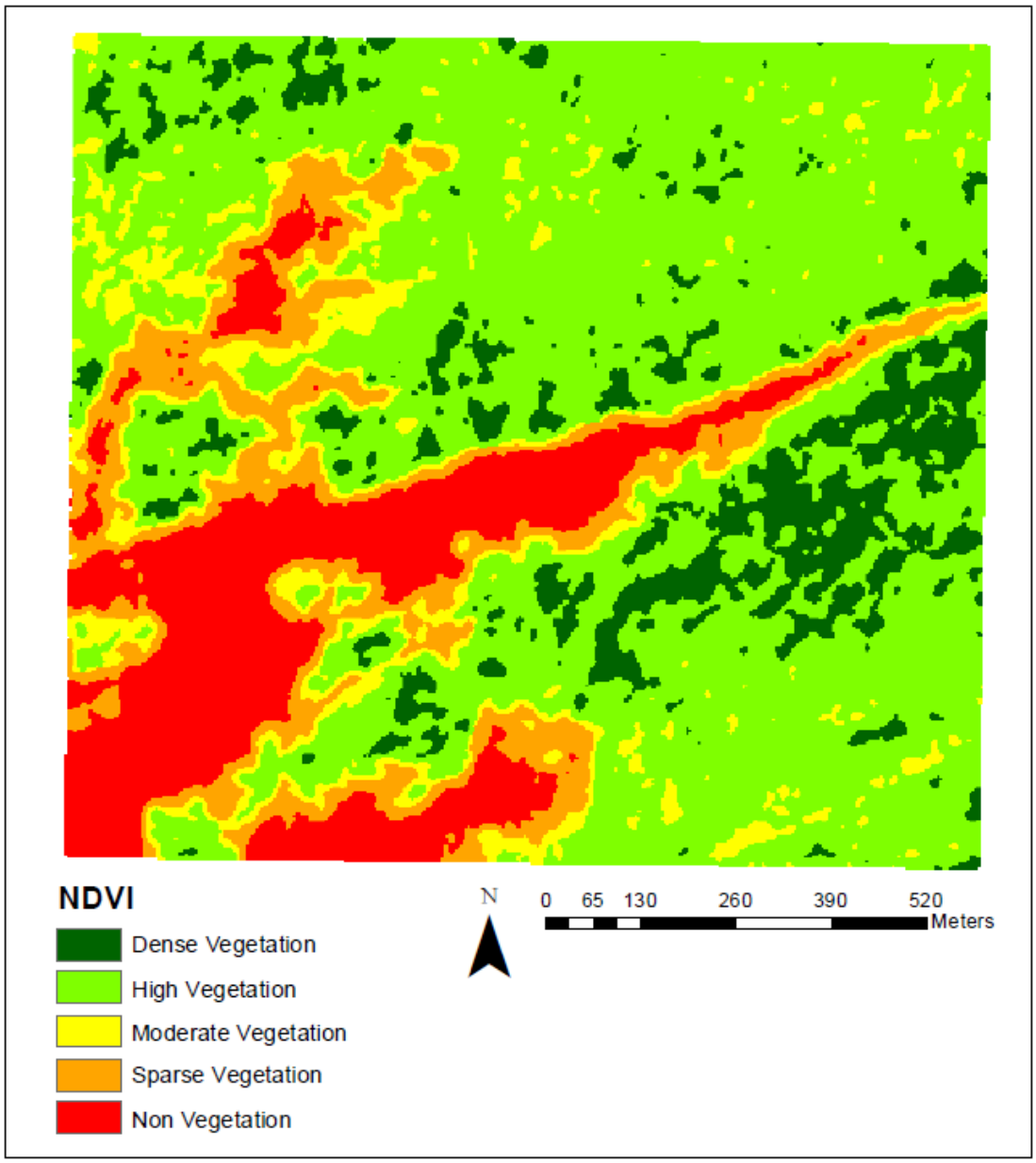

Figure 74: Area 7 NDVI Classification for January 2018.

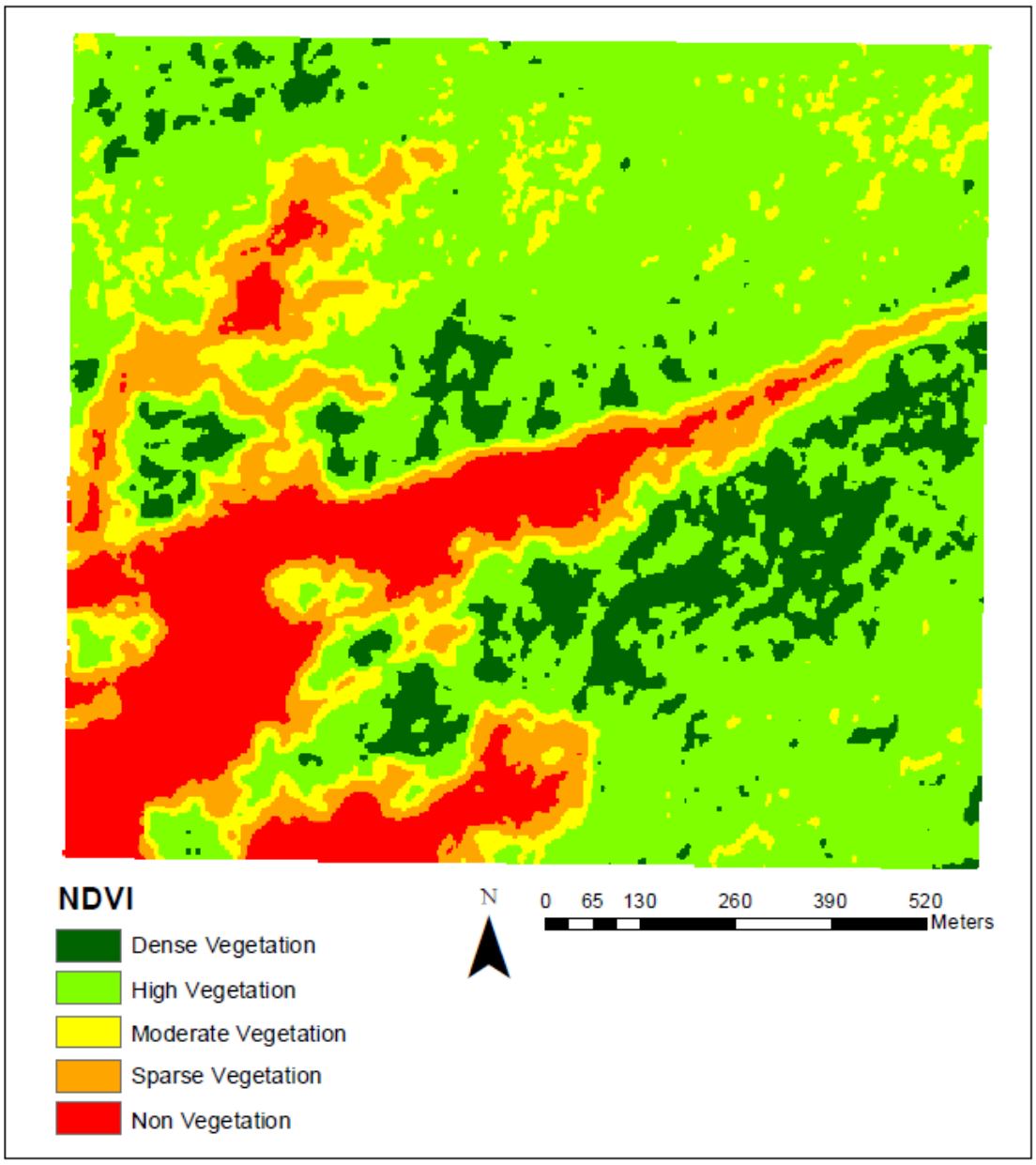

Figure 75: Area 7 NDVI Classification for February 2018.

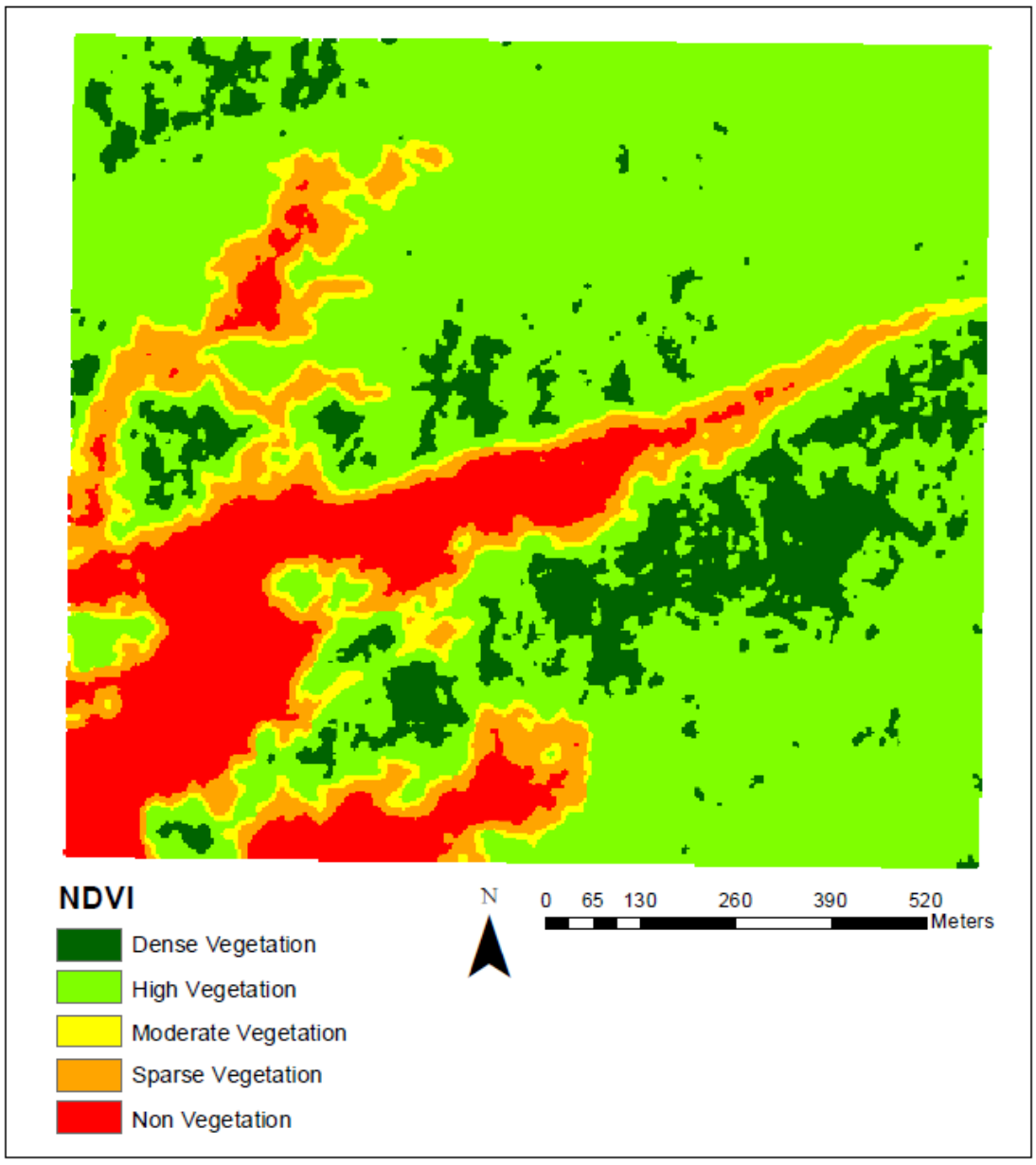

Figure 76: Area 7 NDVI Classification for May 2018.

B Python Scriptsf

B.1 Python Script Downloaded From Planet Labs

```
#----------------------------------------------------------------------------

#Program Title: Planet Tutorial

#Program Author: Que Bekkering

#Date Started: 11/08/2018

#Date Updated or Revised:12/05/2018

#Program Description: Learn to calculate a vegetation index to assess the

#quality of vegetation within an area of interest

#----------------------------------------------------------------------------


#set working environment path so you can path to a download folder - necessary? Not in tutorial

import os

#path = ("e:\\Thesis\\planet_order_288207\\20161218_101700_0e0d\\")

#os.chdir(path)


#STEP 1:Export your Planet API Key to your environment:

#export PLANET_API_KEY=(Your API Key Here)


#STEP 2: Download a 4 band image:

#planet data download --item-type PSScene4Band --asset-type analytic, analytic_xml --string-in id 20161218_101700_0e0d


#STEP 3: Extract the Visible Red and NIR bands
```

```
import rasterio

import numpy


image_file = "20161218_101700_0e0d_3B_AnalyticMS.tif"


#Load red and NIR bands - note all PlanetScope 4-band images have order RGBN

with rasterio.open (image_file) as src:

    band_red = src.read (3)


with rasterio.open (image_file) as src:

    band_nir = src.read (4)


#STEP 4: Normalize to Top of Atmosphere Reflectance

#Converting the pixel values to TOA Reflectance makes the analysis more accurate, and comparable

#with other scenes. Load the TOA Reflectance coefficients from the metadata XML asset.

from xml.dom import minidom


xmldoc = minidom.parse ("20161218_101700_0e0d_3B_AnalyticMS_metadata.xml")

nodes = xmldoc.getElementsByTagName ("ps:bandSpecificMetadata")


#XML parser refers to bands by numbers 1-4

coeffs = {}

for node in nodes:
```

```
    bn = node.getElementsByTagName ("ps:bandNumber")[0].firstChild.data

    if bn in ['1', '2', '3', '4']:

        i = int(bn)

        value = node.getElementsByTagName
("ps:reflectanceCoefficient")[0].firstChild.data

        coeffs[i] = float (value)


#Multiply the band values by the TOA (top of atmosphere) Reflectance Coefficients

#Multiply by corresponding coefficients

band_red = band_red * coeffs[3]

band_nir = band_nir * coeffs[4]


#STEP 5: Perform the NDVI Calculation

#This is done by the subtraction and division of pixel values

#Allow division by zero

numpy.seterr (divide='ignore', invalid='ignore')


#Calculate NDVI

ndvi = (band_nir.astype(float) - band_red.astype(float)) / (band_nir + band_red)


#STEP 6: Save the NDVI image

#We will output these new pixel values to a new image file. Make sure we mirror the
GeoTiff spatial metadata

#Set spatial charachteristics of the output object to mirror the input

kwargs = src.meta
```

```
kwargs.update (
    dtype=rasterio.float32,
    count = 1)

#Create the file
with rasterio.open ('ndvi.tif', 'w', **kwargs) as dst:
    dst.write_band (1, ndvi.astype (rasterio.float32))

#STEP 7: Apply a color map
#This will help to visually distinguish vegetation.
import matplotlib.pyplot as plt
plt.imsave ("ndvi_cmap.png", ndvi, cmap=plt.cm.summer)
```

B.2 Modified Python Script

```
#rasterio==1.0.11 updated to rasterio==1.0.28
import rasterio
import numpy as np
filename = "20170421_175041_1_0c59_3B_AnalyticMS.tif"
# Load red and NIR bands - note all PlanetScope 4-band images have band order BGRN
with rasterio.open(filename) as src:
    band_blue_radiance = src.read(1)
with rasterio.open(filename) as src:
    band_green_radiance = src.read(2)
with rasterio.open(filename) as src:
```

```
    band_red_radiance = src.read(3)
with rasterio.open(filename) as src:
    band_nir_radiance = src.read(4)


from xml.dom import minidom


xmldoc = minidom.parse("20170421_175041_1_0c59_3B_AnalyticMS_metadata.xml")
nodes = xmldoc.getElementsByTagName("ps:bandSpecificMetadata")


# XML parser refers to bands by numbers 1-4
coeffs = {}
for node in nodes:
    bn = node.getElementsByTagName("ps:bandNumber")[0].firstChild.data
    if bn in ['1', '2', '3', '4']:
        i = int(bn)
        value =
node.getElementsByTagName("ps:reflectanceCoefficient")[0].firstChild.data
        coeffs[i] = float(value)


print("Conversion coefficients: {}".format(coeffs))


# Multiply the Digital Number (DN) values in each band by the TOA reflectance
coefficients
band_blue_reflectance = band_blue_radiance * coeffs[1]
band_green_reflectance = band_green_radiance * coeffs[2]
```

```
band_red_reflectance = band_red_radiance * coeffs[3]

band_nir_reflectance = band_nir_radiance * coeffs[4]


import numpy as np

print("Red band radiance is from {} to {}".format(np.amin(band_red_radiance),
np.amax(band_red_radiance)))

print("Red band reflectance is from {} to {}".format(np.amin(band_red_reflectance),
np.amax(band_red_reflectance)))

print("nir band radiance is from {} to {}".format(np.amin(band_nir_radiance),
np.amax(band_nir_radiance)))

print("nir band reflectance is from {} to {}".format(np.amin(band_nir_reflectance),
np.amax(band_nir_reflectance)))

print("blue band radiance is from {} to {}".format(np.amin(band_blue_radiance),
np.amax(band_blue_radiance)))

print("blue band reflectance is from {} to {}".format(np.amin(band_blue_reflectance),
np.amax(band_blue_reflectance)))

print("green band radiance is from {} to {}".format(np.amin(band_green_radiance),
np.amax(band_green_radiance)))

print("green band reflectance is from {} to {}".format(np.amin(band_green_reflectance),
np.amax(band_green_reflectance)))


# Set spatial characteristics of the output object to mirror the input

kwargs = src.meta

kwargs.update(

    dtype=rasterio.float32,

    count = 4)
```

```
print("Before Scaling, red band reflectance is from {} to
{}".format(np.amin(band_red_reflectance),
                                                    np.amax(band_red_reflectance)))


# Here we include a fixed scaling factor. This is common practice.

scale = 100

blue_ref_scaled = scale * band_blue_reflectance

green_ref_scaled = scale * band_green_reflectance

red_ref_scaled = scale * band_red_reflectance

nir_ref_scaled = scale * band_nir_reflectance


print("After Scaling, red band reflectance is from {} to
{}".format(np.amin(red_ref_scaled),
                                                  np.amax(red_ref_scaled)))


print("Before Scaling, nir band reflectance is from {} to
{}".format(np.amin(band_nir_reflectance),
                                                    np.amax(band_nir_reflectance)))


print("After Scaling, nir band reflectance is from {} to
{}".format(np.amin(nir_ref_scaled),
                                                  np.amax(nir_ref_scaled)))


print("Before Scaling, blue band reflectance is from {} to
{}".format(np.amin(band_blue_reflectance),
```

```
                                        np.amax(band_blue_reflectance)))


print("After Scaling, blue band reflectance is from {} to
{}".format(np.amin(blue_ref_scaled),

                                        np.amax(blue_ref_scaled)))



print("Before Scaling, green band reflectance is from {} to
{}".format(np.amin(band_green_reflectance),

                                        np.amax(band_green_reflectance)))


print("After Scaling, green band reflectance is from {} to
{}".format(np.amin(green_ref_scaled),

                                        np.amax(green_ref_scaled)))



# Write band calculations to a new raster file

with rasterio.open('ref042117m7b.tif', 'w', **kwargs) as dst:

    dst.write_band(1, blue_ref_scaled.astype(rasterio.float32))

    dst.write_band(2, green_ref_scaled.astype(rasterio.float32))

    dst.write_band(3, red_ref_scaled.astype(rasterio.float32))

    dst.write_band(4, nir_ref_scaled.astype(rasterio.float32))


import matplotlib.pyplot as plt

import matplotlib.colors as colors
```

"""

The reflectance values will range from 0 to 1. You want to use a diverging color scheme to visualize the data,

and you want to center the colorbar at a defined midpoint. The class below allows you to normalize the colorbar.

"""

```
class MidpointNormalize(colors.Normalize):
    """
    Normalise the colorbar so that diverging bars work there way either side from a prescribed midpoint value)
    e.g. im=ax1.imshow(array, norm=MidpointNormalize(midpoint=0.,vmin=-100, vmax=100))
    Credit: Joe Kington, http://chris35wills.github.io/matplotlib_diverging_colorbar/
    """
    def __init__(self, vmin=None, vmax=None, midpoint=None, clip=False):
        self.midpoint = midpoint
        colors.Normalize.__init__(self, vmin, vmax, clip)

    def __call__(self, value, clip=None):
        # I'm ignoring masked values and all kinds of edge cases to make a
        # simple example...
        x, y = [self.vmin, self.midpoint, self.vmax], [0, 0.5, 1]
        return np.ma.masked_array(np.interp(value, x, y), np.isnan(value))
```

```
# Set min/max values from reflectance range for image (excluding NAN)
min=np.nanmin(band_nir_reflectance)
max=np.nanmax(band_nir_reflectance)
mid=0.20

fig = plt.figure(figsize=(20,10))
ax = fig.add_subplot(111)

# diverging color scheme chosen from https://matplotlib.org/users/colormaps.html
# note that appending '_r' to the color scheme name reverses it!
cmap = plt.cm.get_cmap('RdGy_r')

cax = ax.imshow(band_nir_reflectance, cmap=cmap, clim=(min, max),
norm=MidpointNormalize(midpoint=mid,vmin=min, vmax=max))

ax.axis('off')
ax.set_title('NIR Reflectance', fontsize=18, fontweight='bold')

cbar = fig.colorbar(cax, orientation='horizontal', shrink=0.65)

fig.savefig("ref042117m7b.png", dpi=200, bbox_inches='tight', pad_inches=0.7)

plt.show()
```

C Planet Labs Tutorial

The link to the various tutorials that Planet Labs offers is as follows: developers.planet.com/tutorials/

The necessary tutorial for using Mapshaper is called, “Simplifying Geometry”.

D Supervised Classification Tutorial

ERDAS Imagine 2015 Signature Editor Tutorial for Supervised Classification

This tutorial explains how to use the signature editor within ERDAS Imagine in order to complete a supervised classification on uploaded raster data. Using the signature editor creates a training data set for the supervised classification tool to pull from. Essentially, the training set tells the classification what each class should "look" like (from a spectral standpoint), and gives better guidance to the tool than an unsupervised classification can.

1. Open ERDAS Imagine 2015. Right click within the 2D view, and click Open Raster Layer. Choose the file that you will use to complete the supervised classification.

2. Open the same file within ArcGIS. This file will be used along with the identify tool to ascertain the reflectance values of individual pixels within the image. You will also use Google Earth or ground truth data (if you've collected this) to correctly verify land cover.

3. To begin, set your growing properties. This is discussed in the methods section and shown in the flowchart for *Region Growing Properties*.

4. Open the signature editor by clicking the raster tab ribbon, then supervised, and then signature editor. Click to open. The signature editor will look like the window below.

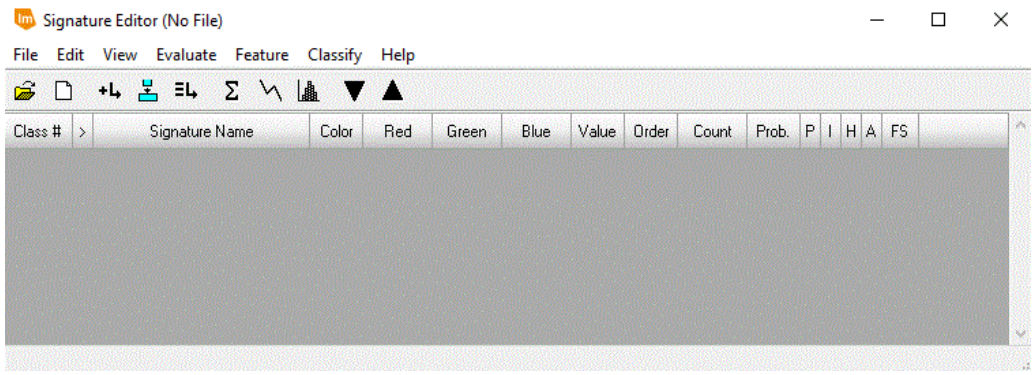

5. Select 30 points for each vegetative or land cover class. This is done by clicking on a pixel within the raster file loaded in ERDAS, and then clicking the "Create New Signature(s) From AOI" button within the signature editor window. Once you have selected 30 points, the signature editor window should look like the window shown on the following page.

Signature Editor (No File)

File Edit View Evaluate Feature Classify Help

Class #	Signature Name	Color	Red	Green	Blue	Value	Order	Count	Prob.	P	I	H	A	FS
1	Class 1		0.284	0.284	0.284	1	1	23	1.000	✔	✔	✔	✔	
2	Class 2		0.261	0.261	0.261	2	2	27	1.000	✔	✔	✔	✔	
3	Class 3		0.123	0.123	0.123	3	3	30	1.000	✔	✔	✔	✔	
4	Class 4		0.000	0.000	0.000	4	4	30	1.000	✔	✔	✔	✔	
5	Class 5		0.056	0.056	0.056	5	5	30	1.000	✔	✔	✔	✔	
6	Class 6		0.324	0.324	0.324	6	6	30	1.000	✔	✔	✔	✔	
7	Class 7		0.190	0.190	0.190	7	7	30	1.000	✔	✔	✔	✔	
8	Class 8		0.151	0.151	0.151	8	8	30	1.000	✔	✔	✔	✔	
9	Class 9		0.150	0.150	0.150	9	9	30	1.000	✔	✔	✔	✔	
10	Class 10		0.195	0.195	0.195	10	10	30	1.000	✔	✔	✔	✔	
11	Class 11		0.145	0.145	0.145	11	11	30	1.000	✔	✔	✔	✔	
12	Class 12		0.151	0.151	0.151	12	12	30	1.000	✔	✔	✔	✔	
13	Class 13		0.087	0.087	0.087	13	13	30	1.000	✔	✔	✔	✔	
14	Class 14		0.105	0.105	0.105	14	14	30	1.000	✔	✔	✔	✔	
15	Class 15		0.061	0.061	0.061	15	15	30	1.000	✔	✔	✔	✔	
16	Class 16		0.000	0.000	0.000	16	16	30	1.000	✔	✔	✔	✔	
17	Class 17		0.000	0.000	0.000	17	17	30	1.000	✔	✔	✔	✔	
18	Class 18		0.000	0.000	0.000	18	18	30	1.000	✔	✔	✔	✔	
19	Class 19		0.132	0.132	0.132	19	19	30	1.000	✔	✔	✔	✔	
20	Class 20		0.080	0.080	0.080	20	20	30	1.000	✔	✔	✔	✔	
21	Class 21		0.122	0.122	0.122	21	21	30	1.000	✔	✔	✔	✔	
22	Class 22		0.280	0.280	0.280	22	22	30	1.000	✔	✔	✔	✔	
23	Class 23		0.401	0.401	0.401	23	23	30	1.000	✔	✔	✔	✔	
24	Class 24		0.141	0.141	0.141	24	24	30	1.000	✔	✔	✔	✔	
25	Class 25		0.193	0.193	0.193	25	25	30	1.000	✔	✔	✔	✔	
26	Class 26		0.178	0.178	0.178	26	26	30	1.000	✔	✔	✔	✔	
27	Class 27		0.354	0.354	0.354	27	27	30	1.000	✔	✔	✔	✔	
28	Class 28		0.305	0.305	0.305	28	28	30	1.000	✔	✔	✔	✔	
29	Class 29		0.000	0.000	0.000	29	29	30	1.000	✔	✔	✔	✔	
30	Class 30		0.027	0.027	0.027	30	30	30	1.000	✔	✔	✔	✔	

6. After you have selected 30 pixels, click on “Class 1” and change it to a significant name for that class. Each signature needs to have a unique name. This means that you will relabel Class 1 to (example: n1, for nonveg signature 1), and continue labeling n2, n3, etc. until you have renamed all 30 signatures. An image is shown on the following page of what your signature editor window should look like at this point.

Signature Editor (No File)

File Edit View Evaluate Feature Classify Help

Class #	Signature Name	Color	Red	Green	Blue	Value	Order	Count	Prob.	P	I	H	A	FS
1	n1		0.284	0.284	0.284	1	1	23	1.000	✔	✔	✔	✔	
2	n2		0.261	0.261	0.261	2	2	27	1.000	✔	✔	✔	✔	
3	n3		0.123	0.123	0.123	3	3	30	1.000	✔	✔	✔	✔	
4	n4		0.000	0.000	0.000	4	4	30	1.000	✔	✔	✔	✔	
5	n5		0.056	0.056	0.056	5	5	30	1.000	✔	✔	✔	✔	
6	n6		0.324	0.324	0.324	6	6	30	1.000	✔	✔	✔	✔	
7	n7		0.190	0.190	0.190	7	7	30	1.000	✔	✔	✔	✔	
8	n8		0.151	0.151	0.151	8	8	30	1.000	✔	✔	✔	✔	
9	n9		0.150	0.150	0.150	9	9	30	1.000	✔	✔	✔	✔	
10	n10		0.195	0.195	0.195	10	10	30	1.000	✔	✔	✔	✔	
11	n11		0.145	0.145	0.145	11	11	30	1.000	✔	✔	✔	✔	
12	n12		0.151	0.151	0.151	12	12	30	1.000	✔	✔	✔	✔	
13	n13		0.087	0.087	0.087	13	13	30	1.000	✔	✔	✔	✔	
14	n14		0.105	0.105	0.105	14	14	30	1.000	✔	✔	✔	✔	
15	n15		0.061	0.061	0.061	15	15	30	1.000	✔	✔	✔	✔	
16	n16		0.000	0.000	0.000	16	16	30	1.000	✔	✔	✔	✔	
17	n17		0.000	0.000	0.000	17	17	30	1.000	✔	✔	✔	✔	
18	n18		0.000	0.000	0.000	18	18	30	1.000	✔	✔	✔	✔	
19	n19		0.132	0.132	0.132	19	19	30	1.000	✔	✔	✔	✔	
20	n20		0.080	0.080	0.080	20	20	30	1.000	✔	✔	✔	✔	
21	n21		0.122	0.122	0.122	21	21	30	1.000	✔	✔	✔	✔	
22	n22		0.280	0.280	0.280	22	22	30	1.000	✔	✔	✔	✔	
23	n23		0.401	0.401	0.401	23	23	30	1.000	✔	✔	✔	✔	
24	n24		0.141	0.141	0.141	24	24	30	1.000	✔	✔	✔	✔	
25	n25		0.193	0.193	0.193	25	25	30	1.000	✔	✔	✔	✔	
26	n26		0.178	0.178	0.178	26	26	30	1.000	✔	✔	✔	✔	
27	n27		0.354	0.354	0.354	27	27	30	1.000	✔	✔	✔	✔	
28	n28		0.305	0.305	0.305	28	28	30	1.000	✔	✔	✔	✔	
29	n29		0.000	0.000	0.000	29	29	30	1.000	✔	✔	✔	✔	
30	n30		0.027	0.027	0.027	30	30	30	1.000	✔	✔	✔	✔	

7. Repeat steps 5 and 6 until you have signatures for every vegetative/land cover class in your study, and giving each signature within each class a significant label.

8. Once you have all classes in the editor, and labeled, save the signature editor file with a meaningful name. For example, I labeled my training data “Train050318m1dist05pix30.sig”. This name means that it is training data for the

imagery date 5/03/18 for Area 6, with growing tool properties of spectral Euclidean distance of 0.5 and a distance of 30 pixels.

9. Once this file is saved, you will merge each set of signatures into their respective classes. To do this for the first class, click, hold, and drag the mouse until the first 30 signatures are selected. Click “Edit”, and then “Merge”, or click the merge button.

10. Scroll to the bottom of the signature editor list. You will now have a new signature called “Class 1” again. Rename this to the name of one of your landcover classes (example: nonveg).

11. Now scroll back to the top of the signature editor window. The 30 selected signatures should still be highlighted. Click “Edit,” then “Delete”.

12. Repeat steps 9 through 11 for your remaining classes.

13. Your signature editor window should now only have 5 signatures, which are your merged class signatures. Your window should look like the image below.

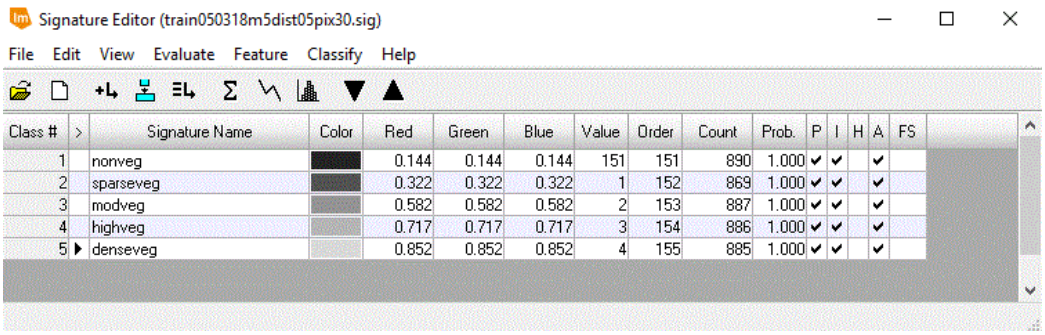

Class #	Signature Name	Color	Red	Green	Blue	Value	Order	Count	Prob.	P	I	H	A	FS
1	nonveg		0.144	0.144	0.144	151	151	890	1.000	✔	✔		✔	
2	sparseveg		0.322	0.322	0.322	1	152	869	1.000	✔	✔		✔	
3	modveg		0.582	0.582	0.582	2	153	887	1.000	✔	✔		✔	
4	highveg		0.717	0.717	0.717	3	154	886	1.000	✔	✔		✔	
5	denseveg		0.852	0.852	0.852	4	155	885	1.000	✔	✔		✔	

14. Select a color for each class from the color drop-down menu. Doing this assigns a color for each landcover class, and gives meaning to the output image from the

supervised classification you will be running in a few steps. Your window should now look like the image below.

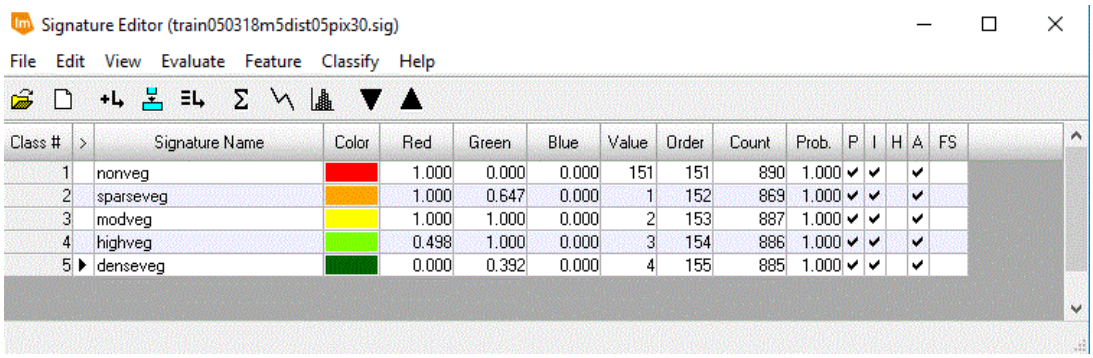

Class #	>	Signature Name	Color	Red	Green	Blue	Value	Order	Count	Prob.	P	I	H	A	FS
1		nonveg		1.000	0.000	0.000	151	151	890	1.000	✔	✔		✔	
2		sparseveg		1.000	0.647	0.000	1	152	869	1.000	✔	✔		✔	
3		modveg		1.000	1.000	0.000	2	153	887	1.000	✔	✔		✔	
4		highveg		0.498	1.000	0.000	3	154	886	1.000	✔	✔		✔	
5	▶	denseveg		0.000	0.392	0.000	4	155	885	1.000	✔	✔		✔	

15. Save this file again with a new meaningful name (example: merge050318m1dist05pix30).

16. Go into the ERDAS window. Click “Raster”, “Supervised”, and then “Supervised Classification”. Path to the files you have saved as shown below. Name the classified file with a significant name, such as “sc” for supervised classification. You may choose to create a distance file. It is not necessary, but in this case, I created one. For the Decision Rules section at the bottom of this window, keep the defaults (“None” for the Non-parametric Rule, and “Maximum Likelihood” for the Parametric Rule). Click “OK” to run the tool.

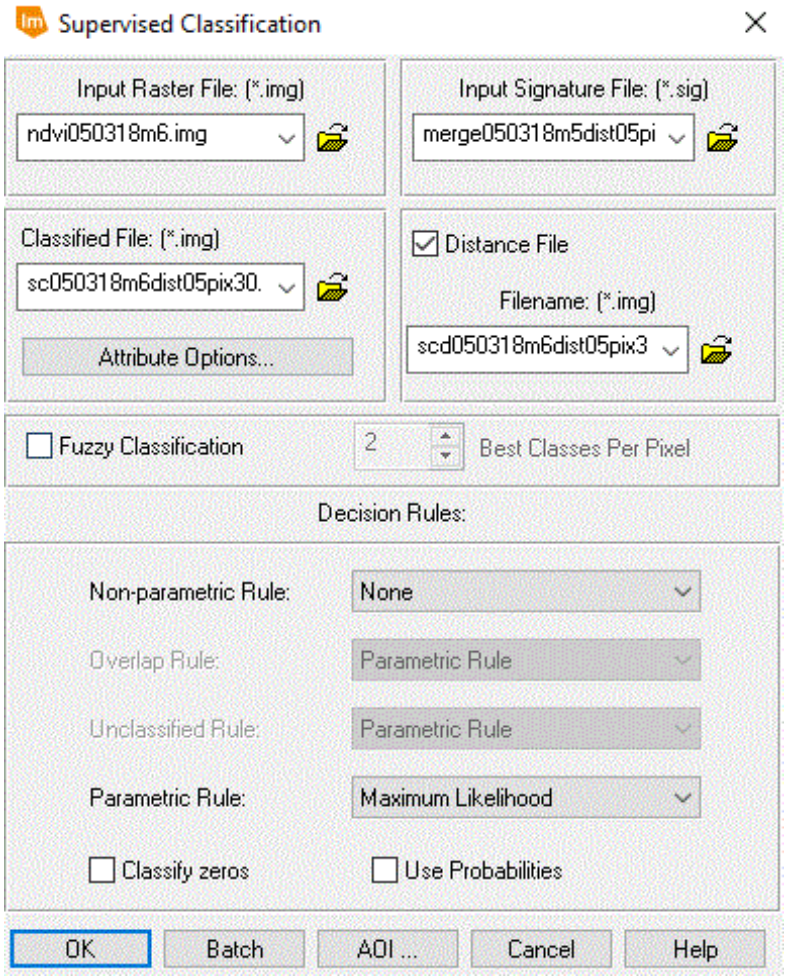

17. To see the supervised classification image you have created, click “File”, “New”, “2D View”. In the new 2D view window, right click and click “Open Raster Layer”. An example of a supervised classification with assigned colormap is shown below.

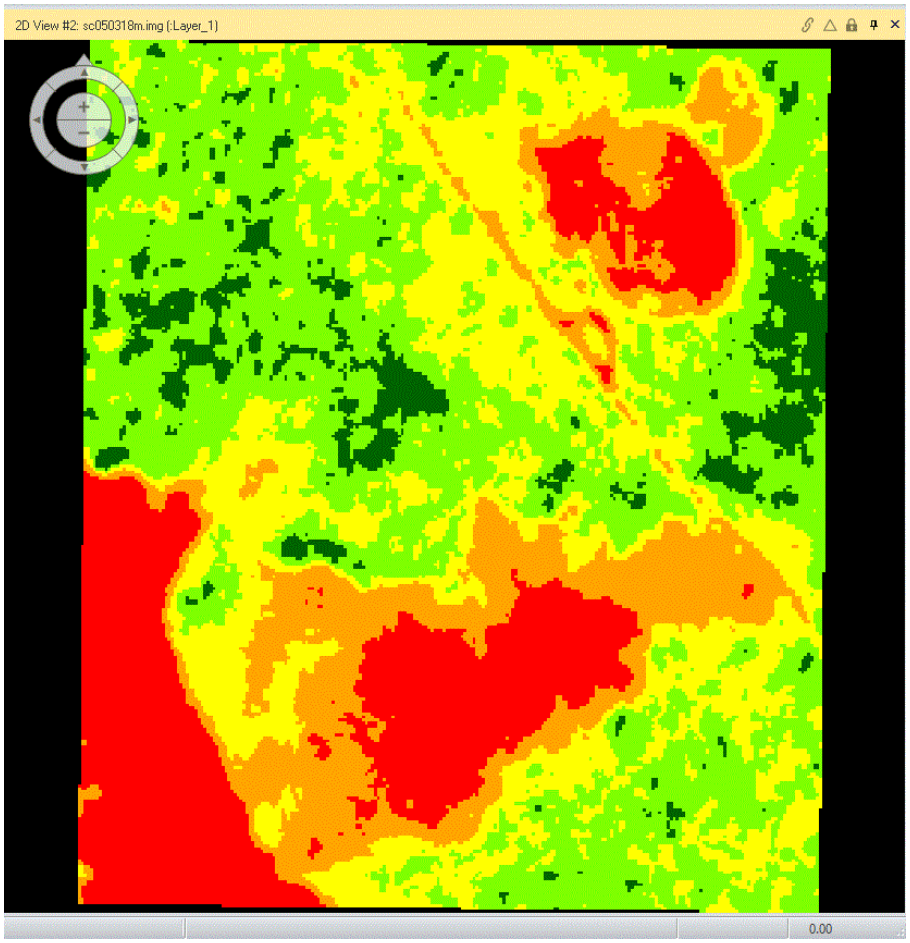
2D View #2: sc050318m.img (:Layer_1)
0.00